Dissertation

submitted to the

Combined Faculties for the

Natural Sciences and Mathematics

of the Ruperto-Carola University of Heidelberg, Germany

for the degree of

Doctor of Natural Sciences

presented by

Dipl.-Ernährungswiss. Nicole Amen

born in Lippstadt, Germany

Oral examination:

14.05.2013

The role of Glucosylceramides in Keratinocyte Differentiation and Epidermal Barrier Function

Referees:

Prof. Dr. rer. nat. Peter Angel

Prof. Dr. med. Hermann-Josef Gröne

Summary

Glycosphingolipids (GSLs) are amphiphatic molecules ubiquitiously expressed in eukaryotes and have been shown to play a crucial role in various (inherited) human disorders such as autoimmune diseases, ichthyoses and cancer. GSLs are one class of sphingolipids (SLs) and are constructed from ceramides (Cers), comprising a sphingoid base (typically sphingosine, a long-chain amino diol) which is amide-linked to a fatty acid (FA) of variable chain length. GSLs are formed by the addition of mono- or oligosaccharides via a glycosidic linkage to sphingosine C1. Glucosylceramides (GlcCers) are precursors for most of the higher GSLs and major compounds of the stratified squamous epithelia. In particular, GlcCers comprise ca. 4% of the total lipid mass in the epidermis and ca. 16% in the esophageal epithelium.

The lipophilic anchor of epidermal GlcCers contains a unique ultra-long-chain amide-linked fatty acid (ULC-FA) with up to 36 carbon atoms. The ULC-FAs are typically ω-hydroxylated to give the so-called OS class of GlcCers, accounting for an essential part of the skin barrier. The ULC-GlcCers reside primarily in the outermost anucleated layers of the epidermis, i.e., the stratum corneum (SC), which is mainly composed of dead, flattened keratinocytes, the so-called corneocytes, embedded in a lipid-enriched extracellular matrix. This barrier protects the body from dehydration, mechanical insult and infection and derives from the interplay between proteins in the corneocyte membrane and the lipids. The lipid matrix surrounding the corneocytes is composed of Cers, cholesterol and free FAs in nearly equimolar ratios, which can be organized into lamellar sheets.

The Cers found in the SC are believed to be derived from GlcCers which have been synthesized at the trans-Golgi network by the enzyme UDP-glucose:ceramide glucosyltransferase (UGCG). Thus, it has been suggested that GlcCers function as intracellular carriers of the hydrophobic Cers and are transferred via vesicular transport within lamellar bodies (LBs) to the apical plasma membrane (PM) of SC keratinocytes. LBs fuse with the PM in the upper stratum granulosum (SG) and at the SG/SC interface, where they exocytose their lamellar lipid content, together with structural proteins, enzymes and antimicrobial peptides, into the extracellular space. By the action of enzymes such as glucosylceramidase and ceramidase, Cers, glucose, FAs and free sphingoid bases are released from GlcCer precursors.

The ω-hydroxy group of ULC-(Glc)Cers enables their esterification to an additional FA, predominantly linoleic acid (18:2, ω–6), to give the EOS subclass of (Glc)Cers. Trans-esterification to proteins of the corneocyte membrane then leads to the formation of protein-linked Cers (POS) and the cornified lipid envelope (CLE). EOS as well as POS species and their corresponding GlcCer-precursors establish the extremely hydrophobic extracellular lipid lamellae of the SC and thereby the skin barrier.

An earlier study using mice with constitutive *Ugcg* deletion in the epidermis (*Ugcg*$^{f/f\,K14Cre}$ mice) highlighted the importance of Cer glucosylation. Mutant mice lost the water permeability barrier (WPB) and died postnatally at day P5. However, the exact molecular and cellular contribution of OS

and specifically POS-Cers for the buildup and stability of the WPB could not be determined. In addition, the differentiation and function of UGCG-deficient epidermis and its function in clinically relevant pathophysiologic states, e.g. wound healing, could not be analyzed.

Inducible $Ugcg^{f/f\,K14CreERT2}$ mice were generated in our laboratory to circumvent the problem of early death experienced with $Ugcg^{f/f\,K14Cre}$ mice. Tamoxifen (TAM)-induced $Ugcg$ gene deletion in keratin K14-positive basal cells resulted in a significant decrease in esophageal and epidermal GlcCers and, in contrast to newborn mice, to an almost complete loss of epidermal POS-Cers three weeks after initiation of TAM induction. Subsequent alterations in keratinocyte differentiation and epidermal barrier homeostasis were evidenced by an increase in transepidermal water loss (TEWL) and pH as well as by keratinocyte hyperproliferation to give a severe ichthyosiform skin phenotype. This skin phenotype was slightly reversed within three months following TAM induction, apparently due to the action of hair follicle stem cells. Furthermore, wound closure and reepithelialization was significantly delayed in mutant vs. control skin.

Gene expression profiling of $Ugcg$ mutant skin vs. control skin revealed a subset of differentially expressed genes which are involved in lipid signaling and epidermal differentiation/proliferation and which correlate with human skin diseases such as psoriasis and atopic dermatitis. Peroxisome proliferator-activated receptor β/δ (PPARβ/δ), a Cer-sensitive transcription factor, was identified as a potential mediator of the altered gene sets. Thus, we conclude that the combined increase in free epidermal Cers and the expression of PPARβ/δ and target genes serves as the driving mechanism for impaired epidermal homeostasis and barrier loss, thereby emphasizing the critical role of GlcCer in epithelial differentiation.

Zusammenfassung

Glycophingolipide („Glycosphingolipids", GSLs) sind ubiquitär vorkommende, amphipathische Lipidmoleküle in Eukaryoten denen eine entscheidende Rolle in verschiedenen humanen Erkrankungen wie z.B. Autoimmunerkrankungen, Ichthyosen und Krebs zugesprochen wird. GSLs bilden eine wichtige Klasse der Sphingolipide (SLs) und werden aus Ceramiden (Cers) gebildet. Ein Cer besteht in seiner Grundstruktur aus einer Sphingoid Base (i.d.R. Sphingosine), die über eine Amid-Bindung mit einer Fettsäure (N-Acyl), sowie im Falle von GSLs am C1 Atom mit einem oder mehreren Kohlenhydratmolekülen verestert ist. Glucosylceramid (GlcCer) ist Vorläuferlipid für alle höheren GSLs und stellt eine wichtige Komponenten von Plattenepithelien dar, wie z.B. in der Epidermis (mit ca. 4% der Gesamtlipidmasse) und im Esophagusepithel (mit ca. 16% der Gesamtlipidmasse).

Der lipophile Anker der epidermalen GlcCers besteht aus ω-hydroxylierten (ωh) Ceramiden (Cers), OS-Cers, die ultra-langkettige („Ultra-Long-Chain", ULC) N-Acylsubstituenten von bis zu 36 C-Atomen besitzen und damit eine essentielle Komponente der Hautbarriere darstellen. Die eigentliche Permeabilitätsbarriere befindet sich in der äußersten, anukleären Epidermisschicht, im Stratum Corneum (SC), welches zum größten Teil aus abgeflachten, terminal-differenzierten Keratinocyten (sogenannten Corneozyten) besteht, die in einer lipidreichen extrazellulären Matrix eingebettet sind. Diese Barriere, die den Körper vor Austrocknung, mechanischen Verletzungen und Infektionen schützt, basiert auf der Interaktion von Proteinen der Corneozytenmembran mit Lipiden. Die äquimolare Zusammensetzung der Lipidmatrix aus Cers, Cholesterol und freien Fettsäuren bedingt ihre lamellare Struktur und damit ihre Funktion als Wasserpermeabilitäts-Barriere (WPB).

Es wird angenommen, dass die Cers im *SC* aus GlcCer-Vorläufern entstehen, die im trans-Golgi-Kompartiment der Keratinozyten in einer UDP-glucose ceramide glucosyltransferase (UGCG) katalysierten Reaktion gebildet werden. GlcCers gelten als intrazelluläre Trägerlipide der extrem hydrophoben Cers und gelangen via vesikulären Transport in sogenannten Lamellar Bodies (LBs) zur apikalen Plasmamembran (PM) der Keratinozyten. An der Grenze zwischen dem *Stratum Granulosum* (SG) und dem *SC* fusionieren die LBs mit der Keratinozytenmembran und extrudieren ihren Inhalt an SLs, Strukturproteinen, Enzymen und antimikrobiellen Peptiden in den Extrazellularraum.

Die ω-hydroxy Gruppe der ULC (Glc)Cers ermöglicht die Veresterung entweder mit Fettsäuren, hauptsächlich mit Linolensäure, was zur Bildung von EOS (Esterified ωh-Spingosine) Cers führt, oder mit Proteinen der Corneozytenmembran, was zur Bildung von POS (Protein-linked ωh-Spingosine) führt. EOS und POS-Cers, sowie die korrespondierenden GlcCer Vorläufer, sind wichtige Bausteine der extrem hydrophoben extrazellulären Lipidlamellae des *SC* und damit der Hautbarriere.

In einer früheren Studie, mit konstitutiv epidermal *Ugcg*-defizienten Mäusen ($Ugcg^{f/fK14Cre}$), konnte die Bedeutung der Cer-Glucosylierung gezeigt werden. Die transgenen Tiere starben ca. fünf Tage postnatal aufgrund der Störung der epidermalen WPB. Aufgrund des frühen Todes der Tiere, konnte die genaue molekulare und zelluläre Funktion der OS, insbesondere der POS-Cers für den Aufbau und

Erhalt der WPB nicht untersucht werden. Darüber hinaus konnten Wundheilungsexperimente zur Untersuchung des Einflusses und der Funktion der UGCG-Depletion auf die Differenzierung der Keratinozyten nicht durchgeführt werden.

Aus diesem Grund wurden induzierbar *Ugcg*-transgene Mäuse ($Ugcg^{f/f\,K14CreERT2}$) generiert, in denen im adulten Stadium (im Alter von 8 Wochen) die Gendeletion mittels tamoxifen (TAM) initiiert wurde. Die *Ugcg*-Deletion in Keratin K14-positiven Basalzellen führte nach drei Wochen zu einem signifikanten Verlust an sowohl esophagealen als auch epidermalen GlcCers und, im Gegensatz zu den Neugeborenen *Ugcg*-defizienten Tieren, zu einem fast kompletten Verlust an POS-Cers. Nachfolgende Störungen der Kertinozytendifferenzierung und der WPB zeigten sich in erhöhtem transepidermalen Wasserverlust („Transepidermal Water Loss", TEWL) und pH, sowie in der resultierenden Hyperproliferation der Keratinozyten, welche letztendlich zu Ichthyose-artigen Hautveränderungen in den transgenen Tieren führte. Nach drei Monaten wurde ein leichter Rückgang der Hautschuppung und des TEWL beobachtet, was wir auf die Aktivierung von Haarfollikel Stammzellen zurückgeführten. Darüber hinaus zeigten Wundheilungsexperimente in Kontrollen und UGCG-defizienten Mäusen, sowie in Hauttransplantaten dieser Tiere, eine signifikant verzögerte Reepithelialisierung der Wunden.

Die Evaluierung der Genexpressionsdaten von Kontroll- und *Ugcg*-transgenen Hautproben hob besonders differentiell exprimierte Gene des Lipidmetabolismus und der epidermalen Differenzierung/Proliferation hervor, die darüber hinaus in humanen Hauterkrankungen (z.B. Ichthyose, Psoriasis, Atopischer Dermatitis) eine Rolle spielen. Peroxisome proliferator-activated receptor β/δ (PPARβ/δ), ein Cer-sensitiver Transkriptionsfaktor, wurde als potentieller Mediator der Genveränderungen identifiziert. Die Ergebnisse deuten darauf hin, dass die Entwicklung der Ichthyose-artigen Hautveränderungen der GlcCer-defizienten Tiere auf Grund eines Anstieges freier Cers und aus einer Cer-getriggerten Aktivierung von PPARβ/δ (sowie dessen Zielgene) resultiert und unterstreicht damit die Bedeutung dieser SL Klasse für die epitheliale Differenzierung.

Table of Contents

List of Figures

List of Tables

1. Introduction

1.1   Sphingolipids

Sphingolipids (SLs) were first described as components of the brain by the German physician Johann L. W. Thudichum (Thudichum, 1884), who named these enigmatic molecules after the sphinx, a Greek mythological creature. SLs are amphipathic molecules ubiquitously expressed in eukaryotic cells and are major constituents of the plasma membrane (PM), promoting its arrangement into a lipid bilayer. SL structure and metabolism have been intensively studied over the past decades, with complementary information coming more recently from the field of *lipidomics*, where the related networks and pathways involving SLs are explored. So far, SLs have been identified as multifunctional molecules involved in proliferation, differentiation and cell signaling. However, the function of only a minor fraction of the known GSLs has been elucidated so far.

The key structural element of all SLs is a ceramide (Cer), composed of a sphingoid base and an amide-linked fatty acid (FA) moiety (Figure 1). Cer is the precursor for more complex SL classes such as the sphingomyelins (SMs) and glycosphingolipids (GSLs), which exclusively differ in their type of substituent at carbon 1 of the sphingoid base (Figure 1).
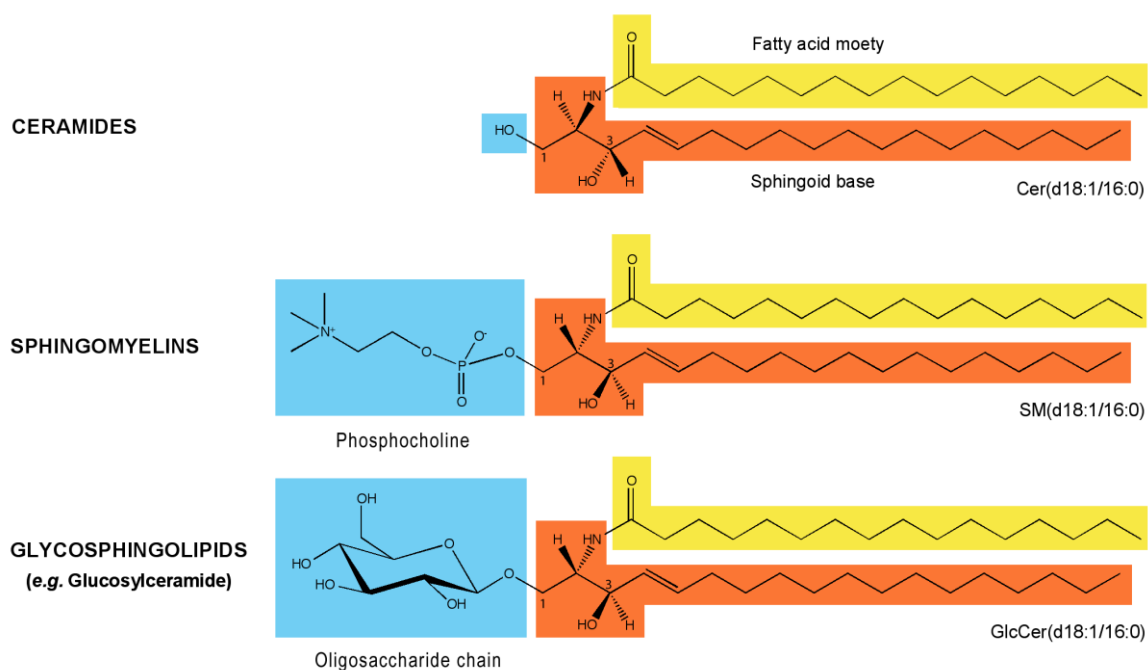
Figure 1.   Major sphingolipid classes.

Sphingolipids are biosynthesized via condensation of the amine group of a sphingoid molecule with an activated fatty acid (acyl CoA). The sphingoid base shown here corresponds to sphingosine (orange), designated d18:1 in the short-hand notation for a "standard" dihydroxy sphingoid with hydroxy groups at carbons 1 and 3 and a *trans* double bond at carbon 4. The amide-linked fatty acid at pos. 2 is represented here by a 16:0 palmitoyl moiety (yellow). The substituent (blue) at the sphingoid carbon 1 determines the SL class and can be either the original hydroxy group (as in sphingosine), a phosphocholine moiety or a mono- or oligosaccharide group. *Modified from* (Rabionet 2011).

The amphipathic character of simple SLs (e.g. Cer) is determined by the amide linkage at C2 (NH as proton donor, C=O as proton acceptor) and the OH group at C3 (proton acceptor or donor), allowing for intermolecular hydrogen bonds (e.g., with cholesterol) (Uchida and Hamanaka, 2006). The amphipathic characteristics of more complex SLs can vary considerably and result from the combined properties of the hydrophobic sphingoid base, its amide-linked FA, and the hydrophilic region of the head group (i.e., phosphocholine (Cho-*P*) in SMs, mono- or oligosaccharide in GSLs). These three structural components: (1) the sphingoid base, (2) the FA, (3) the head group, are also the basis for the structural diversity of most SLs and their functional specialization in various tissues.

The FA moiety may differ considerably in chain length, or in degree of saturation and hydroxylation in a tissue-specific manner. It can be attached to various sphingoid bases: most frequently sphingosine (4*E*-sphingenine, or in short-hand notation 4*E*-d18:1 or simply d18:1), as in the SLs in Figure 1, but also sphinganine (4,5-dihydrosphingosine; d18:0), 4*E*-6-hydroxy-sphingosine (6-t18:1) or phytosphingosine (4-hydroxysphinganine; 4-t18:0), (reviewed in (Kendall and Nicolaou, 2012; Pruett et al., 2008)). The short-hand notation for sphingoids used here and in the Figures is based on the scheme used for fatty acids: numbers x:y denote carbon chain length and number of double bonds; prefix m, d, or t denotes a mono-, di-, or trihydroxy molecule, where by default d = 1,3-dihydroxy; *n*-t denotes the position of a third hydroxyl group; for y = 1 the default is 4*E* while other double bonds are denoted by an appropriate prefix such as 8*Z* for 8-*cis*. This variety in SL structures is enhanced by the different possible head groups, e.g., phosphocholine in SMs or a carbohydrate in GSLs (e.g., monosaccharide in cerebrosides, oligosaccharide in globosides and gangliosides), whereby the oligosaccharides identified for GSLs include combinations of ca. 500 different sugar residues (Kolter et al., 2002).

GSLs were initially studied in lipid storage diseases and brain tissue to investigate their role in the nervous system (Yates, 1986). More recently, mouse models lacking specific glycosyltransferases have faciliated the investigation of distinct GSL classes. Tissue-specific deletion of a key enzyme in GSL synthesis, glucosylceramide synthase (UGCG), in brain (Jennemann et al., 2005), epidermis (Jennemann et al., 2007) and intestine (Jennemann et al., 2012a) proved to be lethal in mice and evidenced the important role of GSLs in tissue development. Moreover, Nordström and coworkers have shown that inducible deletion of the *Ugcg* enzyme in the forebrain impairs energy homeostasis in mice (Nordström et al., 2013). In addition, glucosylceramide (GlcCer), the simplest GSL, has been observed to accumulate in kidneys of humans or mice afflicted with polycystic kidney disease (PKD) (Natoli et al., 2010) as well as in multidrug-resistant tumors expressing high levels of GlcCers (Lavie et al., 1996).

A more complex GSL (GM3) was shown to influence cell-surface receptor function, e.g., the insulin receptor or epidermal growth factor (EGF) receptor, thereby regulating signal transduction (Aerts et al., 2007; Liu et al., 2008; Yamashita et al., 2003). Furthermore, GSLs can act as cell-specific recognition sites for bacterial toxins (e.g., tetanus or shiga toxin) or viruses (e.g., sendai virus), which can bind to specific carbohydrate moieties of these lipids and invade and infect the organism (Angstrom et al., 1994; Karlsson, 1989; Keusch et al., 1991; Markwell et al., 1981). Regarding the

immune system, glycolipid structures (e.g., GlcCer, GalCer) have been shown to activate T lymphocytes, and these findings launched the development of GSL-based therapies for auto-immune diseases such as diabetes or multiple sclerosis (De Libero et al., 2002; Van Kaer, 2005).

The simpler SLs such as Cer, ceramide 1-phosphate (Cer-1-*P*) or sphingosine 1-phosphate (Sph-1-*P*) function as signaling molecules and regulate different cell fates such as proliferation, differentiation and apoptosis, either directly as a signaling lipid or via G-protein-coupled receptor cascades (Chalfant and Spiegel, 2005; Geilen et al., 1997).

Cer is known as a potent inducer of apoptosis and is elevated following various external or internal stress signals. These signals lead to intracellular Cer synthesis and activation of Cer-responsive enzymes such as protein kinases (e.g., janus kinase (JNK), protein kinase C (PKC)), phosphatases (e.g., ceramides activated protein phosphatase (CAPP)), or phospholipase A2 (PLA2), phospholipase D (PLD)) (Bourbon et al., 2000; Huwiler et al., 2001; Perry and Hannun, 1998; Westwick et al., 1995). Moreover, Cer may act via nuclear hormone receptors, as evidenced for the transcriptional regulator peroxisome proliferator-activated receptor beta/delta (PPARβ/δ), and induce the expression of the lipid transporter ABCA12 in keratinocytes (Jiang et al., 2009).

Furthermore, signal transduction can be modified by so-called lipid raft microdomains in the PM. Such rafts are thought to be composed of Cers, GSLs and cholesterol; they trap and concentrate signaling molecules (e.g. FAS receptor) (Bollinger et al., 2005), thereby potentiating the signal.

Much of the present research on SLs is certainly motivated by their recognized role in inherited and acquired human diseases such as sphingolipidoses (Doering et al., 1999b; McGovern and Schuchman, 1993; Sandhoff, 1969), cancer progression (Kannagi et al., 2004; Raffaghello et al., 2003) and inflammatory skin diseases (Macheleidt et al., 2002).

1.2   Sphingolipid Biosynthesis

The cellular pathways involving SLs have been partially elucidated using synthetic as well as radiolabeled precursor lipids (Rosenwald and Pagano, 1993; van Echten-Deckert et al., 1997).

SL biosynthesis begins at the cytosolic leaflet of the endoplasmic reticulum (ER) with the condensation of l-serine and palmitoyl-CoA (CoA = Coenzyme A) to form 3-keto-sphinganine (Figure 2). This rate-limiting step of *de novo* Cer synthesis is catalyzed by the enzyme complex serine C-palmitoyltransferase (SPT) and is crucial for Cer homeostasis in the skin (Hanada, 2003; Mizukoshi et al., 2011). The reduction of 3-keto-sphinganine to sphinganine (dihydrosphingosine) and the subsequent coupling to a particular FA by an acyl-CoA-specific ceramide synthase (CerS) results in dihydroceramide (Pewzner-Jung et al., 2006). A desaturase enzyme (DES1) introduces the 4,5-trans-double bond to give Cer, which can enter the SL metabolic pathways, where it can be deacylated to give sphingosine, which, in turn, can be derivatized to Sph-1-P, for example, or where it can serve as a precursor for more complex SMs or GSLs (Figure 2).

Cer degradation via deacylation to give sphingosine and an FA is catalyzed by a family of ceramidases, which may have a neutral, alkaline or acidic pH optimum, depending on cellular localization (Lahiri and Futerman, 2007). Sphingosine or sphinganine derived from Cer can also be recycled for Cer synthesis via ceramide synthases (CerS) (Geilen et al., 1997).
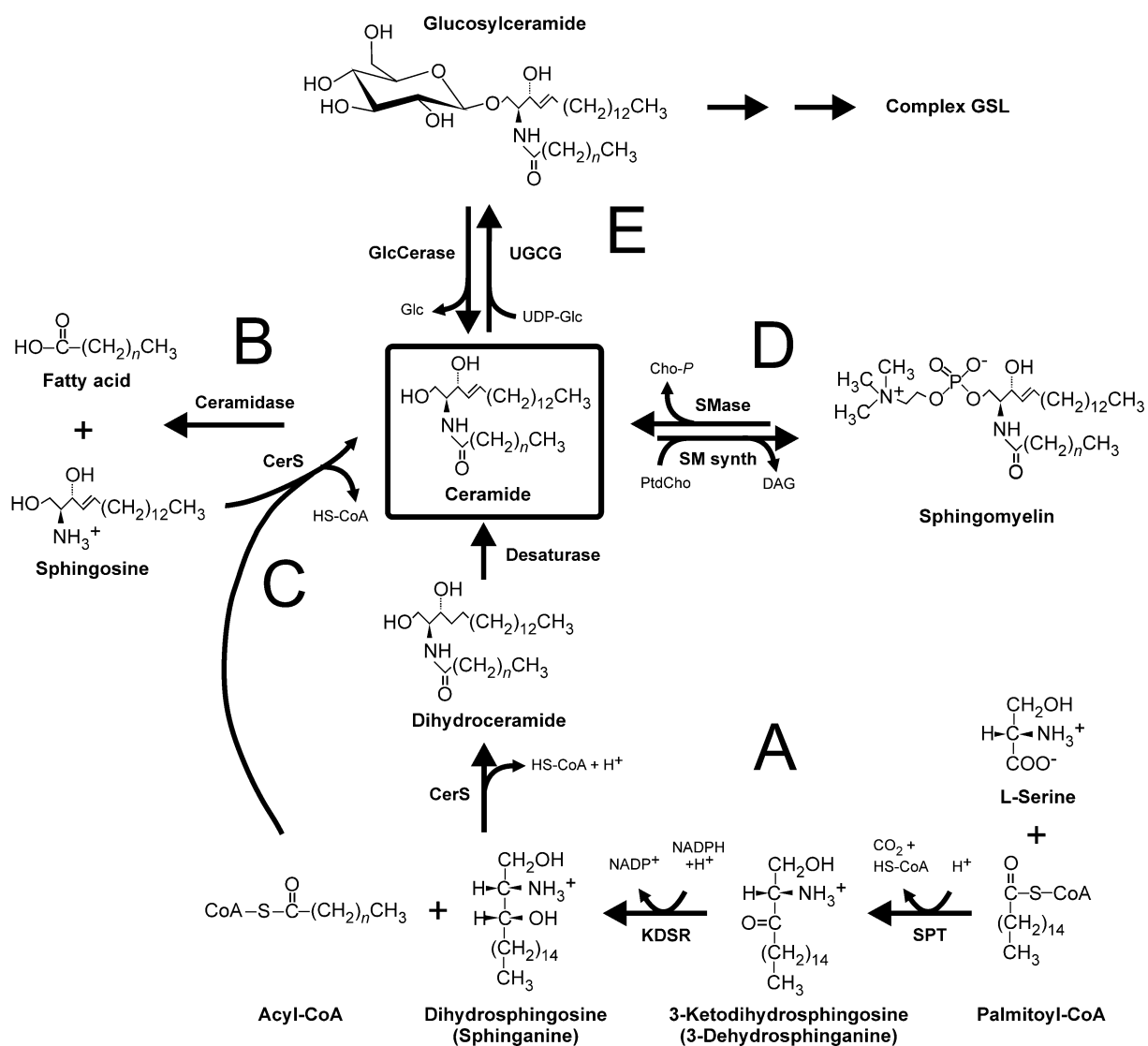
Figure 2. *De novo* **ceramide synthesis, recycling and processing to higher SLs.**

(**A**) *De novo* ceramide synthesis begins with the condensation of L-serine and palmitoyl-CoA catalyzed by serine palmitoyltransferase (SPT). The product 3-keto-dihydrosphingosine is reduced to dihydrosphingosine (sphinganine) via 3-ketodihydrosphingosine reductase (KDSR) and acylated by a ceramide synthase (CerS) to give dihydroceramide and finally ceramide via a desaturase. Ceramide can be degraded by a ceramidase (**B**) to give sphingosine and a fatty acid. Sphingosine can be recycled (**C**) for ceramide formation in a CerS reaction. Ceramide serves as a precursor for more complex SLs such as sphingomyelin (**D**), glucosylceramide (**E**) or higher glycosphingolipids (GSLs).

In contrast to the Cer processing described above, SM synthesis takes place at the luminal side of the Golgi (Jeckel et al., 1992) and requires that the ceramide transport protein (CERT) transfers Cer (with

acyl chain-lengths of C16-C20) from the ER to the Golgi (Hanada, 2006). Within the so-called SM cycle, Cer is converted into SM in a reaction catalyzed by SM synthase in which phosphatidylcholine (PtdCho) is utilized to transfer phosphocholine (Cho-*P*) to the C1 position of the Cer backbone with release of a diacylglycerol (DAG) moiety. Cer can be recycled from SM by the action of a sphingomyelinase with release of Cho-*P* (Geilen et al., 1997). In response to extracellular stimuli (e.g., TNFα, IL-1, endotoxin), Cer can also be synthesized from PM-derived SM (Levade et al., 1999).

In general, for GSL synthesis, Cer is shuttled from the ER by vesicle transport to the cytosolic face of the Golgi (Jeckel et al., 1992), except for galactosylceramide (GalCer) formation (Sprong et al., 1998). One of the key enzymes of GSL formation, glucosylceramide synthase (UDP-glucose:ceramide glucosyltransferase (UGCG); EC 2.4.1.80), is a transmembrane protein which transfers glucose from UDP-Glc to the sphingoid C1 of the Cer backbone, generating glucosylceramide (GlcCer) (Figure 2) (Jeckel et al., 1992). Higher GSLs are formed at the luminal side of the Golgi by enzymatic addition of further monosaccharides, sulfatides or neuraminic acid to give glucocerebrosides (e.g., Gb3, Gb4), sulfatides (e.g., SM4) or gangliosides (e.g., GM1, GM3), respectively. The majority of these GSLs contain GlcCer as a core structure. Only a few, the so-called galactocerebrosides, are derived from GalCer. Two major groups of GSLs can be distinguished by chromatography: neutral GSLs (nGSL) typically contain unsubstituted, uncharged carbohydrates (such as in Gb3 and Gb4); acidic GSLs (aGSL) contain carbohydrates with carboxyl, sulfate, or phosphate groups attached (such as in SM4, GM1 or GM3). After synthesis, complex GSLs either move via vesicular transport to the PM, where they are incorporated, or metabolized to give Cer and bioactive metabolites (Bartke and Hannun, 2009).

1.3   Epidermal Sphingolipids

1.3.1   Distinction between LC-, VLC- and ULC- sphingolipids

Whereas the mammalian PM primarily contains saturated long-chain (LC) and very-long-chain (VLC) FAs with 16 to 24 carbon atoms, the epidermis expresses not only LC- (C16-C20) and VLC-FAs (C22–C26) but also a unique diversity of Cers with ultra-long-chain (ULC) acyl FA moieties with 28 to 36 carbon atoms (Figure 3). The lower epidermal layers contain higher amounts of LC and VLC Cers, localized in the nucleus, mitochondria, Golgi or PM (Uchida and Hamanaka, 2006). In contrast, barrier lipid synthesis becomes more important in the higher differentiated epidermis layers, whereby LC-, VLC-, or mainly ULC-FAs are incorporated into the Cers and localized in compartments such as trans-Golgi network, LBs, CE, or within corneocyte interstices (Vielhaber et al., 2001). The acylated FA chains in ULC-Cers may be saturated or mono-unsaturated and are essential for epidermal barrier function (Jennemann et al., 2012b). To a great extent, ULC-FA moieties are hydroxylated either at α or ω position. Furthermore, an ω-hydroxy group of a ULC-SL can be esterified to an additional FA, predominantly to linoleic acid (C18:2, ω–6) or to a protein sidechain on corneocytes to establish the CLE, a prerequisite for epidermal barrier formation (Figure 3) (Uchida and Hamanaka, 2006).

1.3.2   Major classes of epidermal ceramides

In addition to cholesterol and free FAs, Cers are the major lipid class comprising almost half of the total SC lipid mass by weight (Hamanaka et al., 2002; Weerheim and Ponec, 2001). Twelve major Cer subclasses have been identified in human SC , which differ in the sphingoid backbone (i.e., sphingosine, phytosphingosine (4-hydroxysphinganine) or 6-hydroxysphingosine with C18 or C20 chain length) as well as in the amide-linked FA moiety (Uchida and Hamanaka, 2006). Altogether, more than 340 different Cer species in the SC have been described (Masukawa et al., 2008).
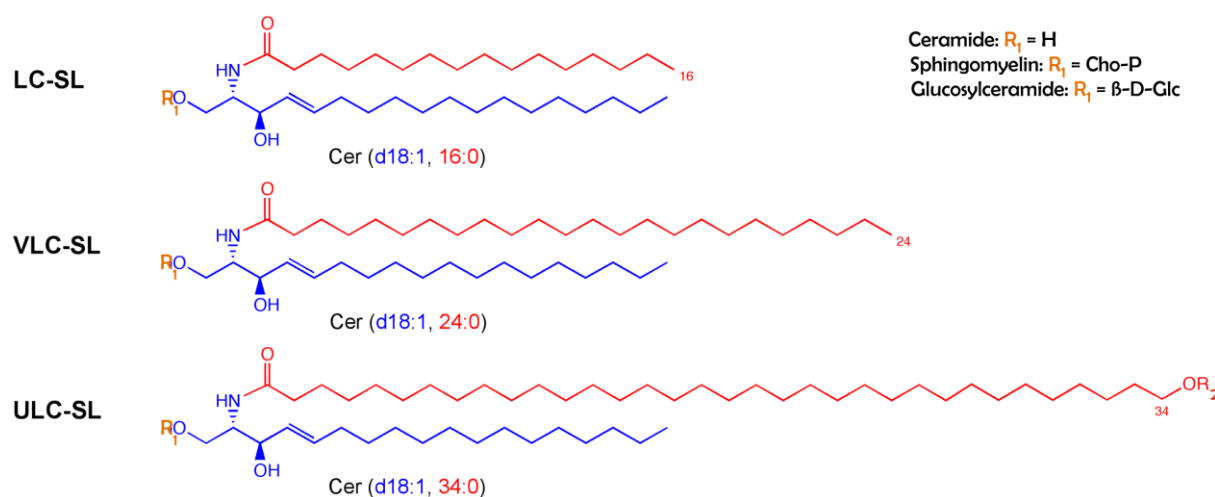
Figure 3.   Acyl FA chain length in sphingolipids.

Plasma membrane sphingolipids (SLs) typically contain FAs with chain lengths of C16 (palmitic) to C24 (nervonic) (red) amide-linked to the sphingoid base (blue) and are designated here as long-chain (LC-) and very-long-chain (VLC-) SLs. The sphingolipid class is determined by the head group R1. However, in the epidermis differentiated keratinocytes produce SLs with ultra-long-chain (ULC-) FAs with 32 to 36 carbons, which may be hydroxylated in the terminal ω position. The ω-hydroxyl group may be esterified to an additional FA, typically linoleic acid (C18:2, ω–6), designated here as R_2. The ULC-SL depicted here contains C34:0 geddic acid, which is the most abundant ULC-FA in epidermal ω-hydroxylated Cers. *Modified from* (Rabionet 2011).

SC Cers derived from sphingosine can be classified according to the characteristics of their FA residue. As shown in Figure 4, a commonly used scheme distinguishes between nonhydroxylated FAs (NS), α-hydroxy FAs (AS), and ω-hydroxy FAs (OS), which, in turn, may be esterified to a protein amino acid sidechain (POS) or to an FA (EOS), typially Lin.

More than 62% of SC Cers are hydroxylated (subclasses AS, OS, EOS, POS) (Hamanaka et al., 2002). AS- and minor NS-Cers are typically linked to saturated FAs with 16 to 26 carbon atoms, but do not contain ULC-FAs (Coderch et al., 2003). Hydroxylated Cers with acyl FA moieties longer than C26 are primarily ω-hydroxylated (OS) and can be esterified to FAs (EOS) or to proteins on corneocytes (POS), thereby establishing the CLE, a prerequisite for epidermal barrier function. In Gaucher's disease and related mouse models, loss of OS-type Cers, particularly POS, coincides with severe

epidermal barrier defects (Doering et al., 1999b), indicating the significance of these Cers for barrier function (Jennemann et al., 2012b).
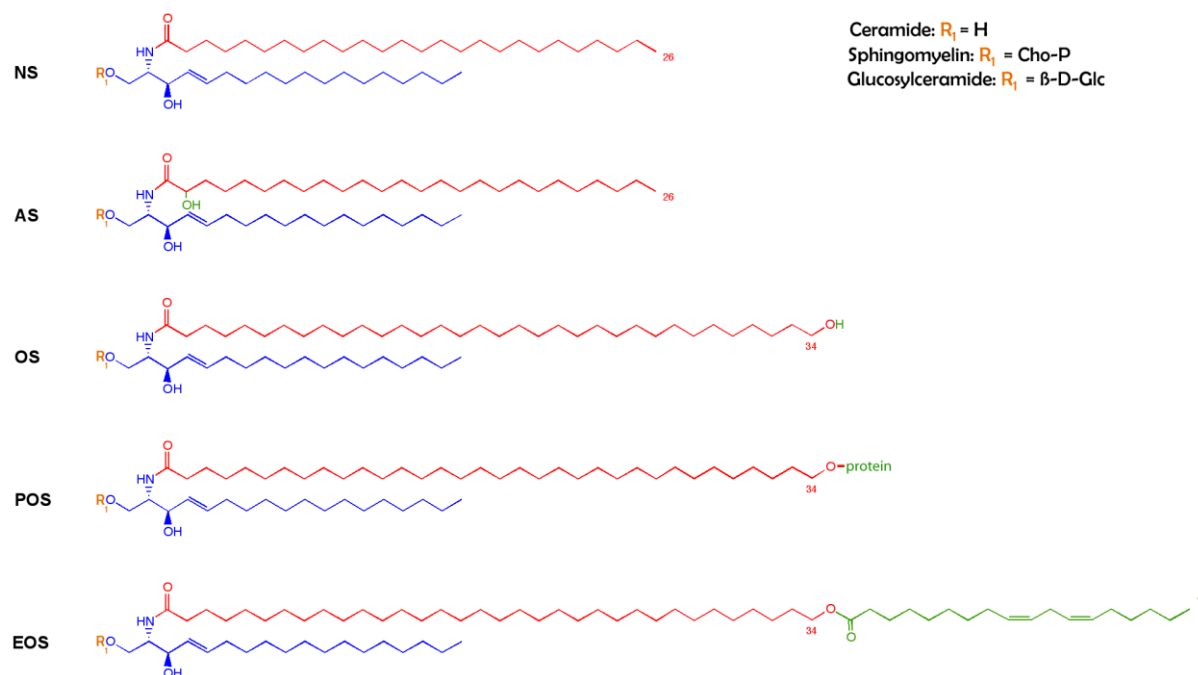
Figure 4.   Major epidermal ceramide subclasses distinguished by acyl FA chain length and hydroxylation.

In keratinocyte-produced ceramides the amide-linked FA residues with chain lengths of C16 (palmitic) to C26 (cerotic) are typically nonhydroxylated (NS) or α-hydroxylated (AS). The ceramides with FA chain lengths of C32 (lacceroic) to C36 (hexatriacontylic)) generally carry an ω-hydroxy group (OS), which may be esterified to a protein sidechain (POS) or the unsaturated FA Lin (EOS). *Modified from* (Rabionet 2011).

EOS-Cers are the most prominent Cer class in the epidermis. In human epidermis ca. 95% of the ω-linked FAs are Lin, but only 45% in mouse epidermis (Uchida and Hamanaka, 2006). Altered epidermal lipid composition has been observed in essential fatty acid deficiency (EFAD), where Lin (C18:2, ω–6) in EOS-Cers was replaced by oleic acid (Ole: C18:1, ω–9), leading to abnormal lamellar formation and leakiness of the epidermal permeability barrier (Hou et al., 1991; Melton et al., 1987).

Most epidermal Cers are believed to derive from the corresponding GlcCer classes, serving as essential precursors for epidermal barrier formation, except for Cer2 (NS) and Cer5 (AS), deriving from SMs (Hamanaka et al., 2002; Uchida et al., 2000).

1.4   The Epidermis

The skin consists of an outer squamous epithelium (epidermis and hair follicles) and an insulating mesenchymal compartment (dermis and dermal papilla) connected via a basement membrane. The dermis is mainly composed of fibroblasts and fibroblast-derived proteins of the extracellular matrix (ECM) such as collagen, elastin and glycosaminoglycans, which confer the skin with tensile strength and elasticity. The dermis provides nourishment for the lower epidermal layers via dermal papillae. The primary function of the epidermis is to maintain the skin barrier and protect the body from environmental stressors such as pathogen invasion, mechanical insult and desiccation. The epidermis synthesizes a unique pattern of various long-chain FA-containing SLs, which, together with specific junction proteins (such as claudins), allow for the formation of a competent barrier confined to the outermost epidermal layer.

1.4.1   Epidermis structure and keratinocyte differentiation

The epidermis is a self-renewing, cornifying epithelium composed of different strata. Keratinocytes, which comprise ca. 95% of all epidermal cells, derive from stem cells in the lower basal layer (Watt, 2002b). Minor components include melanocytes, Langerhan's cells, Merkel cells and lymphocytes. In the stratum basale (SB), proliferating keratinocytes exit the cell cycle and undergo several stages of differentiation while migrating upwards through the epidermal strata, i.e., stratum spinosum (SS), stratum granulosum (SG) and stratum corneum (SC) (Figure 5). Upon terminal differentiation the cells become dead, flattened corneocytes of the SC and finally shed off during desquamation (Candi et al., 2005), a repetitive process with a period of 6 to 7 weeks in humans (Halprin, 1972) and 8 to 10 days in mouse skin (Ghazizadeh and Taichman, 2001; Potten et al., 1987).

At each stage of differentiation keratinocytes change their cytoskeletal structure and composition, expressing distinct sets of structural proteins, of which the most prominent are keratin intermediate filaments. In basal keratinocytes, the cytoskeleton is composed of keratin K5 and K14, as well as of microtubular and microfilamentous proteins. Via transmembrane receptors (e.g., integrins) basal keratinocytes are anchored to adhesive proteins of the underlying basement membrane (e.g., laminins), thereby regulating epidermal homeostasis (Watt, 2002a). When keratinocytes leave the SB, proliferation ceases and differentiation begins with the expression of keratins K1 and K10 in the SS. At this stage the keratinocytes are attached by stabilizing desmosomal junctions which serve as important adhesion sites for structural proteins. Late SS keratinocytes synthesize epidermal-specific lipids and early structural proteins such as involucrin (IVL) and transglutaminases (TG), as required for the cornified envelope (CE). With further keratinocyte maturation, a more granular-like pattern develops, and the cells become keratinocytes of the SG. These granular cells contain high amounts of keratohyalin granules (KG) storing profilaggrin (proFLG) and loricrin (LOR), important structural proteins for cornification. SG keratinocytes eventually enter terminal differentiation, initiated by filaggrin-assisted keratin condensation, and extrude their cellular contents, becoming anucleate corneocytes of the SC.
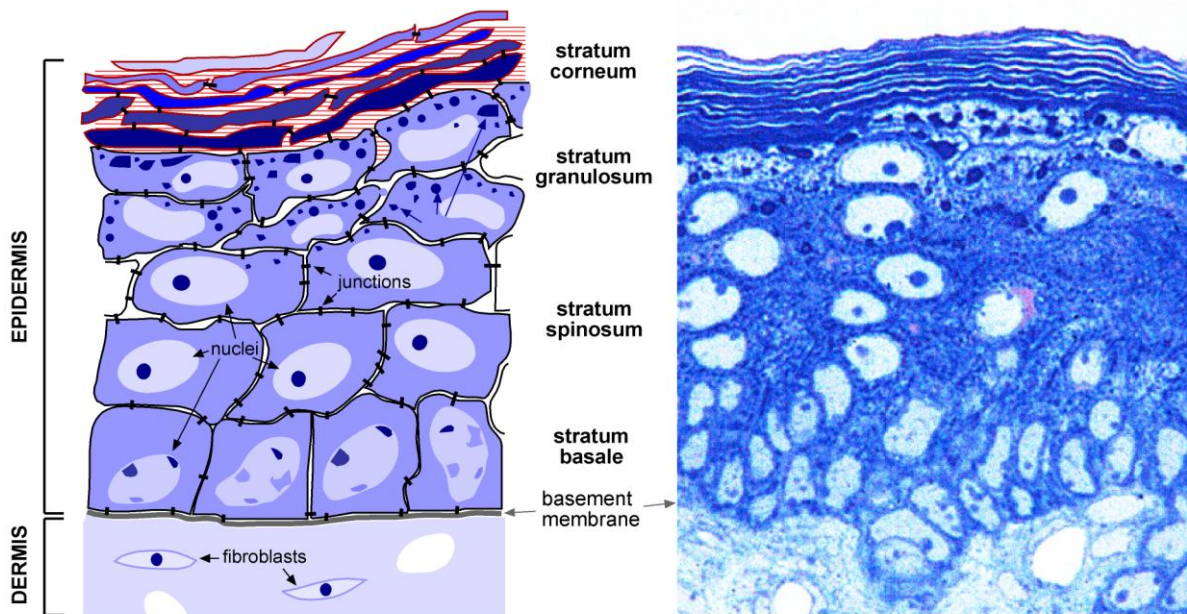
Figure 5. **Epidermis structure: schematic view and microscopy of neonatal mouse skin.**

Left panel: schematic diagram of the epidermis, a squamous epithelium composed of different strata. Keratinocytes in the stratum basale proliferate and eventually enter several steps of differentiation, passing through the epidermal layers (stratum spinosum and stratum granulosum) to terminally differentiate into the dead flattened cells (corneocytes) of the stratum corneum. The corneocytes are surrounded by lipid lamellae (indicated in red) and finally shed off during desquamation. **Right panel**: light microscopy of cross section of neonatal mouse skin stained with PAS-methylene blue-Azure II. *Taken from* (Rabionet 2011).

Upon onset of this cornification process, the corneocyte PM is gradually replaced by a scaffold of cross-linked structural proteins such as IVL and LOR with envoplakin (EVPL) and small proline-rich proteins (SPRRs) bound to lipids. The result is an insoluble, rigid CE, which is a prerequisite for epidermal barrier function (Candi et al., 2005).

In parallel, lipid synthesis increases in SG keratinocytes, forming small secretory organelles, so-called lamellar bodies (LBs), which deliver lipids (SLs, phospholipids, cholesterolester), catalytic enzymes and antimicrobial peptides to the apical PM. The content of the LBs is externalized by exocytosis in the upper SG and at the SG/SC interface (Jennemann et al., 2012b). Extracellular lipids are enzymatically processed and form intercellular lipid lamellae or are covalently bound to proteins of the CE, forming the cornified lipid envelope (CLE) as the first barrier against epidermal water loss (Nemes et al., 1999; Sandhoff, 2009). This barrier demands permanent renewal of the outer cornified layer, which is achieved by steady, highly regulated corneocyte shedding (desquamation).

The integrity of the epidermis is supported by cell-cell junctions, i.e., tight junctions, adherens junctions and desmosomes. Tight junctions (TJs, zonula occludens) are expressed in the more differentiated layers of the epidermis and have been shown to built up a potent barrier against epidermal water loss (Furuse et al., 2002). They form so-called "kissing-points" to neighboring cells,

sealing off the paracellular pathway. Typical epidermal TJ proteins are claudins (e.g., CLDN1) or tight-junction proteins (e.g., TJP1).

Adherens junctions (AJs) are created by multifunctional adhesive proteins (e.g., AJAP1) which interconnect the cytoskeleton of neighboring cells, thereby ensuring keratinocyte cohesion. Furthermore, AJs create transcellular networks, thus regulating cytoskeletal remodeling and cell polarity (reviewed by (Brandner et al., 2010)). AJs are composed of cytoplasmic actin-associated plaque proteins called catenins (CTNNn), e.g., β-catenin (CTNNB1) and calcium-sensitive transmembrane proteins, the cadherins (CDHn), such as E-cadherin (CDH1) and P-cadherin (CDH3).

The most characteristic epidermal junctions are desmosomes with a structure similar to that of the adherens junctions. Desmosomes function as "mechanical junctions" connecting the keratin cytoskeleton via catenins (e.g., plakoglobin (JUP), desmoplakin (DSP)) and transmembranous cadherins, such as the desmogleins (DSGn) and desmocollins (DSCn), to neighboring cells or to the ECM (in the form of hemidesmosomes). At the onset of terminal differentiation, desmosomes serve as templates for more specialized junctions in the SC, the corneodesmosomes. In the lower SC layers the latter are regularly expressed on corneocytes as integral compounds of the CE. In contrast to the desmosomes of the viable epidermal layers, corneodesmosomes contain a keratin-fused plaque protein on the inner cell side which is bound predominantly to the SC-unique corneodesmosin (CDSN) or to other cadherins (e.g., desmoglein 1 or desmocollin 1). Controlled proteolytic degradation of corneodesmosomes by LB-derived proteases (e.g., kallikreins of the KLK family) is a key factor for normal desquamation (Ishida-Yamamoto and Kishibe, 2011). Changes in protease (inhibitor) activities, calcium concentration, or SC pH and hydration can impair the regular desquamatory process and result in hyperkeratosis (ichthyosis) and other skin pathologies (Ishida-Yamamoto and Kishibe, 2011).

1.4.2   Epidermal barrier formation

The epidermal (permeability) barrier (Figure 6, left panel) is confined to tight junctions in the granular layer, controlling paracellular transport (Furuse et al., 2002; Kirschner et al., 2010), and to the lipids and lipid-embedded corneocytes in the SC layer, providing a hydrophobic water-proof sheath (Elias, 2005). The lipid matrix is composed of Cers, cholesterol and free FAs accounting, respectively, for 50%, 25% and 15% of the total lipid mass in human SC (Wertz, 2006). Minor components of this barrier are cholesterol-sulfate (2-5% ww), which regulates protease activity during desquamation (Elias et al., 1984; Sato et al., 1998), and free sphingoid bases, important lipids for microbial defense (Bibel et al., 1992). Desquamation is a highly regulated process and ensures the sequential renewal of the outer epidermal layers.

Lipid barrier formation begins with Cer formation at the ER in keratinocytes (Figure 6, right panel). Elongation of the FA moiety in Cers is carried out by a group of ELOVL enzymes (elongation of very-long-chain fatty acyl-CoA), of which ELOVL4 is decisive for the synthesis of OS-type Cers. The significance of this enzyme for the epidermal water permeability barrier (WPB) is supported by the

observation that ELOVL4 –/– mice die shortly after birth due to barrier loss (Cameron et al., 2007; Li et al., 2007).

Ceramide synthases (CerS), encoded by tissue-specific longevity assurance genes (*Lass*), catalyze the condensation of an FA with a sphingoid base. Among the CerS family (comprising CerS1 to CerS6), CerS3 has been identified to specifically use VLC/ULC-FAs to synthesize VLC/ULC-Cers in testes and epidermis (Jennemann et al., 2012b). Deletion of this enzyme caused premature death of newborn mice due to the lack of ULC-Cers and the deficiency in epidermal barrier formation.
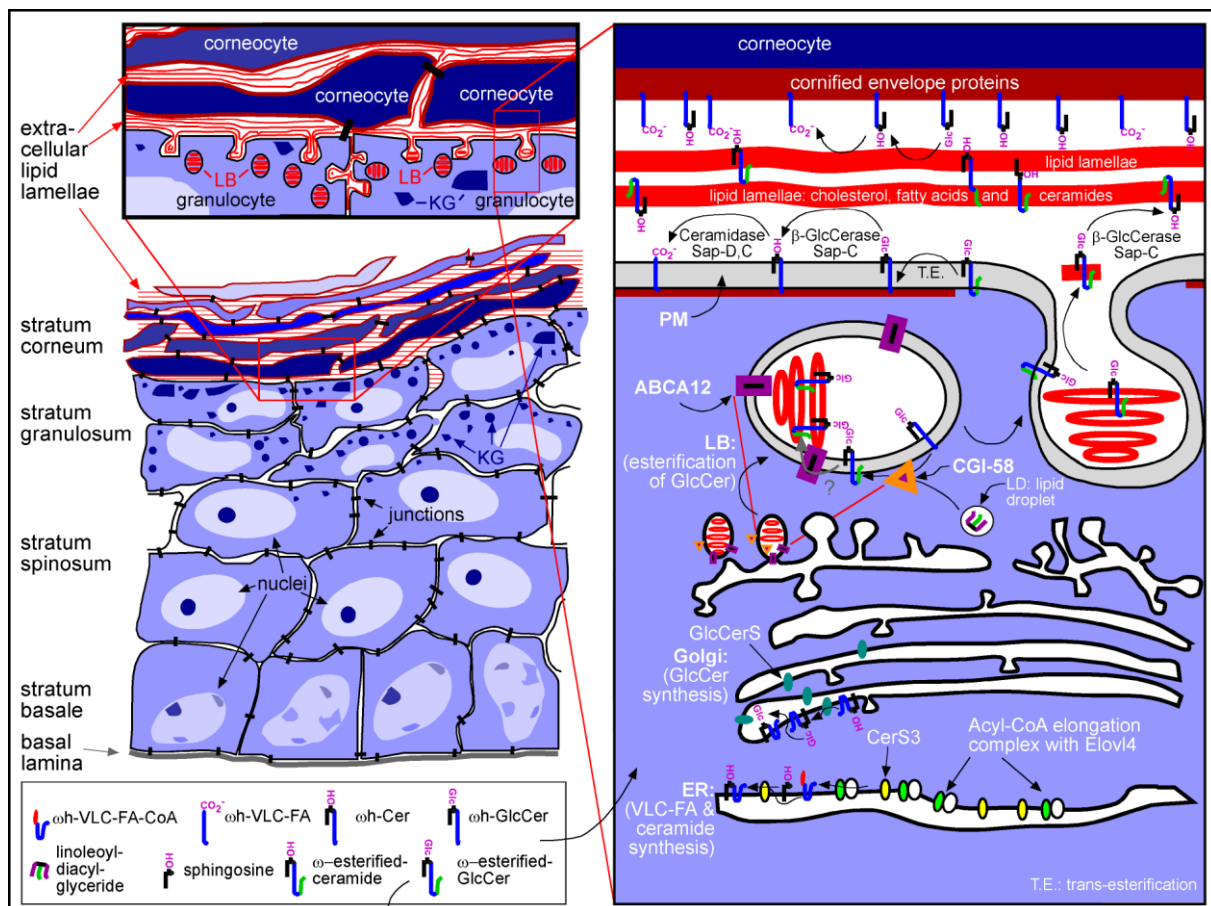
Figure 6.   Epidermal glycosphingolipid synthesis and barrier formation.

Barrier formation takes place at the interface of SG and SC (left panel, top). In the epidermis lipids accumulate with increasing differentiation. Much of the accumulating lipids is packed in lamellar bodies (LBs). The latter export their content by exocytosis near the apical boundary to the SG into the extracellular space, where hydrolytic enzymes act on the lipids to produce Cers, free FAs and cholesterol, the three major barrier lipids. Trans-esterification (T.E.) leads to protein-linked Cers and GlcCers. Unlinked Cers, cholesterol and free FAs form lipid lamellar sheets, thereby sealing the corneocyte interstices and completing lipid barrier formation. *From* (Sandhoff, 2009).

The next important step in barrier formation is the transient formation of glucosylated Cer precursors (GlcCers) by the action of glucosylceramide synthase (UGCG). Constitutive deletion of the *Ugcg* gene causes prenatal death of mice and implies an essential role for GSLs in embryonic development (Ichikawa et al., 1998).

Further processing and transport of precursor lipids (GlcCers and SMs) to the apical PM involves small secretory granules, the LBs (Figure 6 right panel). These oval-shaped organelles consist of a unit-bounding membrane surrounding one or several stacks of lipid lamellar discs. Lamellar arrangement of OS/EOS-GlcCers within LBs is supported by the ATP-binding cassette transporter ABCA12. Loss-of-function mutations in the gene encoding for ABCA12 have been described for lamellar ichthyosis type II (LI2) as well as harlequin ichthyosis (HI), both severe autosomal recessive congenital ichthyoses (ARCI), characterized by hyperkeratosis and permeability barrier loss. Ichthyotic lesions revealed an accumulation of EOS-GlcCers, whereas EOS-Cers were significantly reduced (Zuo et al., 2008).

Within the LBs, ULC-GlcCers are believed to become ω-O-acylated, predominantly with Lin, by the action of CGI-58, a lipid droplet-associated acyl transferase (Akiyama et al., 2008). Mutations in CGI-58 are related to the neutral lipid storage disease called Dorfman-Chanarian syndrome. In addition to systemic accumulation of triglycerides, patients develop an ichthyosis-like skin phenotype, indicating the importance of regular lipid processing for epidermal barrier homeostasis (Akiyama et al., 2003; Demerjian et al., 2006).

As barrier formation proceeds, LBs fuse with the apical PM in the upper SG and at the SG/SC interface to exocytose into the extracellular space their content: structural proteins (e.g., corneodesmosin), enzymes (e.g., TG, neutral lipase, GlcCerase, acid SMase), and antimicrobial peptides (e.g., cathelicidine, β-defensin) (Bouwstra et al., 2003; Elias et al., 2006; Madison, 2003). Upon transesterification, GlcCers and SMs are converted back into their corresponding Cers by the action of GlcCerase and acid SMase. Furthermore, FAs, glycerol and cholesterol are released (from phospholipids and cholesterol esters, respectively) by secretory phospholipase A$_2$ (sPLA2) and cholesterol sulfatase. These components, together with Cers (OS, EOS), establish the extremely hydrophobic extracellular lipid lamellae of the skin barrier (Candi et al., 2005). Mutation or loss of function of the enzymes involved results in severe skin barrier defects (Doering et al., 1999b; Elias et al., 1984; McGovern and Schuchman, 1993). For instance, in Gaucher's disease, depletion of GlcCerase or its activator protein prosaposin (PSAP) inhibits Cer formation from GlcCer precursors leading to impaired lipid lamellar membranes and subsequent WPB loss (Doering et al., 1999b).

In the SC/SG interface, transglutaminase 1 (TG1) catalyzes the ω-esterification of ULC-Cers to glutamine-glutamate rich regions of CE proteins (e.g. involucrin, loricrin, envoplakin (EVPL), periplakin (PPL)), establishing the CLE (Nemes et al., 1999) (Doering et al., 1999a; Jennemann et al., 2012b; Marekov and Steinert, 1998). Deletion of TG1 causes lamellar ichthyosis type I (LI1) , marked by clefts in the SC interstices and increased transepidermal water loss (TEWL) (Elias et al., 2002).

Specific SLs (e.g. sphingosine) also serve in antimicrobial defense. They are synthesized in the epidermis and carried to the surface as cells differentiate or are secreted from sebaceous glands onto the skin surface (Drake et al., 2008).

1.4.3   Stratum corneum pH

Under normal physiologic conditions, the SC pH of human epidermis ranges from pH 6.8 in the lower up to pH 4.5 in the uppermost SC layer, forming the so-called acid mantle of the skin. The pH gradient is maintained by acidic microdomains dispersed across the SC, which contain free FAs, protons (secreted from keratinocytes via the Na^+/H^+ antiporter SLC9A1 (formerly NHE1) and trans-urocanic acid (tUCA), the endproduct of the FLG metabolic pathway. Further contributors to the acidic pH can be lactate from sweat or microbial products (Fluhr and Elias, 2002).

The SC pH is imperative for epidermal barrier homeostasis and regulates four key functions of the SC: (1) lipid processing (and thereby WPB formation), (2) antimicrobial defense, (3) cohesion and (4) desquamation. Whereas the extracellular ion concentration (Ca^{2+}, K^+) affects LB secretion, the pH determines the activity of LB-derived hydrolases and proteases such as GlcCerase and acid SMase (with its acidic pH optimum) as well as sPLA2, steroid sulfatase or the KLKs with neutral pH optimum.

Elevation of the SC pH is fatal for skin barrier function since activated proteases such as KLKs accelerate CD degradation, thereby leading to impaired SC cohesion. A neutral pH has been observed in most skin disorders such as ichthyosis, psoriasis and atopic dermatitis (AD), and can aggravate their associated pathophysiologies (Fluhr and Elias, 2002).

1.5   Loss of Barrier Function

The important role of lipids, in particular of Cers, in skin barrier function has been determined from *in vivo* and *in vitro* studies of cutaneous disorders such as ichthyosis, lysosomal storage diseases, psoriasis and AD. These diseases may result from environmental factors such as allergens and irritants (UV radiation, detergents, carcinogenic agents, and stress) or are based on genetic defects affecting proteins of the lipid metabolic pathways.

Ichthyosis (the so-called fish scale disorder) comprises a heterogeneous family of dry hyperkeratotic skin disorders but may also be a symptom of more systemic diseases such as lysosomal storage diseases (e.g., Gaucher's disease or Niemann-Pick disease) (Doering et al., 1999b; McGovern and Schuchman, 1993). Niemann-Pick disease has been related to mutations in the *SMPD1* gene for acid SMase, leading to loss of Cers and subsequent leakiness of the WPB and ichthyotic skin lesions (McGovern and Schuchman, 1993). Similar barrier disruption has been described in Gaucher's disease, in which a defect in the GlcCerase enzyme eliminated the GlcCers degradation pathway, resulting in loss of Cers, in particular POS-Cers and permability barrier breakdown (Doering et al., 1999b).

Congenital ichthyosis (CI) represents a heterogenous group of skin disorders with deficits in Cer and FA processing, leading to epidermal WPB loss. Mutation in the genes encoding for the ABCA12 transporter or lipoxygenases (12R-LOX, eLOX3) were identified as further predisposing factors for the development of ichthyosis (Akiyama et al., 2005; Jobard et al., 2002). Moreover, deletion of the steroid sulfatase represents a putative risk factor for X-linked recessive ichthyosis (XRI), characterized by severe defects in desquamation (Elias et al., 1984).

Psoriasis is a complex inflammatory skin disease of unknown etiology, which may derive from genetic (e.g., FLG gene mutation), infectious or environmental (e.g., stress) factors. Psoriatic lesions are characterized by a thickened dry scaling skin and basal inflammation. The overall reduction of Cers in some psoriatic patients has been related to a decrease in SPT activity and reduced *de novo* Cer synthesis (Hong et al., 2007). Moreover, AD is a chronic relapsing inflammatory skin disorder, also of unknown etiology. For long time, AD was regarded as an immune-mediated disease until FLG gene mutations leading to disturbed barrier function were shown to be associated with atopy in some populations (Palmer et al., 2006). Patients suffering from AD display dry, itchy skin with inflammatory rashes, and have a high risk for bacterial or viral infections, about fourfold higher than in psoriasis (Elias, 2005). In both diseases, depletion of POS-Cers and an impaired lamellar organization were considered to be responsible for the subsequent WPB breakdown (Macheleidt et al., 2002). However, in skin, a potent regulator of lipid biosynthesis is the epidermis itself, as indicated by an increase in synthesis of major SC lipids (Cer, FA and cholesterol) upon barrier disruption (e.g., induced by wounding) (Holleran et al., 1991).

The importance of (Glc)Cers in permeability barrier function has been demonstrated by the variety of cutaneous disorders which display alterations in (Glc)Cer composition (see above). Furthermore, the function of GlcCers in the esophageal permeability barrier has been recognized (Diaz-Del Consuelo et al., 2005). GlcCers comprise about 16% of the total esophageal lipid content (by weight) in contast to only 1% for Cers. The generally higher content in polar lipids (phospholipids, cholesterol, GlcCers) of nonkeratinized or partially keratinized epithelia confers a higher permeability to these tissues (Wertz et al., 1986). Most of what is known about the esophageal barrier properties has been determined in the context of gastroesophageal reflux disease (GERD) (Katz et al., 2013) and from whole-organ permeability studies *in vitro* (Diaz-Del Consuelo et al., 2005). In particular the distal (abdominal) part of the esophageal duct is prone to mucosal damage by gastric acids, as observed in clinical reflux esophagitis or Barrett esophagus (Yang et al., 2012). Therefore, the esophagus relies on a functional barrier comprising a layer of mucus and unstirred water, surface bicarbonate (HCO_3^-), junction proteins and, in particular, lipids (Diaz-Del Consuelo et al., 2005).

1.6   Wound Healing

Cutaneous injury, specifically skin wounds, trigger a series of epidermal defense and homeostatic mechanisms to repair the skin barrier. These complex mechanisms can be divided into three overlapping phases: (1) inflammation, (2) tissue formation (granulation tissue formation and reepithelialization) and (3) tissue remodeling.

Clot formation and a burst of proinflammatory cytokines released by platelets and polymorphonuclear leukocytes (PMNL) mark the onset of the inflammatory phase. In addition, injured keratinocytes release a preformed pool of cytokines (e.g., interleukins IL-1α, IL-1β, IL-6; TNFα), activating epidermis-specific Langerhan's cells, dermal dendritic cells (DDCs) and fibroblasts (Eming et al., 2007; Wang et al., 2004; Wood et al., 1992). Infiltration of peripheral leukocytes occurs a few hours after wounding. However, the mast cell and neutrophil response normally ceases within 48 h post injury.

In addition to the resident cells, more macrophages migrate to the wound site within two days after injury, assisting in phagocytosis and promoting tissue formation via synthesis of growth factors, e.g., transforming growth factors (TGF-α, TGF-β), basic fibroblast growth factor (bFGF or FGF2). Cells of the adaptive immune system, in particular T-lymphocytes, arrive in the later tissue remodeling phase and modulate the inflammatory response. However, a subpopulation of T-lymphocytes, called γδT-cells, has been identified as dendritic epidermal T-cells (DETCs), which enhance tissue repair (Jameson et al., 2002).

Furthermore, barrier loss provokes enhanced LB secretion (triggered by Ca^{2+} efflux), and enhances lipid processing, as indicated by increased activity of enzymes such as SPT, GlcCerase, neutral SMase, cholesterol sulfatase, HMG-CoA reductase and FA synthase (reviewed by (Feingold, 2007)). The primary goal of the enhanced lipid trafficking is to restore the epidermal permeability barrier. Moreover, barrier disruption and the subsequent boost in lipid synthesis demand an increase in lipid transporters (e.g., fatty acid binding protein 5 (FABP5), cellular retinoic acid binding proteins (CRABP)) (Ogawa et al., 2011) and induces lipid-responsive transcriptions factors (e.g., PPARβ/δ), promoting keratinocyte proliferation, migration and advanced wound healing (Di-Poi et al., 2003; Schmuth et al., 2004; Tan et al., 2007).

The decisive factors for final wound closure and restoration of a competent barrier are (1) reepithelialization and (2) keratinocyte differentiation (Raja et al., 2007). Reepithelialization depends critically on migration of keratinocytes, which, upon injury, are derived initially from hair follicle stem cells and at a later stage of wound healing from stem cells of the basal epidermal layer (Ito et al., 2005).

1.7   Hypothesis and Aim

Permeability barrier formation critically depends on epidermal Cers containing ULC-FAs (C28 to C36) with a unique ω-hydroxyl group. Cers are believed to derive from glucosylated intermediates, GlcCers, as surmised from human Gaucher's disease and related mouse models. In turn, GlcCers are synthesized from Cers by the glucosylceramide synthase (UGCG) reaction and are major precursors for all higher GSLs. However, in the epidermis GSL synthesis stops at the level of GlcCer. Therefore, we chose the skin as an ideal tissue model to test the hypothesis that GlcCers are important regulators in epithelial differentiation.

In an earlier study using mice with constitutive *Ugcg* gene deletion in the epidermis ($Ugcg^{f/f\,K14Cre}$ mice), we found that newborn mice died at postnatal day P5 due to dehydration upon WPB loss, thus demonstrating the importance of Cer-glucosylation in epidermal barrier development. Complete loss of GlcCers and accumulation of the corresponding Cers was observed together with distorted LBs. Surprisingly, POS-Cers were not altered, which might be explained by the early death of mice before the completion of one cycle of epidermal renewal (Jennemann et al., 2007). Therefore, inducible UGCG-deficient mice ($Ugcg^{f/f\,K14CreERT2}$ mutants) have been generated in our department to circumvent early death.

In the present thesis project, a TAM-inducible model of the endogenous *Ugcg* gene deletion in K14-positive cells allowed for the investigation of the role of GlcCers in adult epidermis. This *in vivo* model provides insight into the specific function of GlcCers and Cers in keratinocyte differentiation and further highlights important steps of Cer-processing during epidermal barrier formation. In addition, the function of GlcCer-deficient epidermis in relation to clinically relevant pathophysiologic states, i.e., wound healing, will be examined.

In the context of epithelial barrier function the Discussion will emphasize the relevance of the acquired data with regard to human skin diseases and propose a potential mechanism of Cer action in stages of impaired barrier homeostasis (e.g., dermatoses, gastroesophageal diseases). **This work aims to further clarifiy the pathophysiology of such diseases.**

2. Materials und Methods

2.1 Materials

2.1.1 Chemicals

Standard laboratory chemicals and reagents used for routine analyses in this study were purchased from Sigma-Aldrich (Deisenhofen), Merck (Darmstadt), Life Technologies (Darmstadt), Roche (Mannheim), Carl Roth (Karlsruhe), and Fluka (Neu-Ulm). Tamoxifen and sunflower seed oil were from Sigma-Aldrich (Deisenhofen).

All other chemicals were obtained as indicated in the corresponding method section.

2.1.2 Buffers and solutions

All buffers and solutions were prepared with either *Aqua ad injectabilia* (Braun) or doubly distilled (dd) autoclaved water. Buffers and components are listed in the following Tables (see footnotes at end of Tables).

Buffers for Genotyping	
TAE buffer (50x) 2 M Tris/AcOH, pH 8.0 0.1 M EDTA	**NID buffer** 10 mM Tris/HCl, pH 8.3 50 mM KCl 2.5 mM $MgCl_2$ 0.01% w/v Gelatin 0.45% v/v IGEPAL CA-630 0.45% v/v Tween-20
Xylene cyanol loading buffer (10x) 20 mM Tris/HCl, pH 7.5 0.001% xylene cyanol (w/v) 50% glycerol (v/v)	

Buffers for Southern blot	
Denaturing solution 1.5 M NaCl 0.5 N NaOH 0.25 N HCl	**Neutralization buffer** 0.5 M Tris-HCl, pH 7.0 1.5 M NaCl
SSC buffer (20x) 0.3 M sodium citrate tri-basic, pH 7 3 M NaCl	**Church (hybridization) buffer** 0.5 M sodium phosphate, pH 7.2 7% SDS

MBS washing solution	**Blocking buffer**
100 mM NaCl 0.3% (v/v) Tween-20 pH 7.5	100 mM maleic acid, pH 7.38 10% blocking reagent (DIG Luminescent Detection Kit, Roche) 150 mM NaCl
Developing buffer	**DNA isolation buffer**
100 mM Tris-HCl, pH 9.5 100 mM NaCl	50 mM Tris-HCl, pH 8.0 100 mM EDTA 100 mM NaCl 1% (v/v) SDS
TE buffer	
10 mM Tris, pH 8 1 mM EDTA	

Buffers for western blot	
Digitonin lysis buffer [1] (1x)	**LämmLi loading buffer** [1] (4x)
20 mM HEPES-NaOH buffer, pH 7.4 25 mM KCl 250 mM sucrose 2 mM $MgCl_2$ 0.5 mM DTT 1x protease inhibitors mixtures [2] 1% digitonin [2,3]	250 mM Tris, pH 6.8 40% glycerol (v/v) 0.02% bromophenol blue (w/v) 8% SDS (w/v) 0.4 M DTT
Resolving gel buffer (8x)	**Stacking gel buffer** (4x)
3 M Tris-HCl, pH 8.8 0.1% SDS (w/v)	0.5 M Tris-HCl, pH 6.8 0.1% SDS (w/v)
Running buffer (10x)	**Transfer buffer** (10x)
250 mM Tris, pH 8.3 1.92 M glycine 1% SDS (w/v)	250 mM Tris, pH 8 1.92 M glycine

PBS buffer (10x)	**PBS-Tween® buffer (PBST)** (1x)
0.1 M Na_2HPO_4, pH 6.8 1.4 M NaCl 27 mM KCl	1x PBS buffer, pH 7.4 0.1% Tween® 20 (v/v)
Ponceau red	**Blocking buffer** [4,5]
0.5% Ponceau red (w/v) 1% AcOH (v/v)	1x PBST, pH 7.5 5% skimmed milk (w/v)

Buffers for RNA isolation	
Citrate buffer (1x)	**Guanidine thiocyanate buffer** [5] (10x)
25 mM sodium citrate, pH 7.5 0.5% N-laurylsacrosine (w/v)	1x citrate buffer [6], pH 6.4 4.23 M guanidine thiocyanate 0.2 M 2-mercaptoethanol

Buffers and solutions for immunohistochemistry and immunofluorescence	
Citrate buffer (for antigen retrieval) 2 mM citric acid, 0.9 M sodium citrate, pH 6	**TBS (for antigen retrieval)** 0.01 M Tris base, pH 9 0.15 M NaCl
Tris-HCl (for washing) 0.05 M Tris base + HCl, pH 7.4	**TBS (for washing)** 0.05 M Tris base, pH 7.4 0.15 M NaCl
EdU staining buffer 0.1 M TBS, pH 8.5 0.1 M Vitamin C [5] 0.001 M CuIISO$_4$ 0.01 mM Alexa Azid antibody in H$_2$O Braun	**2% PFA Fixative** [5] 10x PBS, pH 7.4 2% paraformaldehyde

Buffers and solutions for β-galactosidase staining	
X-Gal staining solution [5] 1 mg/mL X-Gal* in *N*,*N*-dimethylformamide 10 mM K$_3$Fe(CN)$_6$ 10 mM K$_4$Fe(CN)$_6$ 0.1% Triton X-100 2 mM MgCl$_2$ *5-bromo-4-chloro-3-indolyl-D-galactosidase	**X-Gal washing buffer** [4] 10x PBS, pH7.4 0.1% Triton X-100 2 mM MgCl$_2$
	1% PFA Fixative 10x PBS, pH7.4 1% paraformaldehyde 0.2% glutaraldehyde (w/v) 0.02% Triton X-100 (v/v)

Buffers and solutions for separating epidermis from dermis	
Thermolysin buffer [1,7] (500 μg/mL) 10 mM HEPES, pH 7.4 142 mM NaCl 6.7 mM KCl 0.43 mM NaOH 1 mM CaCl$_2$	**Trypsin solution** [1,8] 0.25% Trypsin in 1x PBS, pH7.4
	Sodium thiocyanate buffer [9] (0.5 M) 0.5 M Na$_2$HPO$_4$, pH 6.8 0.1 M KSCN

[1] Store at −20 °C.

[2] Add freshly.

[3] A 10% stock solution was prepared by dissolving the powder in boiling water and keeping the solution at 95 °C for 10 min.

[4] Store at 4 °C.

[5] Freshly prepared.

[6] Freshly sterile filtered.

[7, 8, 9] Buffers used to separate epidermis from dermis according to further analysis: lipid analysis[7], Southern blot[8], western blot[9].

2.1.3   Primers

All of the following primers were obtained from BioSpring GmbH (Frankfurt/M, Germany).

2.1.3.1   Primers used for the genotyping of ES cells

Name	Primer sequence (forward; reverse)
Ugcg	5′-TGATAGCCACTGTCTGCTCTGC-3′ ; 5'-CGAAGTTATGTTTAAACGCGGC-3′
Used to synthesize the Southern probe!!	5′-CAAAAAGGTTGGCATTAACCCTAAA-3′ ; 5'-TGTCATCTGATTCACCATGTCAGTT-3'
Ugcg flox/flox	5′-GATATCATGGTCTTCTTCATGTGCC-3′ ; 5′-TTTCCTTCACGTCATTTTTCTGAAC-3′

2.1.3.2   Primers used for the amplification of K14-5′- and 3′-homology arms of the targeting construct

Name	Primer sequence (forward; reverse)
5′ probe	5′-ATAGGTACCCCGCGGCATTTGTTTGGGATCCTTGGC-3′ ; 5′-TAGCTACCGGGAGATATCCATGGCTTTGAGAGAGGTGAG-3′
3′ probe	5′-CACATTAATTAAGCCACCTGCAGCCGCCAGTTCA-3′ ; 5′-TATGCTAGCAAACCGACCTGGGACCTGAGCCAAGC-3′

2.1.3.3   Primers used for the synthesis of the K14-DIG outside Southern probes

Name	Primer sequence (forward; reverse)
5′ probe	5′-TACTGCTGGGTCCTAGTCACCTG-3′ ; 5′-CAACTTCTACAGCAAGGCTCCAA-3′
3′ probe	5′-GTTCTCGATCCTGTCCCAGTTCT-3′ ; 5′-CTAACCTTGGCCCTGCTCTGTAT-3′

2.1.3.4   Primers used for the genotyping of mice

Gene	Primer sequence (forward; reverse)	T_a (°C)	Product size (bp)
Ugcg[wt]	5′-GATCTAAGAGGGTGAAGGCGCA-3′	58	259
Ugcg[wt/flox]	5′-AAGCCAGTCCAGTCAAACCGAG-3′	58	383
K14–wt-F	5′-AGGGATCTGATCGGGAGTTG-3′		442
K14–wt-R	5′-ATCCATCAAATCGACCACCA-3′		442
K14CreERT2Δneo-F	5′-CGCCAATTAACCCTCACTAAAGG-3′;	55	357
Rosa26R (1)	5′-TCTGCTGCCTCCTGGCTTCTGA-3′	63	wt: 270 mutant: 420
Rosa26R (2)	5′-CCAGATGACTACCTATCCTCCCA-3′	63	
Rosa26R (3)	5′-AAGCGCATGCTCCAGACTGCCT-3′	63	

2.1.3.5   Primers used for qRT-PCR analysis

Gene (gene ID)	Primer sequence (forward; reverse)
Smpd3 (ID 58994)	ATCCCTGACCACACAGGAAG; TTAGAGGTCCCAACCACAGG
Sgpp2 (ID433323)	CTCTGGGCCAAGTCATCAAT; ACCCAAGTTACCAGGCACAG
Pparβ/δ (ID19015) [1]	CTGAAGGGAAGGGGGTAGAG; CCAGTCTGGATGCTGCTACA
Krt77 (ID406220)	GTAGAGATCGCCACCTACCG; CCAATGGTCACCTGGCTACT

2.1.4 Antibodies

2.1.4.1 Primary antibodies

Antibody	Gene name	Host[a] – clonality[b]	Application[c] (dilution)	Supplier (clone)	Order number
β-Actin	*Actb*	rb – p	WB (1:200)	Santa Cruz [d]	sc-1616-R
Claudin 1	*Cldn1*	rb – p	WB (1:1000) Cryo (1:10)	Thermo Scientific [e]	RB-9209
Desmoglein 1/2	*Dsg1/2*	m – m	WB (1:100) Paraffin (1:10)	H. Heid [f] (DG3.10)	-
Desmoplakin 1/2	*Dsp1/2*	m – m	WB (1:50) Paraffin (pure)	H. Heid [f] (DP447)	-
Fatty acid binding protein 5	*Fabp5*	g – p	WB (1:2000)	R&D Systems [g]	AF 1476
(Pro-) Filaggrin	*Flg*	rb – p	WB (1:1000) Paraffin (1:50)	Covance [h]	PRB-417P
ER-HR3	-	r – m	Paraffin (1:50)	Acris [i]	
Integrin α6	*Itga6*	r – m	Cryo (1:50)	Progen [j] (GoH3)	10709
Integrin *β*4	*Itgb4*	r – m	Cryo (1:100)	BD [k]	553745
Involucrin	*Ivl*	rb – p	WB (1:100) Paraffin (1:100)	Covance [h]	PRB-140C
Keratin 6	*Krt6*	gp – p	Paraffin (1:100)	L. Langbein [l]	-
Keratin 10	*Krt10*	gp – p	Paraffin (1:100)	L. Langbein [l]	-
Keratin 14	*Krt14*	gp – p	Paraffin (1:2000)	L. Langbein [l]	-
Ki-67	*MKi67*	r – m	Paraffin (1:200)	Dako [m] (TEC-3)	M7249
Laminin 5	*Lama-5*	rb – p	Cryo (1:300)	Abcam [n]	ab14509
Loricrin (LOR)	*Lor*	rb – p	WB (1:1000) Paraffin (1:100)	Covance [h]	PRB-145P
Peroxisome proliferation-activated receptor *δ*	*Ppard*	rb – p	WB (1:500)	Thermo Scientific [e]	PA1-823A

[a] g, goat; gp, guinea pig; m, mouse; rb, rabbit; r, rat.

[b] m, monoclonal; p, polyclonal.

[c] Cryo: cryosections; IHC: immunohistochemistry; Paraffin: paraffin sections; WB: western blot.

[d] Santa Cruz Biotechnology Inc., Heidelberg, Germany; [e] Thermo Scientific (Pierce Antibodies), Germany;

[f] H. Heid, Dept. of Cell Biology , DKFZ, Heidelberg, Germany; [g] R&D Systems, Wiesbaden, Germany;

[h] Covance, Munich, Germany; [i] Acris Antibodies, Hiddenhausen, Germany; [j] Progen Biotechnik, Heidelberg, Germany;

[k] BD Biosciences, Heidelberg, Germany; [l] L. Langbein, Dept. of Genetics and Skin Carcinogenesis, DKFZ, Heidelberg, Germany;

[m] Dako, Hamburg, Germany; [n] Abcam plc, Cambridge, UK.

2.1.4.2   Secondary antibodies

Antibody[a]	Host[a]	Application[b] (dilution)	Supplier (Clone)	Order num.
Alexa FluorR 488 anti-rb	d	IHC (1:500)	Invitrogen [c]	A21206
Alexa FluorR 546 anti-r	g	IHC (1:500)	Invitrogen [c]	A11081
Alexa Fluor® 594 azide	-	Click chemistry (1:1000)	Invitrogen [c]	A10270
Cy3TM anti-gp	g	IHC (1:500)	Abcam [d]	ab102370
Cy3TM anti-m	d	IHC (1:500)	dianova [e]	715-165-150
Cy3TM anti-rb	d	IHC (1:500)	dianova [e]	715-165-152
Biotinylated anti-r	rb	Paraffin (1:200)	Vector Laboratories [f]	BA-4001
Goat-HRP	d	WB (1:1000)	Santa Cruz [g]	sc-2020
Mouse-HRP	g	WB (1:1000)	Santa Cruz [g]	sc-2005
Rabbit-HRP	g	WB (1:1000)	Santa Cruz [g]	sc-2004

[a]d, donkey; g, goat; gp, guinea pig; m, mouse; rb, rabbit; r, rat.

[b]IHC: immunohistochemistry; Paraffin: paraffin sections; WB: western blot.

[c] Life Technologies (Invitrogen™), Darmstadt, Germany; [d] Abcam plc, Cambridge, UK;

[e] dianova (Jackson ImmunoResearch), Hamburg, Germany; [f] Vector Laboratories, Burlingame, CA, USA.

[g] Santa Cruz Biotechnology Inc., Heidelberg, Germany

2.1.5   Enzymes

Restriction Endonucleases	Source
BglII (50,000 U/mL) PacI, SpeI	New England Bio (NEB) Labs, Ipswich, UK
ClaI, EcoRV, KpnI, SstII	Life Technologies (Invitrogen™), Darmstadt, Germany

Other Enzymes	Source
alkaline phosphatase (AP, EC 3.1.3.1)	Dako, Hamburg, Germany
Proof reading polymerase (PFU)	Promega, Mannheim, Germany
Proteinase K (peptidase K, EC 3.4.21.64)	Sigma-Aldrich, St. Louis, MS, USA
Platinum® Taq DNA Polymerase, RNase A (bovine pancreatic, EC 3.1.27.5) SuperScript® II Reverse Transcriptase	Life Technologies (Invitrogen™), Darmstadt, Germany
Turbo DNA-free™ DNase treatment kit	Life Technologies (Ambion®), Darmstadt, Germany

2.1.6   Kits, standards, stains, chromatography, electrophoresis

Agilent RNA 600 nano reagents	Agilent, Böblingen, Germany
CSPD® solution (25 mM) DIG Probe Synthesis Kit DIG Luminescent Detection Kit, Light Cycler® FastStart DNA Master SYBR Green I Kit	Roche Diagnostics Deutschland, Mannheim, Germany (Roche Applied Sciences)
DNA ladder (1 kb), RNaseOUT™ (recombinant RNase inhibitor)	Life Technologies (Invitrogen), Darmstadt, Germany
ECL™ western blotting analysis system (Kit)	Amersham GE Healthcare, München, Germany
PageRuler™ SM0671, prestained protein ladder	Fermentas, St. Leon-Rot, Germany
Turbo DNA-free™ Kit: DNase treatment & removal, WT Expression Kit	Life Technologies (Ambion), Darmstadt, Germany
WT Terminal Labeling and Controls Kit	Affymetrix, Santa Clara, CA, USA
Nitrocellulose membrane	Roche, Switzerland
Hyperfilm^{TM} ECL, X-ray film	Amersham Biosciences, UK
C18 Porasil silica, 125 Å, 55-105 μm	Waters, Eschborn, Germany
Acquity UPLC® BEH C18, 130 Å ,1.7 μm, 2.1 × 50 mm column	Waters, Eschborn, Germany
DEAE Sephadex A-25	Pharmacia Biotech, Uppsala, Sweden
HPTLC plates (Silicagel 60 F$_{254}$)	Merck Millipore, Darmstadt, Germany
SL lipid standards for MS	Avanti Polar Lipids, USA
Bradford reagent for protein determination	Sigma-Aldrich, Deisenhofen, Germany
H&E stain (hematoxylin & eosin)	Chroma, Köngen, Germany
Streptavidin, alkaline phosphatase conjugated (SA-5100)	Vector Laboratories, Burlingame, CA, USA
Giemsa stain	Merck, Darmstadt, Germany
Vitro-Clud® mounting media	Langerbrink, Emmendingen, Germany
DAPI stain	Sigma-Aldrich, Deisenhofen, Germany
EdU reagent	Invitrogen

2.1.7   Cell lines

Embryonic stem cells (ES), cell line E14 were obtained from the Transgen-Service of the German Cancer Research Center (DKFZ, Heidelberg, Germany).

2.1.8 Mouse lines

Mouse Strain	Origin
C57/Bl6	Charles River, L'Arbresle, France
K14CreERT2 $Ugcg^{f/f\,K14CreERT2}$	Generated by R. Jennemann [1]
FLP-deleter Rosa26 reporter	Kindly provided by G. Schütz [1]

[1] DKFZ Heidelberg

2.1.9 Instrumentation

Instrument	Company

Instruments used for genotyping (PCR analysis)

Agarose gel electrophoresis chamber	Carl Roth, Karlsruhe, Germany
Agarose gel chamber	Carl Roth, Karlsruhe, Germany
GelDoc^{TM} 2000 Gel Documentation System	Bio-Rad, München, Germany
GeneAmp® PCR System 2400, 2720 Thermal cycler – PCR	Life Technology (Applied Biosystems), Darmstadt, Germany

Instruments used for lipid extraction and analysis

Alpha 1-2 Lyophilizer	Christ, Osterode, Germany
Evaporator	Liebisch, Bielefeld, Germany
Linomat IV	Camag, Muttenz, Switzerland
Sonorex Super RK 102H Sonicator	Bandelin, Berlin, Germany
Variofuge 3.0 R	Heraeus Sepatech, Osterode, Germany
Xevo® TQ-S Tandem MS Acquity UPLC® I-class	Waters, Eschborn, Germany

Instruments used for protein extraction, western & Southern blots

Branson Sonifier® 250	G. Heinemann, Schwäbisch Gmünd, Germany
Classic autoradiography film developing machine	AGFA E.O.S., Bonn, Germany
Electrophoresis blotting apparatus	Bio-Rad, Munich, Germany
Mini-PROTEAN 3 Cell electrophoresis system	Bio-Rad, Munich, Germany
SM-30 Control rotary shaker	Neolab, Heidelberg, Germany
Ultrospec 2000 UV/visible spectrophotometer	Pharmacia Biotech, Uppsala, Schweden
UV Stratalinker 2400	Stratagene, USA

Instruments used for RNA analysis

Agilent 2100 Bioanalyzer	Agilent Technologies, Böblingen, Germany
Avanti J-25 centrifuge	Beckman Coulter, Krefeld, Germany
GeneChip® Mouse Gene 1.0 ST Arrays GeneChip® Scanner 3000	Affymetrix, Santa Clara, USA
Light Cycler 2.0 system	Roche Diagnostics, Mannheim, Germany
Ultra-Turrax® T25 Basic homogenizer	IKA Labortechnik, Staufen, Germany

Instruments used for surgery and surgical dressing

Biopsy punches (5-mm and 8-mm diameter)	Stiefel GmbH, Waiblingen, Germany
Cavilon semipermeable dressing	3M Health Care, Neuss, Germany
Kinesiologic tape	Care Integral, Bad Schwartau, Germany
Narcotic evaporator	Dräger, Lübeck, Germany
Surgical instruments	Geuder, Heidelberg, Germany
Prolene 5-0 surgical thread	Ethicon, Norderstedt, Germany

Instruments used for histology, microscopy and physical measurements

Almemo® 2390-1 rectal thermometer, Sensor: ZA 9040-FS	Ahlborn Messtechnik, Holzkirchen, Germany
Autoanalyzer Hitachi 9-17-E	Hitachi, Frankfurt am Main, Germany
Biorevo BZ-9000 microscope	Keyence, Neu-Isenburg, Germany
Cryostat Leica CM 3050S	Leica Biosystems, Nussloch, Germany
Dako Autostainer	Dako, Hamburg, Germany
Skincheck pH Tester HI 98110	PCE Deutschland, Meschede, Germany
Microtome Microm HM355S	Thermo Scientific, USA
Tewameter TM300 (for TEWL measurements)	Courage-Khazaka Electronics, Cologne, Germany
Ultramicrotom Leica Ultracut	Leica Microsystems GmbH, Wetzlar, Germany

Additional Equipment

Dewar, liquid nitrogen container	KGW-Isotherm, Karlsruhe, Germany
Eppendorf refrigerated table top centrifuge 5417R, Eppendorf table top centrifuge 5415C	Eppendorf, Hamburg, Germany
Heating furnace (56°C)	Heraeus, Hanau, Germany
HP LaserJet 2410 PS	Hewlett-Packard, Böblingen, Germany
Laboratory scale	Ohaus, Pine Brook, USA
Laboratory micro scale	Sartorius, Göttingen, Germany
Minifuge RF (refrigerated centrifuge)	Heraeus, Hanau, Germany
pH Meter	Schott, Mainz, Germany
ScanMaker i800	Microtek, Taiwan
Thermomixer compfort (1.5mL)	Eppendorf, Hamburg, Germany
Vortexer	IKA Labortechnik, Staufen, Germany

2.1.10 Software

Adobe Illustrator CS2	Adobe Systems, USA
Bioconductor, version 2.9	freeware
Endnote X6 ISI Research Software	Berkeley, USA
Genomatix ChipInspector Genomatix Pathway System (GePS)	Genomatix Software GmbH, Munich, Germany
GraphPad Prism® 5	GraphPad Software, San Diego, CA, USA
MADMAX (Management and Analysis Database for Multi-platform microArray eXperiments)	https://madmax.bioinformatics.nl University of Wageningen
Microsoft Office 2007	Microsoft Corp., Redmont, USA
Microsoft Windows Vista	Microsoft Corp., Redmont, USA
R Statistical Package, version 2.14.0	freeware

2.2   Methods

For abbreviations and terminology used in the Methods section, see Appendix 7.3. The materials, enzymes, antibodies, reagents and equipment used and their sources are, for the most part, summarized in Section 2.1

2.2.1   Cloning and generation of transgenic mice

2.2.1.1   *K14CreERT2 knock-in mice*

A ca. 4.5 kb fragment of the keratin K14 promoter region was amplified by PCR using proof-reading polymerase (PFU, Promega). The primers were designed to introduce target sites for the restriction endonucleases KpnI and SstII at the 5′ end as well as an ATG start-codon and an EcoRV site at the 3′ end of the PCR product. A second PCR was performed to amplify a ca. 4.5 kb fragment which included the complete coding sequence of K14 as well as PacI and NheI sites needed for cloning of the PCR fragment. The correctness of both PCR products was proven by sequence analysis. The 5′ homology arm was inserted via KpnI/EcoRV in frame into a modified cloning vector containing regions encoding for iCre, ERT2 and an FRT-flanked neomycin selection cassette (Figure 7). The 3′ homology arm was inserted into Pac I/Nhe I sites at the 3′ end of the neomycin cassette. The targeting construct was then ligated via SstII/ClaI into a cloning vector containing a PGK-DTA cassette (Figure 7) in order to enhance the efficiency of the homologous recombination in embryonic stem (ES) cells. E14 ES cells were transfected in the presence of the SstII-linearized K14-targeting vector and cultivated and genotyped as described previously (Jennemann et al., 2005). Southern blot analysis using digoxigenin-labeled probes revealed that four out of 384 ES cell clones were correctly targeted (Figure 7 B,C). Positive stem cells were injected into blastocysts, and the resulting chimeras were mated with C57BL/6 mice. Germ line transmission was indicated by the agouti-like color of the fur from the offspring, which were additionally genotyped by Southern blot analysis (Figure 7 D) and PCR (Figure 7 E,F). The neomycin selection cassette of the targeted allele was removed by crossing K14CreERT2-neo mice with FLP-deleter mice (kindly provided by G. Schütz, DKFZ-Heidelberg) (Rodriguez et al., 2000). K14CreERT2 delta-neo animals were backcrossed for at least 5 generations until they were combined with *Ugcg*-floxed mice of pure C57BL/6 background.
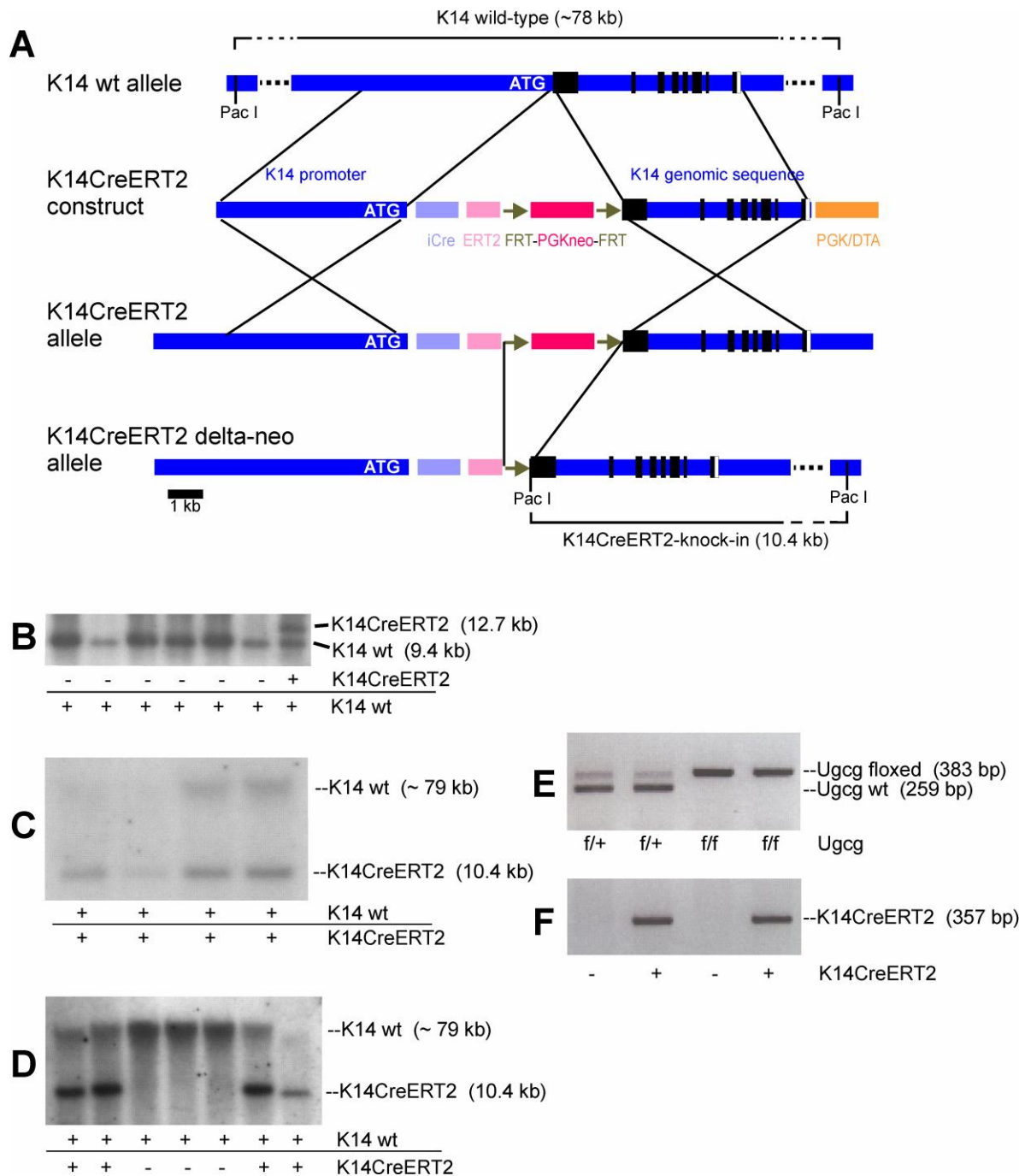
Figure 7.   Generation of K14CreERT2 knock-in mice.

(**A**) A PCR product including the promoter of K14 and the ATG-start codon was cloned in frame into a vector containing an iCre/ERT2 sequence and an FRT-flanked neomycin cassette. Part of the K14 genomic sequence was also inserted at the 3′ end of the neomycin cassette. The construct was transferred into a vector containing the PGK-DTA cassette. Stem cells were targeted and mice successfully generated. The neomycin antibiotic-resistance cassette was finally removed by crossing K14CreERT2-neo with FLP-deleter mice. (**B**–**D**) Genotyping of ES cells and knock-in mice by Southern blot analysis. The correct 5′ (**B**) and 3′ (**C**, **D**) homologous recombination of the targeting construct into E14 ES cells (**A**, **B**) and targeted mice (**C**) was confirmed by Southern blot analysis after KpnI (**B**) and PacI digestion (**C**, **D**) of DNA isolated from ES cells or mouse tail. Mouse tail biopsies from mutant mice were characterized by PCR analysis, detecting wild-type *Ugcg* and floxed *Ugcg* alleles as well as the K14CreERT2 transgene (**E**, **F**).

2.2.1.2   *Ugcg* $^{f/f\,K14CreERT2}$ mice

Homozygous-floxed mice *(Ugcg* $^{f/f}$*)* were generated as described (Jennemann et al., 2005) and crossed with K14CreERT2 mice. In a second mating step heterozygous-floxed *Ugcg* $^{f/+\,K14CreERT2}$ mice were bred with *Ugcg* $^{f/f}$, resulting in tamoxifen-inducible *Ugcg* $^{f/f\,K14CreERT2}$ mice, which were born at the expected Mendelian ratio. TAM induction of *Ugcg* $^{f/f\,K14CreERT2}$ mice resulted in disruption of the *Ugcg* gene by the action of Cre-recombinase, which excised exons 6–8 (including the catalytic domain) of the *Ugcg* gene locus (Figure 8).

PCR analysis was performed to confirm wild-type (+ / +), heterozygous-floxed (*f* / +) or homozygous-floxed (*f* / *f*) alleles (Figure 7E, F). Heterozygous-floxed and *Ugcg* $^{f/+}$ littermates served as controls. The efficiency of gene deletion was validated via Southern blot analysis (Figure 10) and byquantification of UGCG enzyme products, GlcCers, in epidermis samples obtained in week 3 or 4 after initiation of TAM induction (Figure 12 and Figure 13).
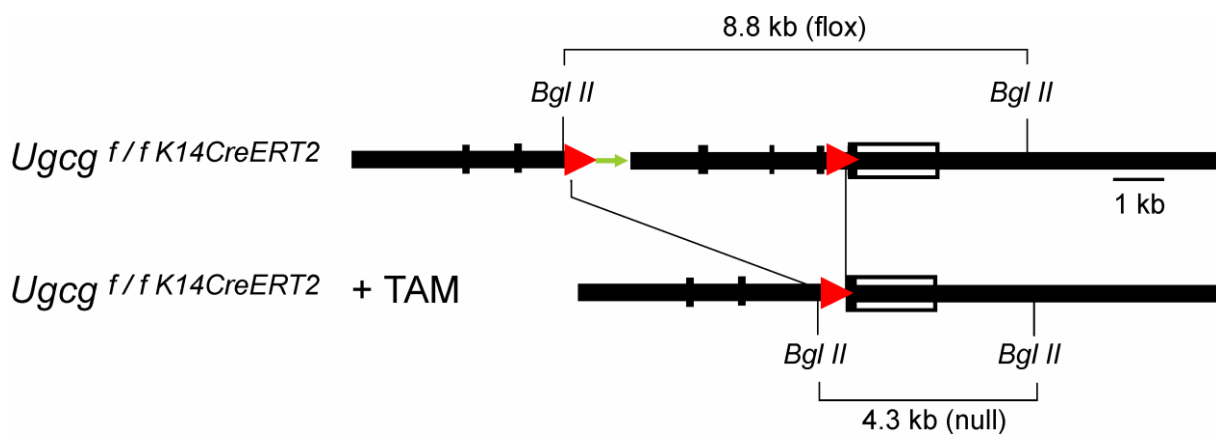
Figure 8.   The tamoxifen-inducible *Ugcg* transgene.

Deletion of the *Ugcg* gene for glucosylceramide synthase in murine epidermis was achieved by TAM-induced Cre-recombinase activation specifically in K14-expressing cells.

2.2.1.3   *Rosa26/K14CreERT2 mice*

Rosa26-LacZ reporter mice (kindly provided by G. Schütz, DKFZ-Heidelberg), bearing a β-galactosidase gene (*LacZ*), were crossed with transgenic K14CreERT2 mice. The resulting offspring (Rosa26/K14CreERT2 mice) were used to investigate TAM-induced Cre-activity before and after injection of 1 mg TAM dissolved in 100 µL oil.

2.2.2   Animal care

Animals were kept under specific pathogen-free conditions in barrier facilities, where a 12 h light / 12 h dark cycle was maintained. Mice were housed in groups of up to five animals at a controlled temperature of 22 °C. They were fed a diet of regular laboratory chow and water, supplied *ad libitum*. All animal experiments were approved by German federal law (Regierungspräsidium Karlsruhe, Germany).

2.2.3 Genotyping

2.2.3.1 *Genotyping of ES cells*

DNA genotyping of ES cells was performed by PCR analysis using an upstream primer located on the 5′ region of the targeted *Ugcg* gene outside the region encompassed by the targeting construct. A PCR product much larger than 1.7 kb was diagnostic for the homologous recombination of the 5′-terminus of the targeting construct (Figure 7). The data obtained from PCR were further confirmed by Southern blot analysis after NdeI restriction digestion using the PCR DIG Probe Synthesis Kit and DIG Luminescent Detection Kit (DIG = digoxigenin) according to the manufacturer's protocol. Confirmation of the insertion of the 3′ single *loxP* site was performed through PCR by using a primer pair to amplify one part of the *Ugcg* gene (>> 100 bp) before and after the single *loxP* integration site. The 3′ homologous recombination of the targeting construct was additionally verified by Southern blot analysis after SpeI digest of the DNA with a 3′ outside DIG probe. Six out of 384 ES clones underwent homologous recombination of the *Ugcg* gene locus.

2.2.3.2 *Genotyping of mice*

Mice were genotyped as previously described (Jennemann et al., 2005). In brief, genomic DNA was isolated from tail biopsies. Tails were digested overnight at 56 °C with 8 µL of proteinase K (10 mg/mL, Sigma) dissolved in 800 µL of NID buffer. Upon heat inactivation of the enzyme at 85 °C for 45 min, 2 µL of DNA solution was used for PCR analysis. Primers used for amplification of specific products corresponding to wild-type or mutant alleles are listed in Section 2.1.3. The results of the PCR analysis were confirmed by Southern blot analysis.

PCR conditions for amplification of the *Krt14* and *Ugcg* transgenes

PCR reaction (50 µL)	µL	PCR program	T [°C]	Time [s]
H_2O	34.75	1. Denaturation	95	300
10x Buffer	5.00	2. Denaturation	95	45
$MgCl_2$ (50 mM)	3.00	3. Annealing	58	30
dNTPs (10 mM)	1.00	4. Elongation	72	40
Forward primer (7.5 pmol/µL)	2.00	5. Elongation	72	300
Reverse primer (7.5 pmol/µL)	2.00	6. Cooling	4	∞
NID-DNA	2.00	Steps 2 to 4 are repeated for 35 cycles.		
Platinum Taq Polymerase (5 U/µL)	0.25			

PCR conditions for amplification of the *Rosa26/LacZ* gene

PCR reaction (50 µL)	µL	PCR program	T [°C]	Time [s]
H$_2$O	17.50	1. Denaturation	95	300
10x Buffer	2.50	2. Denaturation	95	30
MgCl$_2$ (50 mM)	0.75	3. Annealing	63	60
dNTPs (10 mM)	0.50	4. Elongation	72	60
Primer 1	0.50	5. Elongation	72	600
Primer 2	0.50	6. Cooling	4	∞
Primer 3	0.50			
NID-DNA	2.00	Steps 2 to 4 are repeated for 35 cycles.		
Platinum Taq Polymerase (5 U/µL)	0.25			

2.2.4 Preparation and administration of tamoxifen

Ugcg gene deletion was initiated by intraperitoneal (i.p.) injection of 1 mg TAM once per week as indicated in Figure 9. TAM was first dissolved in 100% ethanol and then further diluted with sunflower seed oil. Both steps were performed under sonication for ca. 5 min at 37 °C. The TAM solution was always freshly prepared at a concentration of 1 mg TAM per 100 µL as an ethanol/oil (10:90) suspension. Controls and *Ugcg$^{f/f\,K14CreERT2}$* mice were treated in parallel.

2.2.5 Southern blot

TAM-induced recombination of the *Ugcg* gene was confirmed by Southern blot analysis. Biopsies were taken and snap frozen in liquid nitrogen. Epidermis and dermis were separated after trypsinization (0.25% in PBS) of skin for 16 h at 4 °C (Mertens et al., 2005). Subcutaneous fat tissue was removed from the dermis.

2.2.5.1 DNA isolation

Tissue samples were digested in 500 µL of DNA isolation buffer containing 5.6 mg/mL proteinase K (Sigma/USA) at 56 °C overnight. Then 214 µL of saturated NaCl were added, and samples were gently mixed and centrifuged at 15000×*g* for 20 min at 4 °C. Supernatants were transferred into new Eppendorf tubes and incubated with bovine pancreatic RNAse A (19.6 µL/mL) for 25 min at 37 °C. DNA was precipitated by adding one volume of 2-propanol and gently mixing. Centrifugation was repeated (15000×*g*, 20 min, 4 °C) and the resulting DNA pellet was washed with 500 µL of ice cold 70% ethanol. Next, the DNA was air-dried and dissolved in 50-100 µL of doubly distilled H$_2$O at 37 °C for 1 h. The DNA concentration of each sample was calculated from its optical density (absorbance) at 260 nm (A_{260}) measured with an Ultrospec 2000 UV/vis spectrophotometer.

2.2.5.2   Restriction digest, electrophoresis and denaturation

DNA samples (5 µg) were digested with 50 units of the BglII restriction enzyme overnight at 37 °C. Resulting fragments and a 1 kb DNA ladder were separated by 1% agarose gel electrophoresis in 1x TAE buffer (120 V, 4 h). The lane with the DNA ladder was manually removed, stained with ethidiumbromide and visualized under UV light. To denature DNA fragments, the gel was incubated for 10 min in 250 mM HCl, subsequently washed with dd H_2O and placed for 30 min in denaturing solution. After repeated washing with dd H_2O, the gel was incubated in neutralization solution (2 times, 15 min each).

2.2.5.3   DNA transfer and hybridization with DIG-labeled probe

Further analysis was performed using a digoxigenin-labeled 3′ "outside" Southern probe amplified according to the protocol of the DIG Probe Synthesis Kit and DIG Luminescent Detection Kit according to the manufacturer's instructions (Roche Applied Science). Primers used for the synthesis of the Southern probe are listed in section 2.1.3.3.

The DNA was blotted onto a nitrocellulose membrane in 20x SSC buffer overnight. Upon transfer, the DNA was fixed covalently to the membrane by UV-cross linking in a UV Stratalinker. Thereafter, the membranes were pre-hybridized for 6 h with Church buffer at 65 °C. The DIG probe was diluted 1:10 in TE buffer and subsequently denatured at 95 C for 6 min. The membrane was then incubated at 65 C with Church buffer containing the DIG-labeled probe overnight. The next day, the membrane was washed twice with 2x SSC/0.1% SDS and twice with 0.5x SSC/0.1% SDS (15 min for each wash) and equilibrated with MBS washing buffer for 30 min at RT. Upon blocking (30 min, RT), an anti-DIG solution containing alkaline phosphatase (AP) (1:1000 dilution, of AP stock (150 mU /ml)) in blocking buffer) was applied (30 min, RT). The membrane was washed again, equilibrated in developing buffer and incubated with the chemiluminescence substrate for alkaline phosphatase (CSPD® solution) for 20 min at 37 °C in the dark. Bands were visualized by exposure to an X-ray film (Hyperfilm™) for 2 h at RT.

2.2.6   Lipid analysis

2.2.6.1   Tissue preparation

Skins were incubated in thermolysin buffer (500 µg/mL) at 37 °C for 2 h and subsequently washed with PBS. Epidermis was separated from dermis using forceps. Epidermis samples were lyophilized and powdered; dry weight was determined. Samples were stored air tight at 4 °C until lipid extraction was performed.

Whole esophagus tissue was collected, directly lyophilized and further processed as described for epidermis.

2.2.6.2   Lipid extraction

Lipid extraction of lyophilized epidermis and esophagus tissue was performed according to Doering et al. with slight modifications (Doering et al., 1999a; Jennemann et al., 2007). In brief, 10–50 mg of

epidermis were extracted with 2 mL of chloroform/methanol/distilled water (C/M/W) (30:60:8 v/v) under sonication at 50 °C for 15 min. Extracts were centrifuged at ca. 2000×*g* for 10 min and supernatants were collected. Pellets were extracted again as described above using C/M/W (10:10:1 v/v) and then with C/M (2:1 v/v). The supernatants were pooled with previous fractions and dried under air flow at 37 °C. Crude extracts were stored at 4 °C until further extraction.

Aliquots of crude extracts (2–10 mg) were purified by saponification under mild alkaline conditions (0.1 M methanolic KOH, 4 h, 50 °C) to remove phospholipids. Purified extracts were then desalted using reverse-phase chromatography (RP-18) columns, air-dried and stored at 4 °C.

For the extraction of protein-linked sphingolipids (POS), pellets were first subjected to 3 cycles of methanol "washings" to remove remaining free lipids and then saponified under mild alkaline conditions (1 M methanolic KOH, 2 h, 60 °C) to cleave ester-bonds and to release POS. Supernatants were collected, neutralized with 1 M acetic acid, then dried and desalted as previously described (Jennemann et al., 2012a).

2.2.6.3 DEAE-Sephadex A-25 chromatography

Esophagus crude extracts were subjected to anion-exchange chromatography for the separation of neutral and acidic GSLs as previously described (Jennemann et al., 1990). In brief, pasteur pipettes were packed with 200 µL of diethylaminoethyl (DEAE-) Sephadex A-25 and equilibrated with 2 mL of C/M/W (30:60:8 v/v). Esophagus samples were dissolved in 2 mL of C/M/W (30:60:8 v/v) by sonication and loaded onto freshly prepared columns. The eluate was collected directly. Sample vials were rinsed twice with 1 mL of C/M/W (30:60:8 v/v) and loaded. After additional washing of the columns with 2 mL of C/M/W (30:60:8 v/v) and 2 mL of methanol, the total eluate containing unbound, neutral GSLs (fraction 1), which do not bind to the column material, was air-dried by evaporation. Acidic GSLs (fraction 2) were eluted with 4 mL of 0.5 M potassium acetate (KAc) in methanol, air-dried, and dissolved in H_2O to a final salt concentration of 0.1–0.2 M KAc. The salt was then removed using RP-18 columns.

2.2.6.4 High-performance thin-layer chromatography (HPTLC) analysis

For analysis of GlcCers, aliquots of saponified and nonsaponified crude epidermal extracts and lipid standards were dissolved in C/M/W (10:10:1 v/v) prior to loading of 20–40 µL volumes, corresponding to 1 mg dw of tissue, on an HPTLC glass plate (10 cm × 20 cm × 0.1 mm; Silicagel 60 F_{254}) using a Linomat IV (CAMAG). After a pre-run with chloroform/acetone (1:1 v/v), GSLs were separated using C/M/W (65:25:4 v/v) as running solvents. Plates were sprayed with 0.2% orcinol in 10% sulfuric acid and developed at 120 °C for ca. 10 min and scanned (ScanMaker i800). For the analysis of freely extractable and protein-linked sphingolipids, amounts corresponding to 1 mg of dry epidermis in nonsaponified extracts and 0.25 mg of saponified extracts were separated with chloroform/methanol/glacial acetic acid (190:9:1 v/v) as running solvent. The plates were then sprayed with copper reagent (10% $CuSO_4$ in 8% H_3PO_4), developed at 180 °C for 5–10 min and scanned (ScanMaker i800).

2.2.6.5   Quantification by liquid chromatography-electrospray ionization tandem mass spectrometry (LC-ESI MS/MS)

Sphingolipid quantification was performed by tandem mass spectrometry using a Xevo® TQ-S triple-quadrupole instrument (Waters) equipped with ultra-performance liquid chromatography hardware (Acquity UPLC® I-class, Waters) and a nano-electrospray source.

Lipid extract samples, equivalent to a dried weight of 12.5 µg, were dissolved in 95% methanol (1 mL) and mixed with nonendogenous lipid standards prior to analysis. Lipid standards included the ceramides (d18:1/14:0), (d18:1/19:0), (d18:1/25:0), (d18:1/31:0), 6.25 pmol each; the GlcCers (d18:1/14:0), (d18:1/19:0), (d18:1/25:0), (d18:1/31:0), 3.125 pmol each; and the SMs (d18:1/14:0), (d18:1/25:0), (d18:1/31:0), 3.125 pmol each.

The samples (extract + standard) were injected (10 µL) and separated into the UPLC using a reverse-phase column (Acquity UPLC® BEH C18, 130 Å 1.7 µm, 2.1×50 mm column) which was maintained at 40 °C during the analyses. The chromatographic eluent gradient at a constant flow rate of 0.45 mL/min is given in the following table.

UPLC-gradient elution of sphingolipids for detection by tandem mass spectrometry.

Time [min] [a]	Solvent A [%] [b]	Solvent B [%] [c]	Slope
0.0	100	0	Initial
0.1	100	0	linear
0.2	92	8	linear
5.0	10	90	concave
5.25	10	90	linear
5.50	100	0	linear
6.50	100	0	linear

[a] Flow rate 0.45 mL/min.

[b] Solvent A: 95% methanol, 5% water, 0.05% formic acid, 1 mM ammonium formate.

[c] Solvent B: 99% isopropanol, 1% methanol, 0.05% formic acid, 1 mM ammonium formate.

MS/MS analysis was performed using the positive-ion ESI mode with multiple reaction monitoring (MRM) of daughter-ion fragments specific to each lipid class. For quantification, chromatographic peak areas corresponding to each specific lipid species were normalized to the peak areas of the corresponding internal standards.

2.2.7   Transepidermal water loss (TEWL)

The TEWL was determined using a Tewameter TM300 (Courage-Khazaka Electronics) instrument according to the manufacturer's instructions. Mice were shaved and the water evaporation gradient

was measured at the skin surface by placing a special probe for small sample areas onto a dry depilated area for at least 30 s. The instrument was calibrated before each measurement.

2.2.8 Stratum corneum pH

The stratum corneum pH was determined with a *skincheck* pH Tester (PCE) according to the manufacturer's protocol. In brief, the pH meter was calibrated and the pH electrode was placed on a depilated, moisturized area of skin on the back of a mouse for at least 1 min. Measurements were performed in duplicates.

2.2.9 Body temperature

Body temperature was measured using a rectal thermometer with a special small sensor (Almemo® 2390-1, sensor: ZA 9040-FS). The sensor was covered with Vaseline and inserted into the rectum of a mouse for at least 1 min directly after anesthesia. The core body temperature of *Ugcg* mutants and control mice was determined during weeks 1 and 4 of TAM induction (Figure 14).

2.2.10 Water deprivation experiments

Water deprivation experiments were performed before and during TAM induction (weeks 1, 2 , 3 , 4 and 12) to investigate the onset and impact of epidermal barrier perturbations on weight maintenance of *Ugcg* mutants as compared to controls. Once per week control and mutant mice were deprived of drinking water for 6 h while their body weight was monitored (Figure 17)

2.2.11 Time course of Cre-expression

Long-term Cre-recombinase activity in Rosa26/K14CreERT2 mice was investigated by β-galactosidase staining (el Marjou et al., 2004; Soriano, 1999). Control mice (Rosa26-pos./K14CreERT2-neg.) and double mutant mice (Rosa26-pos./K14CreERT2-pos.) were induced once with TAM and monitored over 3 months (as $Ugcg^{f/f\,K14CreERT2}$ mice). Full thickness skin samples were resected and snap-frozen in isopentane pre-cooled with liquid nitrogen and stored at $-80\,°C$. Skin cryosections (5 μm) were fixed in 1% PFA Fixative, rinsed twice in PBS, and stained overnight at 37 °C in X-gal staining solution (see section 2.1.2). The next day, stained sections were washed twice with PBS and distilled water and then mounted and visualized with a Biorevo BZ-9000 microscope (Keyence).

2.2.12 Western blotting

2.2.12.1 Epidermis preparation

Adult control and mutant mice were depilated in the first week of TAM induction. Two weeks later (day 21 of induction), hair-free back skin of mice was collected and incubated in sodium thiocyanate buffer [check conc. in Table] for 30 min on ice (Diaz et al., 1977). Skins were rinsed with ice-cold PBS and the epidermis was peeled off the dermis using forceps.

2.2.12.2 Protein lysate preparation

Epidermis samples were placed in digitonin lysis buffer and homogenized by sonication (Branson Sonifier 250) using five pulses every 30 s for 5 min. Lysates containing epidermal proteins were cleared by centrifugation at $21000 \times g$ for 15 min.

2.2.13 Determination of protein concentration using Bradford assay

The protein concentration in total lysates was dermined by the Bradford method (Bradford, 1976), a colorimetric assay based on the dye Brilliant Blue G. The formation of a protein-dye complex causes a shift in the absorption maximum of the dye from 465 to 595 nm. Protein-dye mixtures were prepared by mixing either 2.5 or 5 µL of lysate with Bradford reagent (Sigma-Aldrich) up to 1 mL. A dilution series with BSA standards ranging from 0 to 10 µg/mL dissolved in Bradford reagent was prepared in parallel. The absorbance of the protein-dye complex at its maximum at 595 nm was measured for the BSA standards and the epidermal lysates. The protein content of each lysate sample was calculated by interpolation of their absorbance values on the BSA standard curve.

2.2.13.1 SDS polyacrylamide gel electrophoresis (SDS-PAGE)

Equal amounts of epidermal proteins (50 µg) were separated on 10% polyacrylamide gels by sodium dodecyl sulfate polyacrylamide gel electrophoresis (SDS-PAGE) according to their molecular weight. They were blotted onto nitrocellulose membranes (3-4 h, at 180 mA) and equal loading of protein samples was controlled by staining with Ponceau S red solution. Unspecific binding sites were blocked with blocking buffer containing 5% milk for 1 h at RT followed by incubation with primary antibodies overnight at 4 °C (see 2.1.4.1). As reference protein β-actin was used. The next day, membranes were washed with PBST buffer (3 times, 10 min each) and incubated with HRP-coupled secondary antibody (see 2.1.4.2) for 45–60 min at RT. After repeated washings (3 times, 10 min each), antibody binding was detected using the chemiluminescence substrate luminol of the Amersham ECL™ western blotting analysis system and exposure of X-ray film (Amersham Hyperfilm ECL). The films were scanned (Epson Stylus SX435W multifunctional scanner/printer) and protein bands were identified according to their molecular weight using a prestained protein ladder (PageRuler™).

2.2.14 mRNA isolation and analysis

2.2.14.1 Sample preparation

Full-thickness dorsal skin of $Ugcg^{f/f\,K14CreERT2}$ mutants and control mice ($n = 4$, each) was excised using an 8-mm biopsy punch.

2.2.14.2 RNA extraction and DNAse digest

RNA was directly extracted from skin samples by phenol-chloroform extraction (Chomczynski and Sacchi, 2006). Tissue samples were homogenized on ice using an Ultra-Turrax® T25 Basic homogenizer. RNA was digested using the Turbo DNA-free™ DNase treatment kit (Ambion). The RNA integrity was validated with the Agilent Bioanalyzer 1000.

RNA was reverse transcribed into cDNA using SuperScript® II reverse transcriptase (Invitrogen) according to the manufacturer´s instructions.

2.2.14.3   Quantitative reverse transcription PCR (qRT-PCR)

Real-time qRT-PCR was performed using the Light Cycler® FastStart DNA Master SYBR Green I Kit (Roche) under the following conditions.

qRT-PCR conditions

PCR mix	µL	PCR program [a]	T [°C]	time [s]
cDNA (1:10)	2.0	1. Denaturation	95	600
LC® SYBR Green	2.0	2. Denaturation	95	5
MgCl$_2$ (25 mM)	1.6	3. Annealing	56	10
Primers (5 µL each)	2.0	4. Elongation	72	10
dd H$_2$O	12.4	5. Elongation	72	300
		6. Elongation	4	∞

[a] Steps 2 to 4 are repeated for 35 cycles

2.2.14.4   Gene expression profiling

RNA was isolated and treated with DNAse as described above. The RNA integrity was validated with the Agilent Bioanalyzer 1000 and 100 ng of total RNA were further processed using the Ambion WT Expression Kit (Ambion) in order to synthesize cDNA, cRNA and finally ss cDNA. The ss cDNA was fragmented and labeled with the WT Terminal Labeling and Controls Kit (Affymetrix) and hybridized onto GeneChip® Mouse Gene 1.0 ST Arrays according to the manufacturer's instructions (Affymetrix). Experiments were performed as independent triplicates. The microarray chips were scanned with a GeneChip® Scanner 3000.

Quality control and clustering analyses were carried out using the MADMAX (Management and Analysis Database for Multi-platform microArray eXperiments) platform of the University of Wageningen (*https://madmax.bioinformatics.nl*). For these steps the Affymetrix CEL files (containing the results of the intensity calculations on the pixel values of the original DAT files, including an intensity value, standard deviation of the intensity, the number of pixels used to calculate the intensity value) were normalized according to the Robust Multi-array Average (RMA) technique (Irizarry et al., 2003), using the freeware programs R Statistical Package and Bioconductor.

The data were analyzed using Genomatix ChipInspector (for calculating fold changes) and Genomatix Pathway System (GePS). These tools utilize a single probe approach which allows pre-selection of differentially expressed genes. A cut-off of 0% false discovery rate (FDR) was applied to identify significantly regulated genes. The *p*-values for analysis of GO enrichment (Table A2) were determined

using Genomatix software. All gene expression data will be deposited in NCBI's Gene Expression Omnibus (Edgar et al., 2002) upon acceptance of a manuscript for publication.

2.2.15 Wound healing experiments

2.2.15.1   Induction protocol and anesthesia of mice

After three weeks of TAM induction, mice were anesthetized with 2.5 vol.% isofluran (Abbott, Illinois, USA) and wound healing experiments were performed as shown in Figure 9.
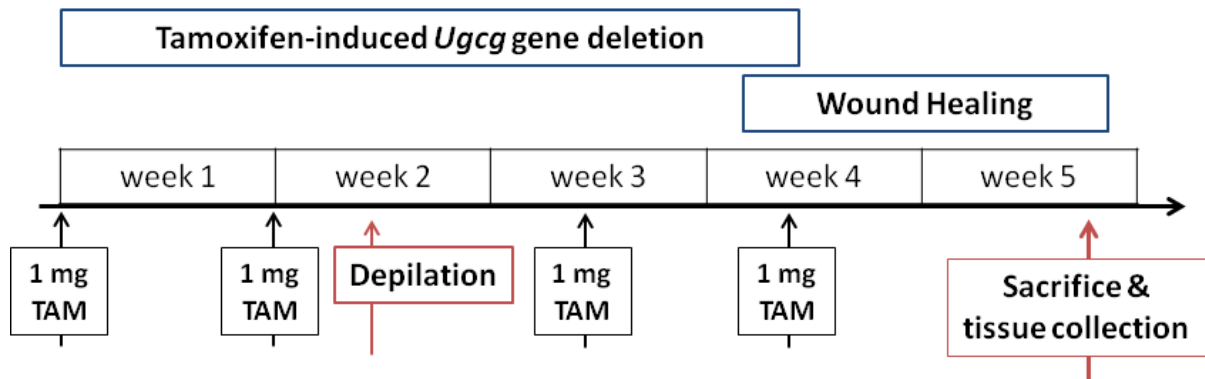
Figure 9.   Experimental scheme for wound healing.

TAM-induction and wound healing experiments. Adult mice (7–8 weeks old) or mice with grafted skin (5 weeks after grafting) were injected i.p. with TAM (1 mg/mL in sunflower oil) once a week for up to four weeks. The hair was removed by depilation in the second week. Three weeks after initiating induction, when the epidermal defect was fully established, wounds were applied on the upper back of mice and monitored for 9-10 days until wounds were closed in controls. Mice were then sacrificed and tissue was collected for further analysis.

2.2.15.2   Wound application and sample collection

Full-thickness skin wounds were applied on the upper back of mice using disposable 5-mm biopsy punches. Wound size, TEWL and body weight of animals were documented over 9–10 days until wounds in control litters were closed. Wounds were collected at 6 h, and on day 2, 6 and 9 following wounding using surgical instruments (scissor, forceps) and subsequently fixed in 4% formaldehyde or snap-frozen in isopentane precooled with liquid nitrogen.

2.2.15.3   Wound healing in skin transplants

Isografting was performed on 7–8 week-old male mice (20 to 25 g). They were anesthetized with tribromoethanol (Avertin, Sigma) and full thickness skin (4 × 4 cm) was excised from donor animals (control and $Ugcg^{f/f\,K14CreERT2}$ mutants) and quickly placed in sterile ice-cold PBS. Skins from acceptor animals (control litters) were resected and disposed of. Grafts were sewn on the back of acceptor mice using a surgical thread, and edges were covered with a semi-permeable dressing (3M, Neuss, Germany). Upon transplantation, mice were single-housed and cages were kept on a heating plate 1-2 days until recovery. Transplants were fully adapted within 2–3 weeks after grafting. The fur started

growing ca. 4 weeks after grafting and had to be shaved before wound healing experiments could be performed, as described above.

2.2.16 Histology and microscopy

2.2.16.1   Sample preparation

Skin samples were collected and were either fixed in formalin (4%) overnight at 4 °C or frozen in isopentane pre-cooled with liquid nitrogen for cryosectioning. The next day, formalin fixed samples were dehydrated in aqueous ethanol solutions of decreasing concentrations (70%, 80%, 96%, 100%) and embedded in paraffin. Prior to staining, paraffin sections (ca. 3 μm) were deparaffinized by immersion in xylol followed by 100%, 96%, 80% and 70% ethanol and were finally rinsed with distilled water.

2.2.16.2   Staining for light microscopy

H&E staining

For routine morphologic analysis, skin and esophagus tissue were stained with hematoxylin and eosin (H&E), which highlights basophilic structures (pink; e.g. DNA) and proteins (blue).

Ki-67 staining

Keratinocyte proliferation was investigated by Ki-67 staining (pink), which is based on the nuclear protein MKI67 associated with proliferation. The procedure was performed using a Dako Autostainer. After permeabilization, blocking and an application of primary antibody for MKI67, sections were incubated with a biotinylated anti-rat antibody and detected with streptavidin conjugated to alkaline phosphatase (dilution 1:200 = 5 μg/mL).

HR3 & Giemsa staining

Skin macrophages and dendritic cells were stained using an anti-hematopoiesis-related antibody (ER-HR3) as described previously (Jennemann et al., 2007). Skin granulocytes and monocytes were stained with Giemsa solution (methylene blue-eosin-Azure B). Sections were rinsed with 1% acetic acid and sequentially immersed in 96% ethanol, 2-propanol (twice for 2 min) and xylol (ca. 1 min).

TUNEL staining

Apoptosis of keratinocytes was investigated by TUNEL staining according to the In Situ Cell DeathDetection kit's instructions (Roche, Mannheim, Germany).

All sections were mounted with Vitro-Clud® mounting media (Langerbrink) and evaluated by counting of respective positive cells in five high-power fields (400×) of each tissue sample (Ki-67, HR3, Giemsa staining).

β-Galactosidase (LacZ) staining

Cryosections (ca. 5 μm) from skins of Rosa26/K14CreERT2 and control mice were subjected to β-galactosidase staining as previously described (el Marjou et al., 2004). Prior to incubation with X-Gal staining buffer overnight at 37 °C, cryosections were fixed in 1% PFA buffer for 15 min and subsequently washed with X-Gal washing buffer. The next day, sections were washed, mounted with

Vitro-Clud® mounting media and directly visualized using a Biorevo BZ-9000 fluorescence microscope (Keyence).

2.2.16.3 Immunofluorescence microscopy

For indirect immunofluorescence microscopy, deparaffinized sections were subjected to antigen retrieval using 10 mM sodium citrate at pH 6 and 96 °C for 3–5 min and permeabilization with triton X-100 in 0.1% PBS at RT for 5 min prior to 1 h blocking with (a) 5% BSA, (b) 5% goat serum or (c) mouse blocking solution (Vector Laboratories). Following several washings with PBS (3 times for 5 min) incubation with primary antibodies (see Materials 2.1.4) was performed for 1 h at RT.

For the detection of CLDN1, LAMA5 and ITGA6 cryosections (5 µm) were fixed in acetone at RT for 10 min followed by blocking with 5% BSA for 45 min and subsequent incubation with primary antibodies for 1 h at RT.

Upon several washings with PBS (3 times for 5 min), incubation with secondary antibodies and DAPI stain (20 ng/mL, for A-T rich DNA regions) was performed for 30 min at RT. Afterwards, sections were washed twice with PBS and 5 min in distilled water. Samples were mounted with FluoroMount (Dako) and visualized.

2.2.16.4 In vivo DNA labeling with EdU

Mice were injected intraperitoneally with 200 µg of 5-ethynyl-2′-deoxyuridine (EdU), a thymidine analogue which is incorporated into the DNA of dividing cells. After 24 h mice were sacrificed, and skin and esophagus were dissected and embedded in paraffin. Sections of 5 µm thickness were taken, and EdU-labeled cells were stained by Click chemistry as described by Salic and Mitchison (Salic and Mitchison, 2008). In brief, deparaffinized sections were washed with TBS and incubated with staining buffer, containing 10 µM of Alexa Fluor® azide antibody (Invitrogen), for 30 min at RT. The 6-azidohexanyl group of this antibody reacts with the terminal alkyne of EdU via a copper-catalyzed Click reaction. Sections were then washed with TBS and distilled water and subsequently mounted with Dako Fluorescent Mounting Medium.

2.2.16.5 Staining for neutral and phospholipids with Nile red

Neutral and phospholipids were analyzed as previously reported (Greenspan et al., 1985). Cryosections (5 µm) were air-dried, embedded with freshly prepared Nile red (5 mg/mL in 75% glycerol) and visualized with a Biorevo BZ-9000 fluorescence microscope.

2.2.17 Statistics

All experiments included a minimum of 3 animals. The results obtained are shown as mean $\pm$ SD. All statistical tests were performed using GraphPad Prism® 5 software, except for the analysis of the lipid data, which was performed with Microsoft Office Excel 2007. Measurements in control (heterozygous [$Ugcg^{f/+\,K14CreERT2}$], wildtype [$Ugcg^{f/+}$, $Ugcg^{+/+}$]) and $Ugcg^{f/f\,K14CreERT2}$ mice were compared by the Student's t-test. Differences between group means were considered significant for $p < 0.05$ (*), $p < 0.01$ (**) and $p < 0.001$ (***). The statistical methods used for the evaluation of the gene array are described in section 2.2.14.4.

3. Results

3.1   The Challenge of TAM Induction and Tissue-specific *Ugcg* Gene Deletion

Constitutive *Ugcg* gene deletion (Exon 6-8 removal) in the epidermis and consequent loss of UGCG activity and GlcCers synthesis caused disruption of the WPB and premature death of newborn $Ugcg^{f/f K14Cre}$ mice (Jennemann et al., 2007). In order to further study the role of Cer glucosylation in epidermal differentiation, in particular the function of GlcCers in barrier homeostasis, TAM-inducible $Ugcg^{f/f K14CreERT2}$ mice were generated and investigated after *Ugcg* gene deletion.

Control and $Ugcg^{f/f K14CreERT2}$ mice were initially induced using a generally approved TAM induction protocol (el Marjou et al., 2004), which recommends 1 mg TAM per day on five consecutive days in the first week and one single injection of 1 mg TAM every second week. With this protocol severe health problems developed in *Ugcg* mutants already in week 2 of induction, hindering the mice to eat or drink. Deletion of *Ugcg* in K14-positive epithelia other than skin (see 3.2.1) was assumed to be responsible for the overall weak condition of the mice. However, no alterations in skin morphology or epidermal barrier function were observed at this time (see Appendix Figure A2, cf. Figure 14 E). Due to the overall health condition of mutant mice, further experiments could not be performed until a much lower TAM dose (1 mg TAM injection/week) was chosen (Figure 7), allowing for normal food intake and viability of UGCG-deficient mice.

3.2   Characterization of Inducible $Ugcg^{f/f K14CreERT2}$ Mice

3.2.1   *Ugcg* gene deletion and lack of GlcCers in the esophageal epithelium

Following TAM induction, *Ugcg* gene deletion was demonstrated by Southern blot analysis in the epidermis and other stratified epithelia, such as tongue, esophagus and forestomach (UGCG-null band; Figure 10) where K14-promotor activity had been previously detected (Huelsken et al., 2001). However, in newborn $Ugcg^{f/f K14Cre}$ mice activity of this promoter was not evident. The UGCG-null band detected in the dermis of adult mutant mice resulted from K14-positive recombinant cells of epidermal appendages (e.g., hair follicle outer root sheath keratinocytes) residing in the dermis (Figure 10).

Lipid analysis of whole esophagus tissue revealed that EOS-GlcCers were expressed in control samples, a result which has not been described previously (Figure 11 A,B). In contast, GlcCers were markedly reduced in the esophagus of mutants. No alterations were observed in the acidic GSLs (aGSLs), despite the upcoming band in samples from mutants (at the position of the GM1 standard band), which was lacking in controls (Figure 11 D). However, this band might derive from GM1-expressing macrophages infiltrating the esophageal tissue of mutant mice. Furthermore, high amounts of GM3, a major ganglioside of muscle tissue, were found in whole tissue extracts of control and mutant esophagi (Figure 11 D).
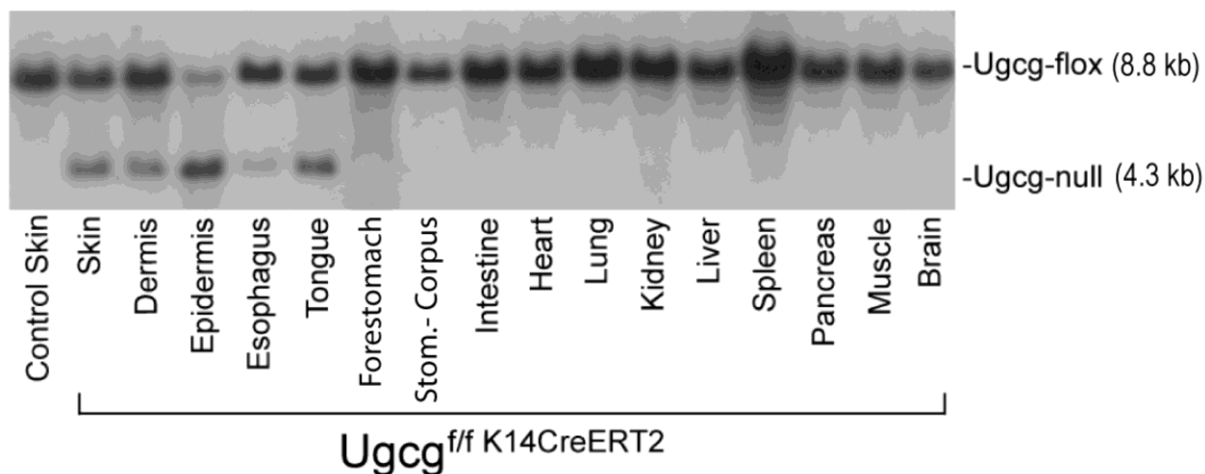
Figure 10. **Investigation of *Ugcg* gene recombination.**

Tissue specificity of *Ugcg* gene recombination was confirmed by Southern blot analysis. Recombinations were detected not only in skin but also in tongue, esophagus and forestomach. Positivity of dermis tissue was derived from recombinations in K14-positive hair follicle outer root sheath keratinocytes.

Morphologic alterations in the esophageal epithelium of *Ugcg*-mutant mice were already detected in week 2 of TAM induction. The esophagus of mutant mice was dilated and displayed a marked decrease in cellular organization and cohesion as compared to controls (Appendix Figure A1 A–F). Hyperproliferation was evidenced in all parts of the esophageal tube (cervical, thoracic, abdominal) by EdU staining, 24 h after EdU injection. EdU-positive cells were present in the esophageal lumen of mutant mice, indicating that a complete epithelial turnover deriving from proliferating basal cells was accomplished within ca. 24 h (Appendix Figure A1 A′–F′). In comparison, only a few EdU-positive cells were detectable in epidermis samples of same animals (not shown).
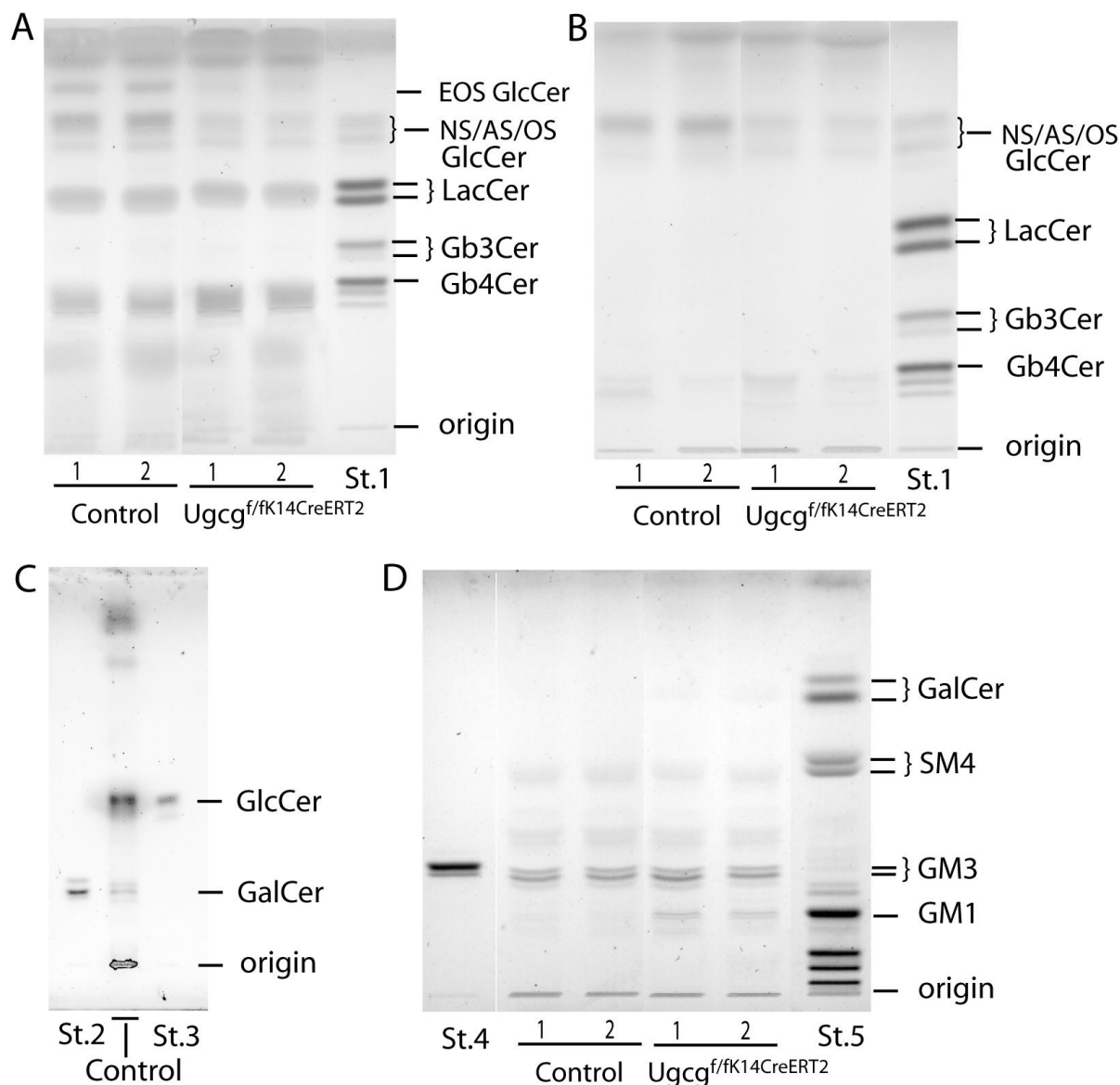
Figure 11. TLC analysis of esophageal lipid extracts: detection of EOS-GlcCers and evidence for the depletion of GlcCers in UGCG-deficient samples.

To investigate differences in the glycosphingolipid (GSL) pattern of whole esophagus tissue, crude extracts (ca. 4 mg dw each) were subjected to anion exchange chromatography (DEAE-Sephadex A-25) for the separation of neutral (n) and acidic (a) GSLs (Jennemann et al., 1990). (**A**) TLC of nGSLs and subsequent orcinol staining (1.5 mg dw each, crude extracts) revealed the presence in esophagus of esterifed EOS-GlcCers (mainly with linoleic acid). All GlcCer species (NS, AS, OS, EOS) were reduced by ca. 66% in mutant tissue compared to controls. (**B**) Further purification of nGSLs by saponification and subsequent TLC (1.5 mg dw each) showed that phospholipids, but also EOS, were removed. (**C**) To discriminate GlcCers from GalCers, peracetylation and subsequent perborate separation of nGSLs (2 mg dw each) was performed (Jennemann et al., 1990). (**D**) TLC analysis of aGSLs (1.5 mg dw each) showed differences between control and mutant extracts (i.e., at the position of GM1 standard), but the exact GSL species could not be identified by TLC. Standards were: human spleen extract (St.1); GalCer (St.2); GlcCer (St.3); GM3 (St.4); ganglioside mixture (St.5).

3.2.2 *Ugcg* ^{f / f K14CreERT2} mice exhibit reduced epidermal GlcCers and lack protein-linked sphingolipids

The efficiency of *Ugcg* deletion was addressed by analysis of the UGCG enzyme products, the GlcCers, via 1D-TLC, which separates SL species according to their polarity (Figure 12 A,A′). Orcinol-staining showed a significant reduction of all free extractable GlcCers (NS, AS, OS, EOS) in UGCG-deficient epidermis as compared to controls (Figure 12 A,A′). In the epidermis EOS-GlcCers, in which the GlcCers are ω-linked predominantly with linoleic acid (Doering et al., 1999a), occur in relatively small amounts compared to EOS-Cers. However, EOS-GlcCers were detectable in nonsaponified crude extracts of controls and appear as an orcinol-positive band in the GlcCer fraction. In contrast, in UGCG-deficient tissue EOS-GlcCers were not detectable, marking a substantial loss of barrier lipids.

A more complex chromatographic pattern was obtained for free extractable Cers (Figure 12 B,B′). In crude extracts of mutants, most Cers seemed to be reduced (Figure 12 B), whereas in saponified extracts (containing nonesterified Cers) compounds running at the positions of the Cer-C16 and -C24 standards and below were clearly elevated (Figure 12 B′).

Most strikingly, protein-linked POS-SLs, key material for the CLE, were drastically reduced (Figure 12 C). More specific information concerning individual SL species could not be obtained from the TLC results, but was available from MS analyses (Figure 13).
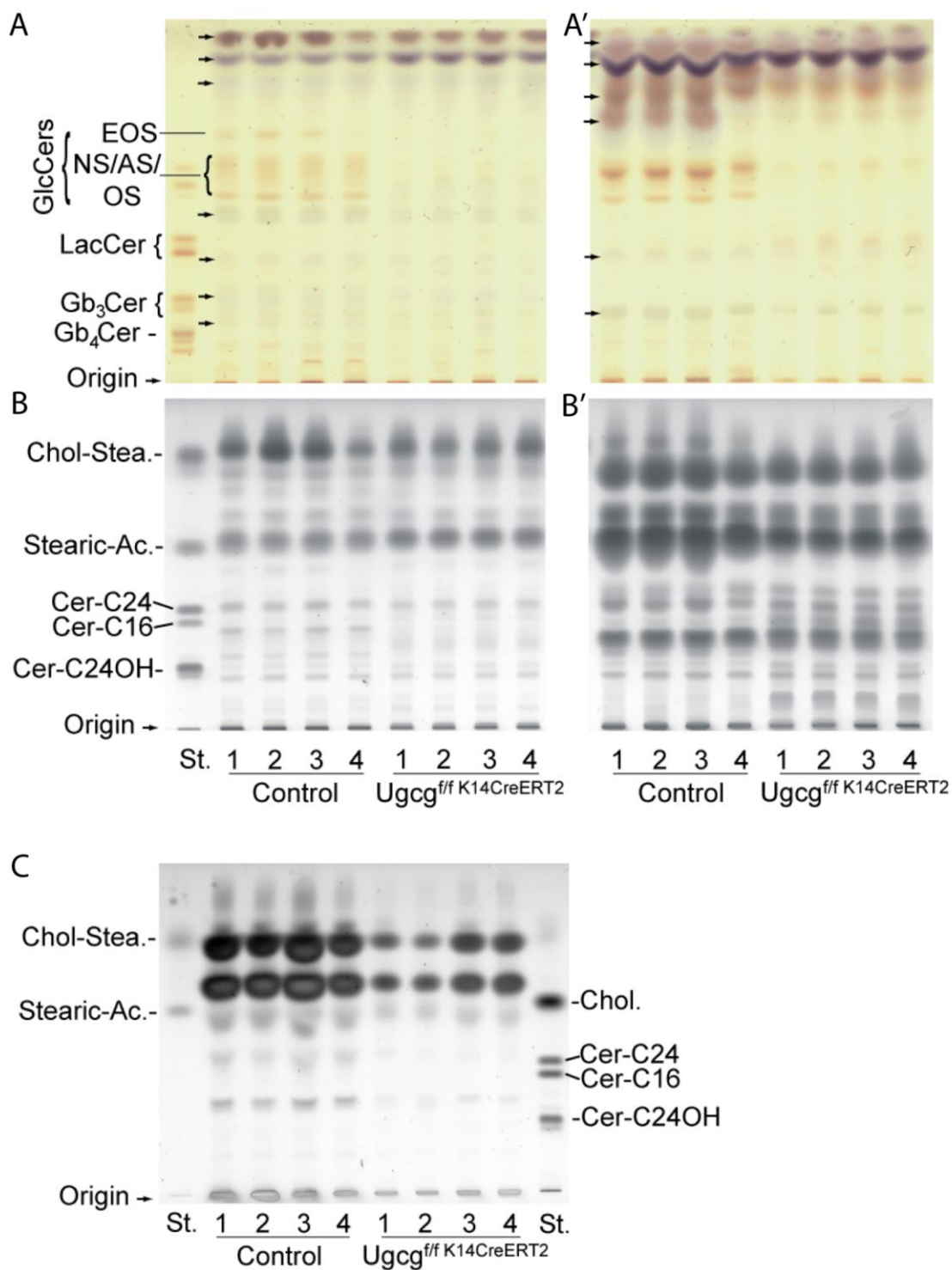
Figure 12. Analysis of epidermal lipids via 1D-TLC for control vs. UGCG-deficient mouse epidermis.

Epidermal sphingolipid composition with regard to freely extractable (**A**, **A′**, **B**, **B′**) and protein-linked sphingolipids (POS-SLs) (**C**) was investigated by separating the lipids according to their polarity. Orcinol staining of GSLs in crude extracts (**A**) and after alkaline treatment (**A′**) revealed a significant reduction of all GlcCers species (NS, AS, OS, EOS) in mutant epidermis. Copper staining of extractable Cers (**B**, **B′**) showed quantitative differences in the Cer profiles for $Ugcg^{f/f\,K14CreERT2}$ vs. controls. POS-SLs (**C**) were drastically reduced in epidermal extracts of $Ugcg$ mutants.
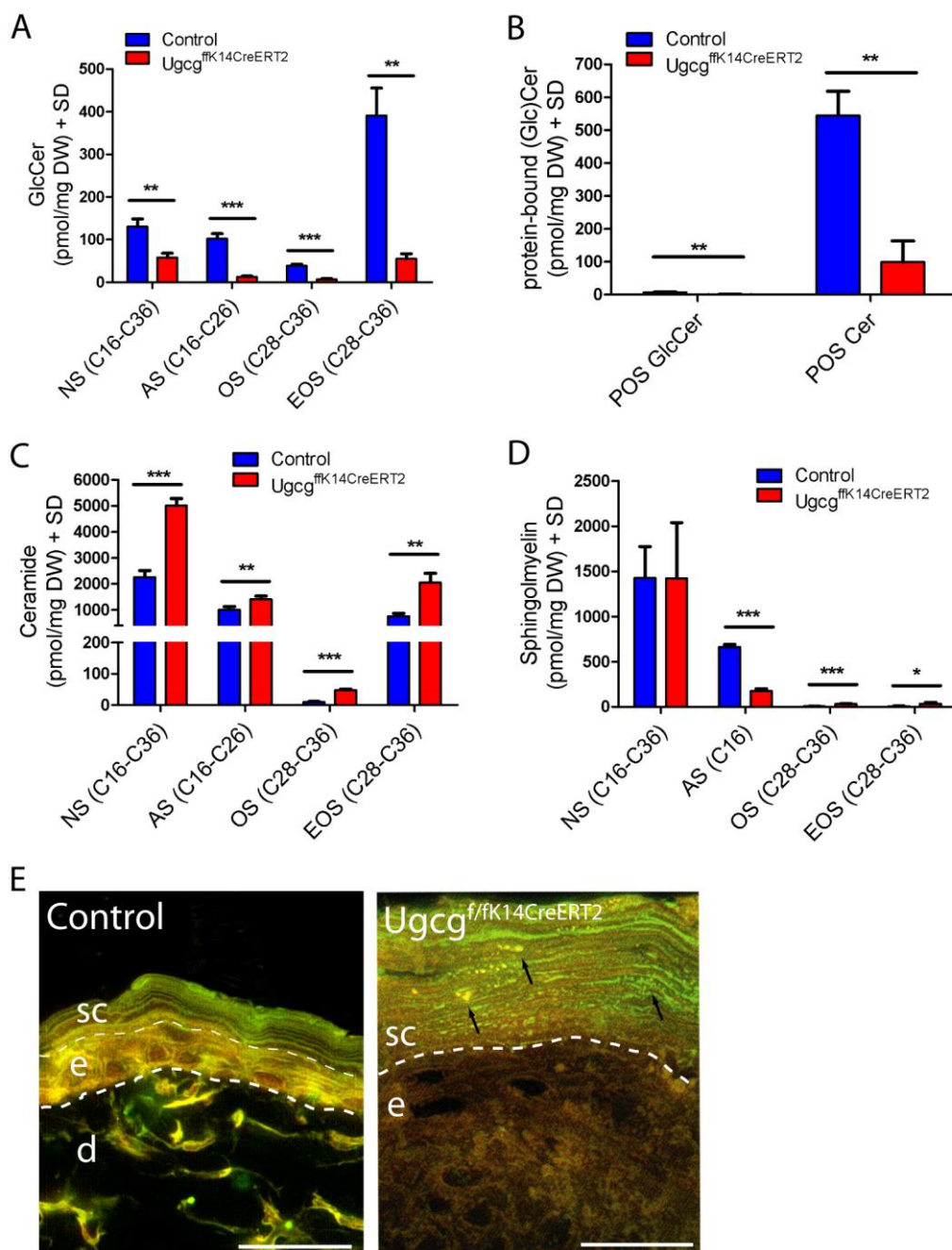
Figure 13. Mass spectrometric analysis of epidermal sphingolipids and comparison of the lamellar lipid structure of the SC for control vs. UGCG-deficient mouse epidermis.

Epidermal sphingolipids were quantified by LC-ESI MS/MS, showing that free GlcCers (**A**) as well as protein-linked species (POS-GlcCers) (**B**) were significantly reduced in the epidermis of $Ugcg^{f/f\,K14CreERT2}$ mutants. The corresponding Cers (**C**) were significantly increased in mutants compared to controls. Among the sphingomyelins (**D**) the levels of C16 to C36 nonhydroxylated species (NS) were the same in mutants and controls, whereas the low levels of ω-hydroxylated ULC-SMs (OS) significantly increased in mutants. Surprisingly, C16 α-hydroxylated SMs (AS) significantly decreased. Under LM (**E**) Nile Red-stained cryosections alterations in the lipid constitution resulted in an abnormal lamellar lipid structure in mutant stratum corneum (SC). Lentil-like lipid aggregates within the lamellae of corneocytes were seen by Nile red staining (black arrows). Mean values ± SD are shown for $n = 4$; differences in group means are significant with $p < 0.05$ (*), $p < 0.01$ (**), or $p < 0.001$ (***).

3.2.3   GlcCer depletion leads to a significant loss of protein-linked Cers and irregular lipid lamellae in the stratum corneum

Quantification of sphingolipids by mass spectrometry (LC-ESI MS/MS) corroborated the results obtained by TLC. Free extractable GlcCers (NS, AS, OS, EOS) were significantly reduced by ca. 80% (Figure 13 A.). The largest reduction (by weight) of ω-hydroxylated (ωh) GlcCers was observed for EOS species with hC32:0, hC34:0 or hC36:1 FAs (see Appendix Figure A3), which are generally the most abundant ωh-GlcCer species in healthy skin (Doering et al., 1999a). Here the prefix h is used to denote a hydroxylated FA, whereby MS can normally only distinguish the number of hydroxyl groups (by mass) but not their positions. Generally, the FAs for epidermis SLs will be hydroxylated in position α for chain lengths C16 to C26 or in the terminal position ω for > C26.

An even larger reduction (by 82%) was observed for POS-Cers and the few POS-GlcCers containing hC32:0 and hC34:1 FAs, essential barrier lipids (Figure 13 B and Appendix Figure A4 B). The POS-Cers containing hC32:0 and hC34:1 FAs were the most prominent in control skin but showed the highest reduction in mutants (Figure A3 B). Loss of POS-Cers has been observed in several human skin diseases such as HI and AD (Akiyama et al., 2005; Macheleidt et al., 2002; Zuo et al., 2008), underlining the importance of these species for epidermal barrier function.

GlcCer-deficient skin showed a significant increase (by 200%) in all free extractable Cers (NS, AS, OS, EOS) (Figure 13 C) with FA composition similar to that of the lost GlcCers. Among the ωh-Cers, EOS with FAs hC34:1, hC32:0, and hC36:1 were the most abundant in control skin (Figure A3). For EOS-Cers in mutant epidermis, the order of decreasing FA abundance was hC34:1, hC32:1, hC36:1, hC32:0, hC34:2. For the NS- and AS-Cers in mutant skin, the most abundant FAs were C24:0, hC16:0, C16:0, C26:0 and C22:0, in decreasing order (Figure A4).

The SMs in mutant vs. control mice showed less uniform trends. Total NS-SMs did not change significantly (Figure 13 D), while the reduction of NS-SMs containing C17:0, C23:0 or C30:1 FAs and AS-SMs with hC16:0 was statistically significant (Figure A4 C). In contrast, the minor amounts of OS- and EOS-SMs were significantly elevated in mutants (Figure 13 C, Figure A3 D). The quantitative mass spectrometry data for the NS-, AS-, OS- and EOS-SLs are listed in Table A1.

The observed alterations in epidermal SLs, in particular in barrier lipids (OS, EOS, POS), led us to the investigation of the SC lamellar lipid organization. Nile Red staining on cryosections displayed orderly structured lipid lamellae in controls, whereas mutant SC was interspersed with granular-like lipid aggregates within disordered lamellar sheets (Figure 13 E).

3.2.4   *Ugcg* mutants develop an ichthyosiform skin phenotype marked by hyperkeratosis and leakiness of the water permeability barrier

$Ugcg^{f/f\,K14CreERT2}$ mice were easily distinguishable from controls in week 3 of TAM induction. The mutants exhibited sticky fur, dark tails and pruritus (data not shown). Dry, flaky skin became visible at the end of week 3 (Figure 14 A). *Ugcg* mutants displayed a hyperstratified and hyperkeratotic epidermis (Figure 14 B and Appendix Figure A2) with a fivefold increase in epidermal thickness (Figure 14 C).

Significant weight loss of mutants was observed parallel to increasing TEWL in week 3 (Figure 14 D,E), indicating the onset of WPB disruption. Mutant mice sufficiently compensated the high water loss by increased water uptake (Figure 14 F). As a consequence of high water evaporation via the skin, the core body temperature (Figure 14 H) as well as the surface temperature (Appendix Figure A5) of mutant mice was reduced in week 4. In addition, impaired barrier function was demonstrated by a significant increase in SC pH, (pH 6.1 in mutant versus pH 5.1 in control mice) (Figure 14 G), which explains in part the visible loss in SC cohesion and obvious desquamation defect of mutant epidermis.

3.2.5 Barrier loss provokes keratinocyte hyperproliferation and chronic inflammation

Hyperkeratosis in UGCG-deficient skin was associated with an increase, relative to controls, in the number of Ki-67-positive cells in basal, para- and lower suprabasal layers of the epidermis as well as in hair follicles (Figure 15 A–C). Furthermore, immune cell activation upon epidermal barrier disruption resulted in an increase of ER-HR3-positive dendritic cells/macrophages in mutant skin (Figure 15 C–F). No significant difference in granulocytes and mast cells was observed between control and mutant mice (Figure 15 G–I). TUNEL staining revealed apoptotic nuclei in the lower and upper SC (Appendix Figure A6) indicating a delay in corneocyte maturation but not an increase in apoptosis. Control samples were TUNEL-negative.
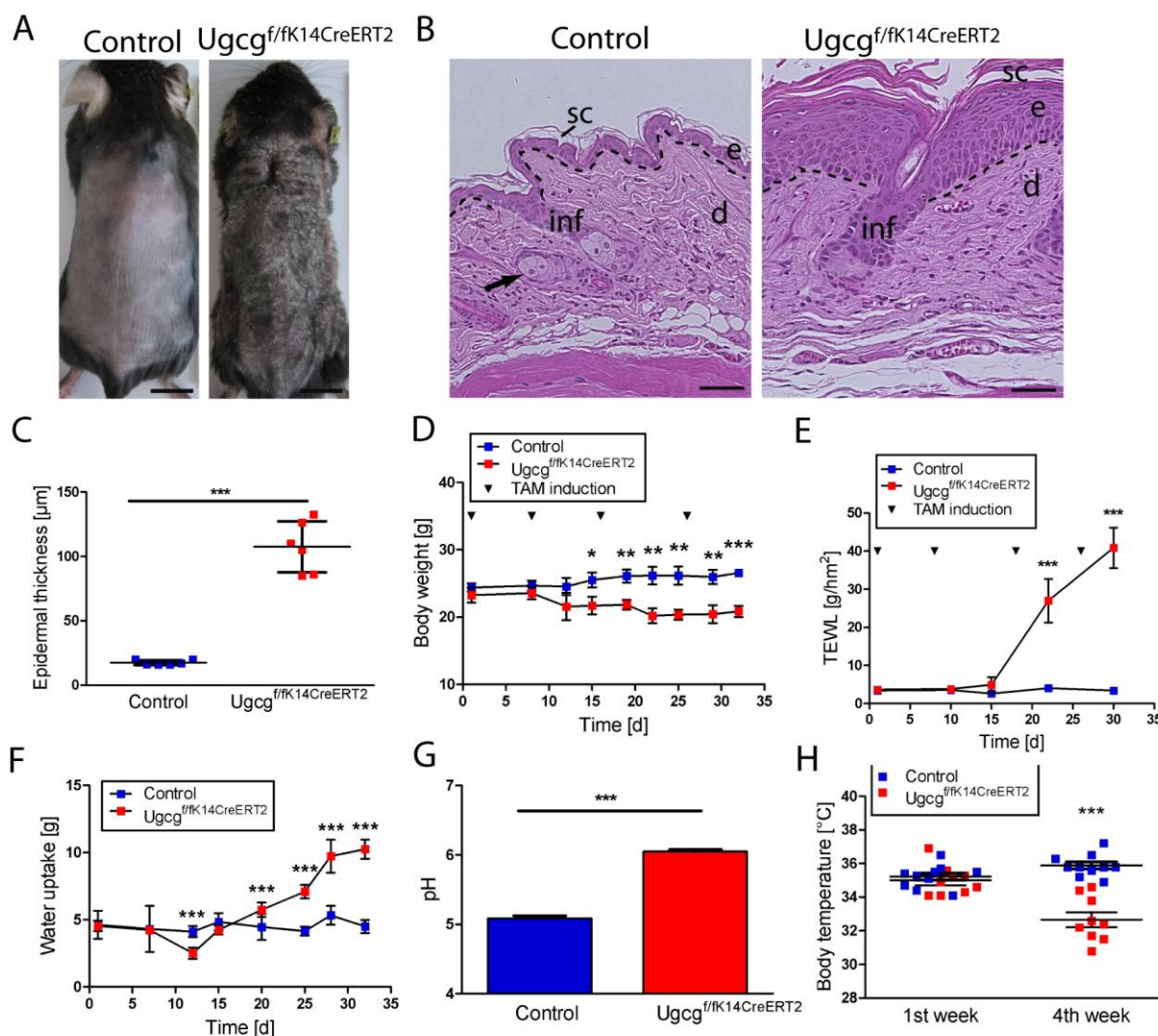
Figure 14. Phenotype analysis of control and *Ugcg^{f/f K14CreERT2}* mice.

(**A**) *Ugcg* mutants showed dry, scaling skin, greasy fur and impaired hair growth at week 3 of TAM induction; scale bar = 0.5 cm. (**B**) LM with H&E staining revealed a hyperstratifed epidermis in mutants (scale bar = 50 µm) with a fivefold increase in epidermal thickness (**C**) in week 4 of induction. The body weight of mutants began to decrease by week 2 (**D**). In week 3 the epidermal barrier failed, as reflected by significant increase of the TEWL (**E**), water uptake (**F**) and stratum corneum (SC) pH (**G**). The body temperature of mutants decreased in week 4 (**H**). In the micrographs dashed lines indicate the dermal/epidermal junction zone; the arrow indicates a sebaceous gland; e = epidermis; d = dermis; inf = infundibulum; sc = stratum corneum; mean values ± SD are shown with significance of differences $p < 0.05$ (*); $p < 0.01$ (**); $p < 0.001$ (***).
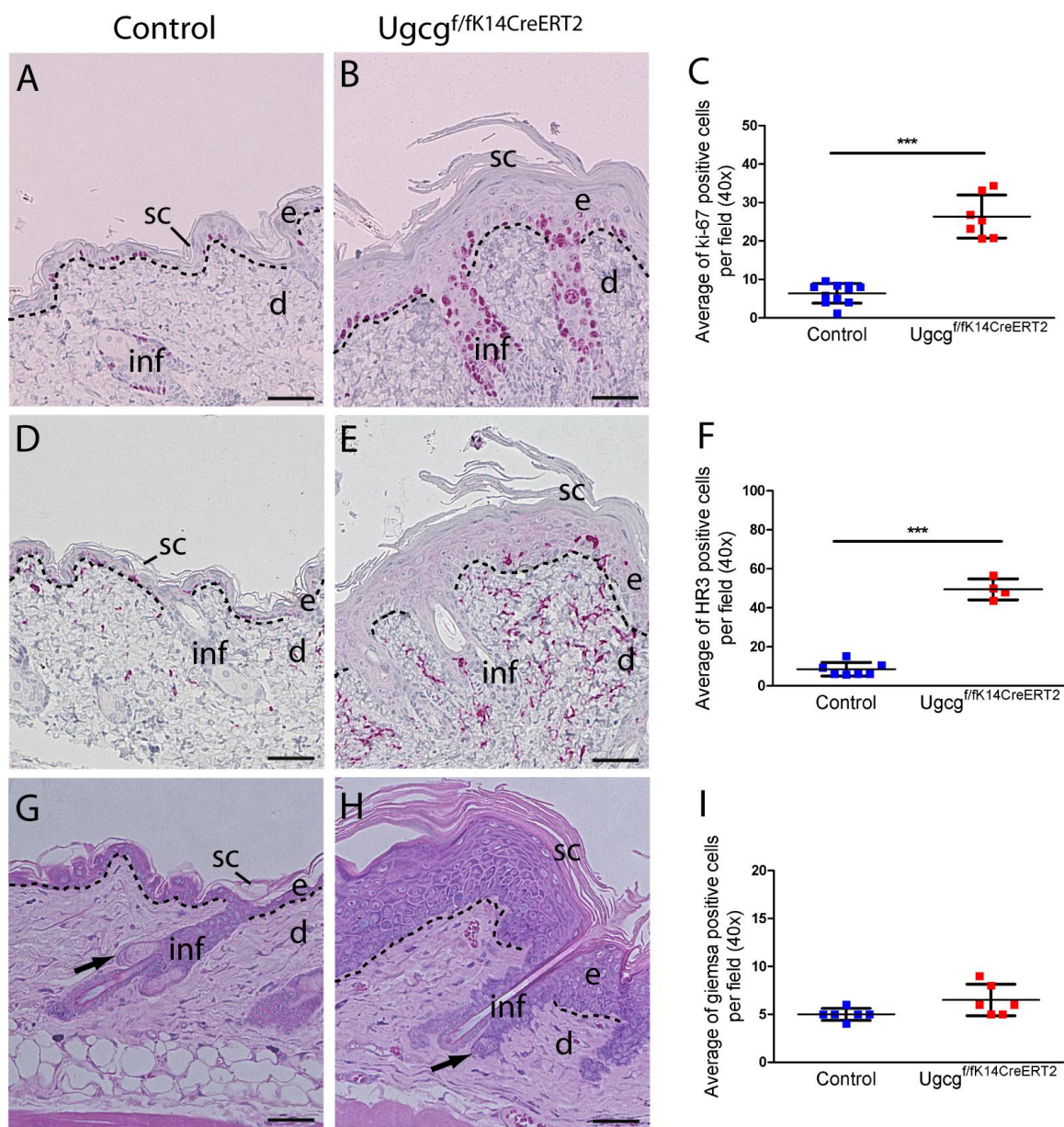
Figure 15. *Ugcg^{f/f K14CreERT2}* **mouse skin is hyperproliferative and exhibits increased apoptosis and chronic inflammation.**

(**A–C**) Keratinocyte proliferation, as judged by the number of Ki-67-positive cells, was markedly enhanced in mutant skin. (**D–F**) In addition, macrophages and dendritic cells (ER-HR3 staining) were significantly increased, whereas no differences were observed for granulocytes and mast cells (**G–I**; Giemsa staining). Dashed lines indicate the dermal/epidermal junction zone; arrows indicate sebaceous glands; e = epidermis; d = dermis; inf = infundibulum; sc = stratum corneum; scale bars = 50 µm; mean values ± SD are shown; significance of difference, $p < 0.001$ (***).

3.2.6 Partial recovery of epidermal barrier dysfunction implies the action of hair follicle stem cells

Long-term Cre-recombinase (Cre) activity was analyzed in Rosa26/CreERT2 mice in order to investigate the enzyme's persistence after TAM induction by injection on day 1 and day 8 (Figure 16 A). Cre activity was observed in the epidermis of Rosa26 mutants at all investigated time points but not in control skin. The highest activity was observed in weeks 2 and 4 after TAM induction. Thereafter, Cre-activity decreased in the epidermis, but persisted even after 12 weeks. However, the infundibulum lost positivity approximately 8 to 10 weeks after TAM induction.

Based on these observations, we decided to investigate whether or not $Ugcg^{f/f\,K14CreERT2}$ mice recover from the WPB defect over time after TAM induction. Hence, TAM-induced mutants were monitored over three months, and the TEWL, water uptake and body weight were documented (Figure 16 B–D).

Barrier disruption occurred in the end of week 3 (Figure 16 B), indicated by a constantly increasing TEWL until week 6. From day 38 onward, water loss and water uptake regressed but remained significantly elevated even three months after TAM induction. In contrast, TEWL and water uptake values for controls remained at baseline. Body weight gain was slightly lower for mutants vs. controls but not significantly different (Figure 16 D).

In line with the observed decline of Cre-activity in Ros26 reporter mice (in particular within the infundibulum), we observed a recovery of the skin phenotype of $Ugcg$ mutants. Dry, scaling skin persisted mostly at locations with low hair follicle density, e.g., ear, paw and tail, implying the action of K14-negative hair follicle stem cells in epidermal barrier restoration. Nevertheless, the permeability barrier did not fully recover, as evidenced by sustained TEWL and water uptake. Furthermore, weight loss of mutant mice during 6-h water deprivation experiments was documented once a week for one month and at the end of the long-term monitoring period (Figure 17 A–E). In $Ugcg$-mutants, weight loss increased significantly from the third week onwards as compared to controls. These results demonstrated the lack of epidermal permeability barrier restoration in GlcCer-depleted skin.
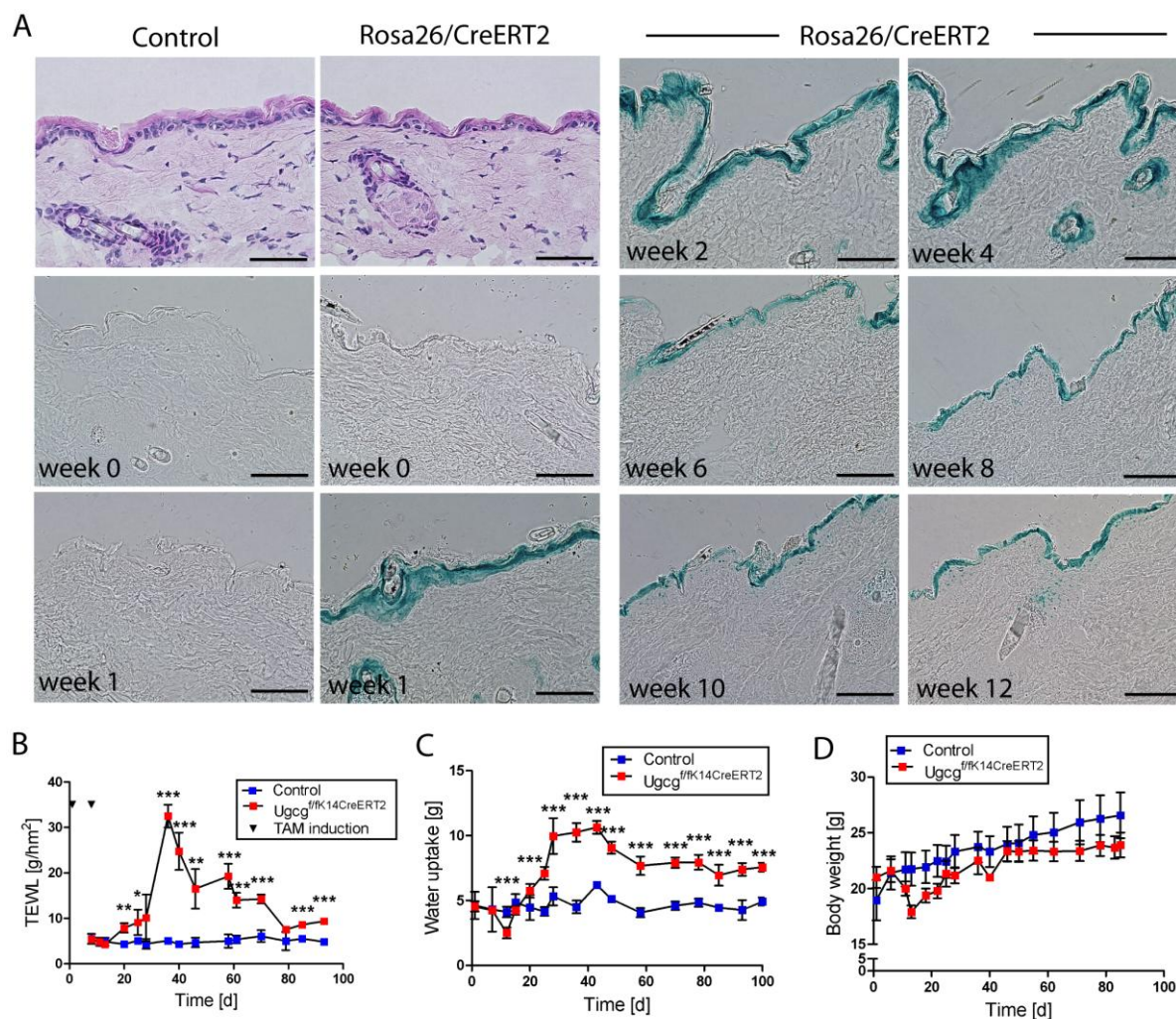
Figure 16. Continuous Cre-activity sustains leakiness of the WPB.

(**A**) X-gal staining was performed to investigate long-term Cre-recombinase activity in K14CreERT2 mice by crossing K14CreERT2⁻ with Rosa26 reporter mice (Rosa26/K14CreERT2). Cre-activity was strongest in epidermis and hair follicles from week 1 to 4. The staining intensity decreased slightly until week 12, and hair follicles stained negative approximately 8 to 10 weeks beyond TAM induction. *Ugcg* mutants and control mice were induced with TAM (two injections) and monitored over the same time period as reporter mice. From the onset of barrier pertubations (week 3), transepidermal water loss (TEWL; **B**) and water consumption (**C**) were significantly higher in mutants. Body weight gain (**D**) was similar in mutant and control mice. Scale bars = 50 µm; mean values ± SD are shown for $n \geq 4$; significance levels are $p < 0.05$ (*); $p < 0.01$ (**); $p < 0.001$ (***).
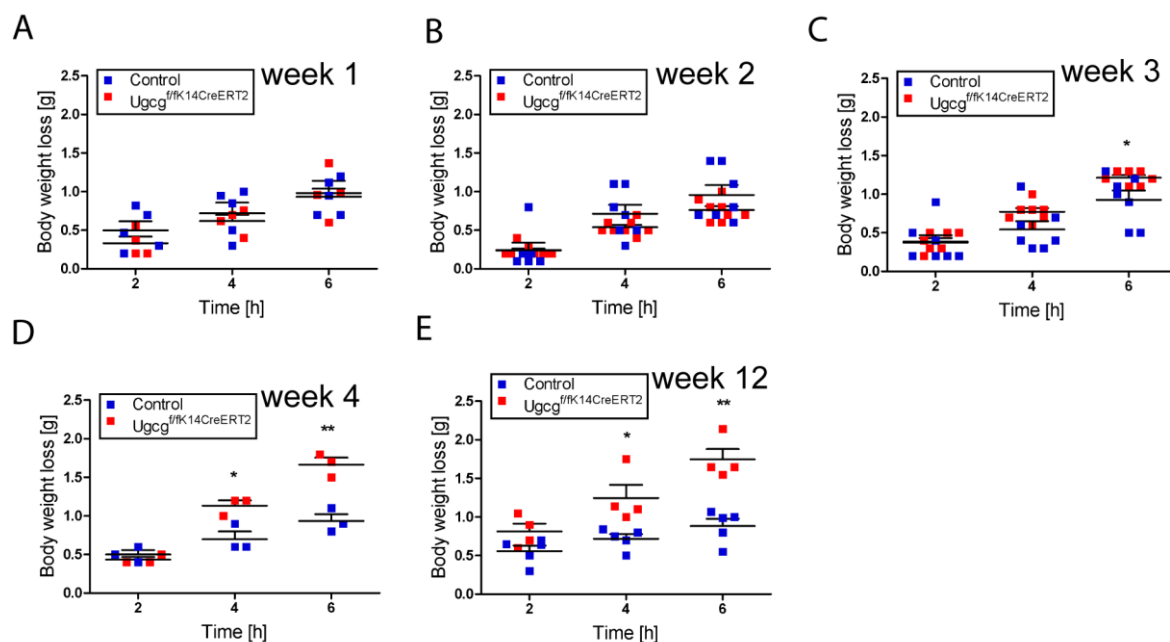
Figure 17. Body weight loss is significantly higher for UGCG-deficient mice vs. controls during 6-h water deprivation.

Water deprivation experiments for one 6-h period in weeks 1-4 and 12 revealed that weight loss for mutants vs. controls was initially the same (**A, B**) but increased significantly following the onset of WPB loss in week 3 of TAM induction (**C–E**). Data for individual mice and mean values ± SD are shown; significance of differences: $p < 0.05$ (*); $p < 0.01$ (**).

3.2.7   Early keratinocyte differentiation and epidermal cohesion is disturbed

Epidermal differentiation is a complex signaling and remodeling process in which proliferating basal keratinocytes exit the cell cycle to move upwards and continuously differentiate until they become keratin-filled anucleate corneocytes, which finally shed off during desquamation (Candi et al., 2005). Immunofluorescence (IF) microscopy was used to characterize keratinocyte maturation by means of the keratin expression pattern (red fluorescence). Keratin K14 was normally expressed in the basal layer keratinocytes in control skin but was additionally present in all suprabasal layers in the GlcCer-deficient skin of UGCG-deficient mice, indicating abnormal keratinocyte differentiation (Figure 18 A,B). Keratin K10 is expressed in the differentiated layers of the SS and SG in control skin. In mutants K10 was distributed in the normal manner, including the fivefold multilayered epidermis (Figure 18 C,D). Keratin K6, a stress-induced intermediate filament, was present in all nonapoptotic epidermal layers in the mutant, reflecting the hyperproliferative state of GlcCer-deficient epidermis, but was absent in control skin (Figure 18 E,F). Abnormal keratinocyte differentiation was further demonstrated by the presence of numerous nuclear remnants in SC layers of mutant skin, indicating not only the inability of GlcCer-deficient keratinocytes to terminally differentiate and shed off during desquamation but also an inability to transit into a state of "full apoptosis" (Figure 18 B,F). In summary, the epidermis of *Ugcg* mutants appeared as a disorganized hyperproliferative layer.
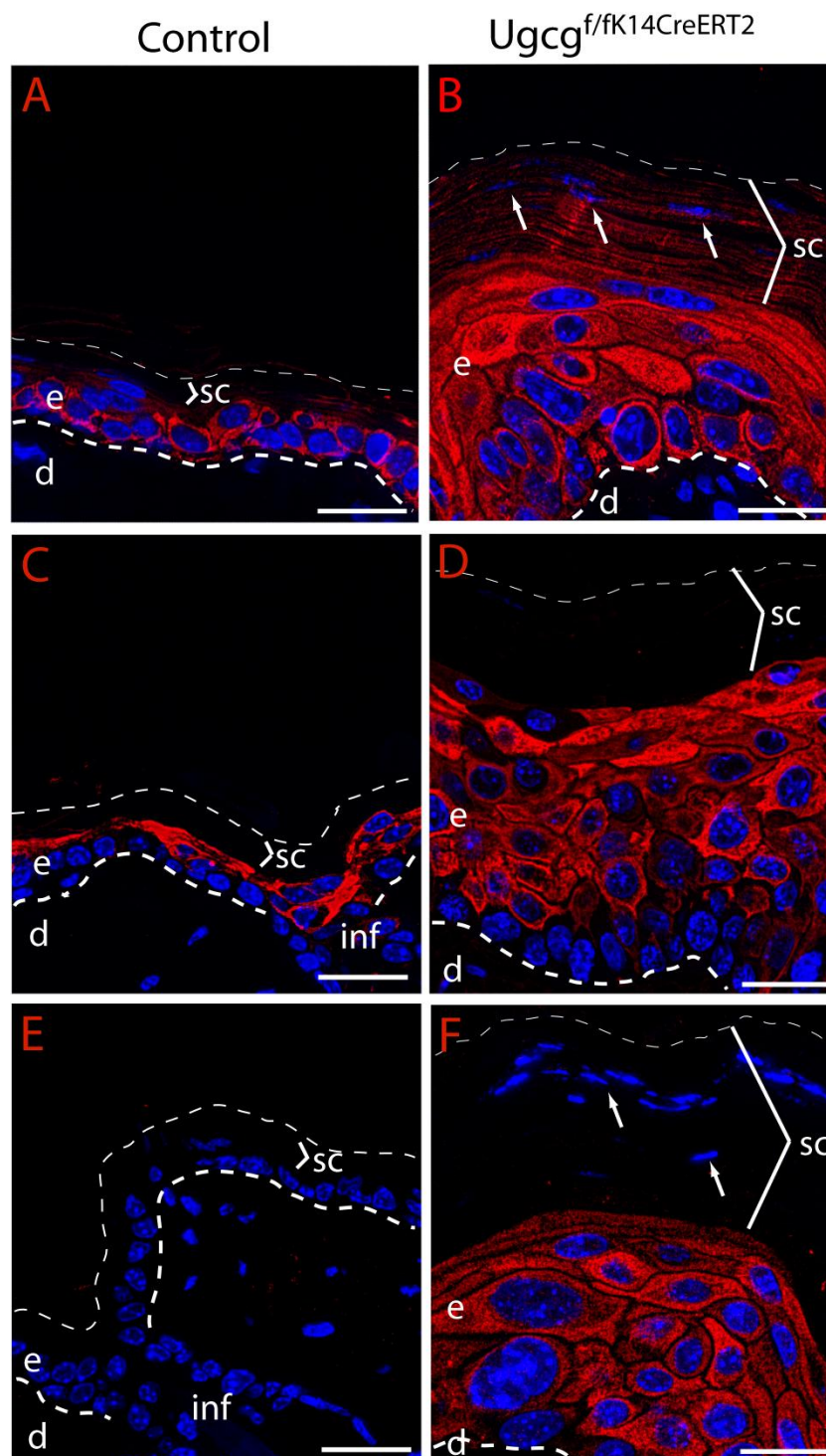
Figure 18.   Early keratinocyte differentiation is delayed in $Ugcg^{f/fK14CreERT2}$ mice vs. controls.

Immunofluorescence (IF) microscopy of mouse skin sections (red = a specific keratin antibody, blue = nuclear staining with DAPI). In control epidermis (**A**) keratin K14 was restricted to the basal layer, whereas in UGCG-deficient mutants (**B**) K14 was expressed in all epidermal layers. Keratin K10 distribution in the SS was normal (**C**), but a larger number of cell layers was evident in mutant epidermis (**D**). Concomitant with the observed hyperkeratosis, stress-induced keratin K6 was detected in mutant epidermis (**F**) but not in controls (**E**). Note the nuclear remnants present in stratum corneum layers of UGCG-deficient skin, reflecting the delay in terminal keratinocyte differentiation (**B**, **F**; arrows). e = epidermis; d = dermis; inf = infundibulum; sc = stratum corneum; scale bars = 50 µm.

Anchorage of the basal epidermal layer to the underlying basement membrane (BM) is imperative for normal keratinocyte maturation and epidermal renewal. Such anchorage is ensured by heterodimeric transmembrane receptors, so-called integrins, located in the PM of basal (and outer root sheet) keratinocytes. They are composed of an α- and β-subunit connecting the keratin cytoskeleton with adhesive proteins of the BM. Integrin-α6β4 (ITGA6B4) is one of the most abundant integrins in basal keratinocytes, connecting the keratin cytoskeleton with adhesive proteins in the BM such as laminin-5 (LAMA5), thereby regulating cell adhesion, proliferation and differentiation (Watt, 2002a).

Deletion or a loss-of-function mutation (in either subunit) of the integrin has been related to the autosomal recessive skin disorder epidermolysis bullosa, causing severe epidermal blistering in humans and mice (Ashton et al., 2001). Furthermore, overexpression of ITGA6B4 is a known feature of several papillomas and squamous cell carcinomas (Owens et al., 2003).

IF microscopy of ITGA6 and its binding partner LAMA5 indicated that their expression patterns were the same in skin from UGCG-deficient mice and controls (Figure 19) and that these proteins are not significantly involved in the observed differentiation defect in mutant skin. Nevertheless, determination of the exact cellular localization of these proteins was difficult with IF microscopic analysis alone; techniques with higher resolution, such as electon microscopy (EM), should be employed.

To closer examine the epidermal integrity of mutant skin, tight junctions (TJs) and desmosomes were investigated with IF microscopy. The expression of TJ protein claudin 1 (CLDN1) (Figure 20 A,B) and the desmosomal cadherins desmoglein 1 and desmoglein 2 (DSG1, DSG2) (Figure 20 C,D) were detectable in all vital epidermal layers in controls – with DSG2 in the basal and DSG1 in the suprabasal strata. Note, the employed desmoglein antibody labeled both isoforms; (Simpson et al., 2011). Compared to controls, mutant skin showed a slightly weaker punctuate staining which was more concentrated at the cell margins of the large hyperproliferative cells and was practically absent in the basal layer (Figure 20 D), indicating a reduction of DSG2. Quantitative differences of CLDN1 and DSG1/2 in GlcCer-depleted epidermis vs. controls were corroborated by western blotting (Figure 21 A) and correlate with the leakiness of the epidermal junction barrier in mutants. Furthermore, the desmosomal catenin desmoplakin (DSP), was strongly expressed in all viable strata in mutant epidermis, as demonstrated by its typical diffuse punctuate staining pattern in the basal and spinous layers, and was more concentrated at cell membranes in the upper layers (Figure 20 E,F). These results suggest that deficient junction formation (regarding CLDN1 and DSG2) contributes to the epidermal barrier loss as well as the leakiness of the SC lipid barrier.
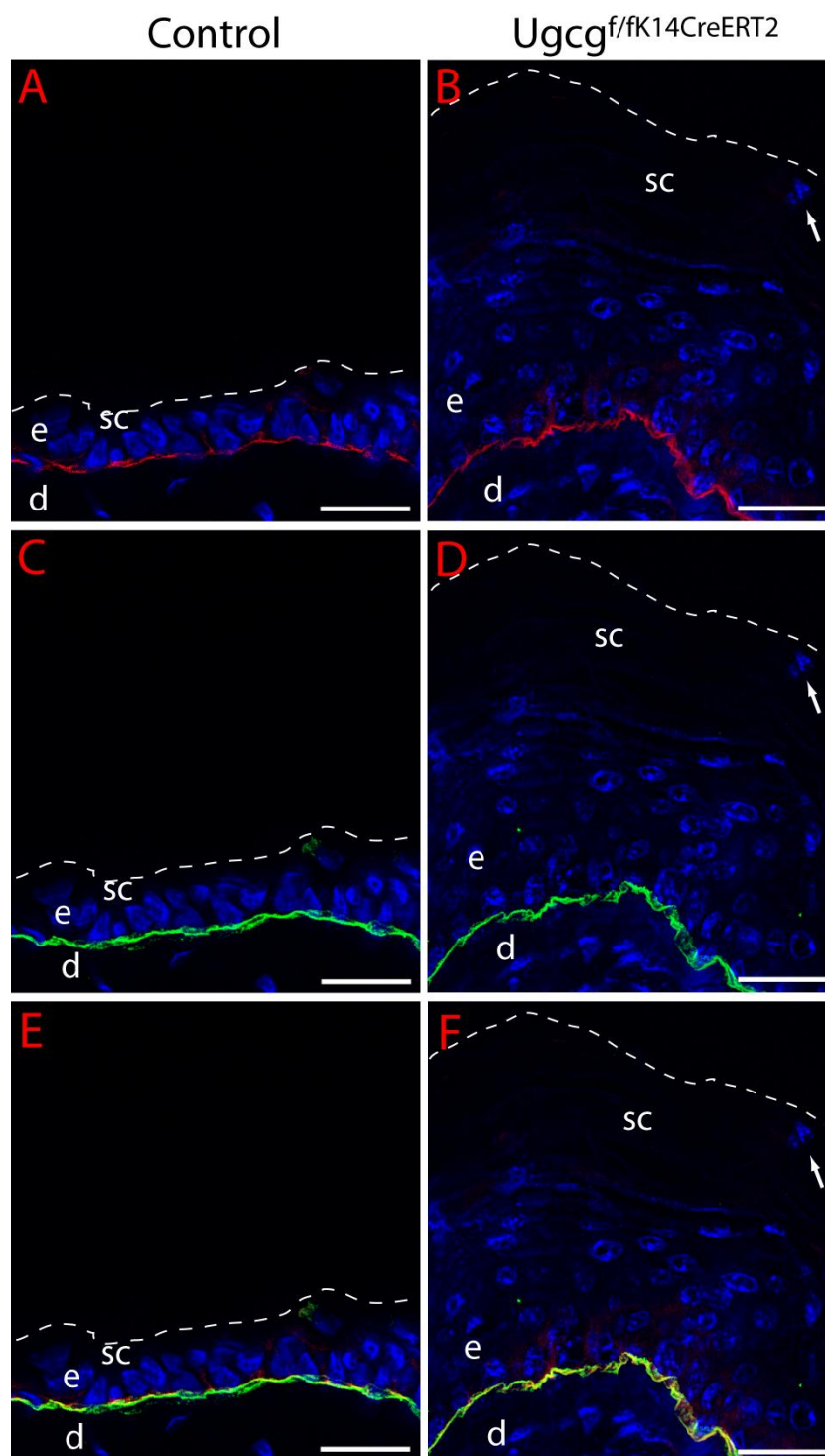
Figure 19. Anchorage of basal layer keratinocytes to the underlying basement membrane via integrin and laminin is not altered in $Ugcg^{f/f\,K14CreERT2}$ mutants vs. controls.

IF microscopy of mouse skin sections from UGCG-deficient mutants vs. controls. Single IF staining of basal cell-specific integrin-α6 (red; **A**, **B**) or its basement membrane binding partner laminin-5 (green; **C**, **D**) were performed. Overlays of the two types of protein stainings are shown in **E**, **F** to demonstrate co-localization. Nuclear staining with DAPI is shown in blue. No differences in the protein staining pattern between control and UGCG-deficient skin were observed; e = epidermis; d = dermis; sc = stratum corneum; scale bars = 50 µm.
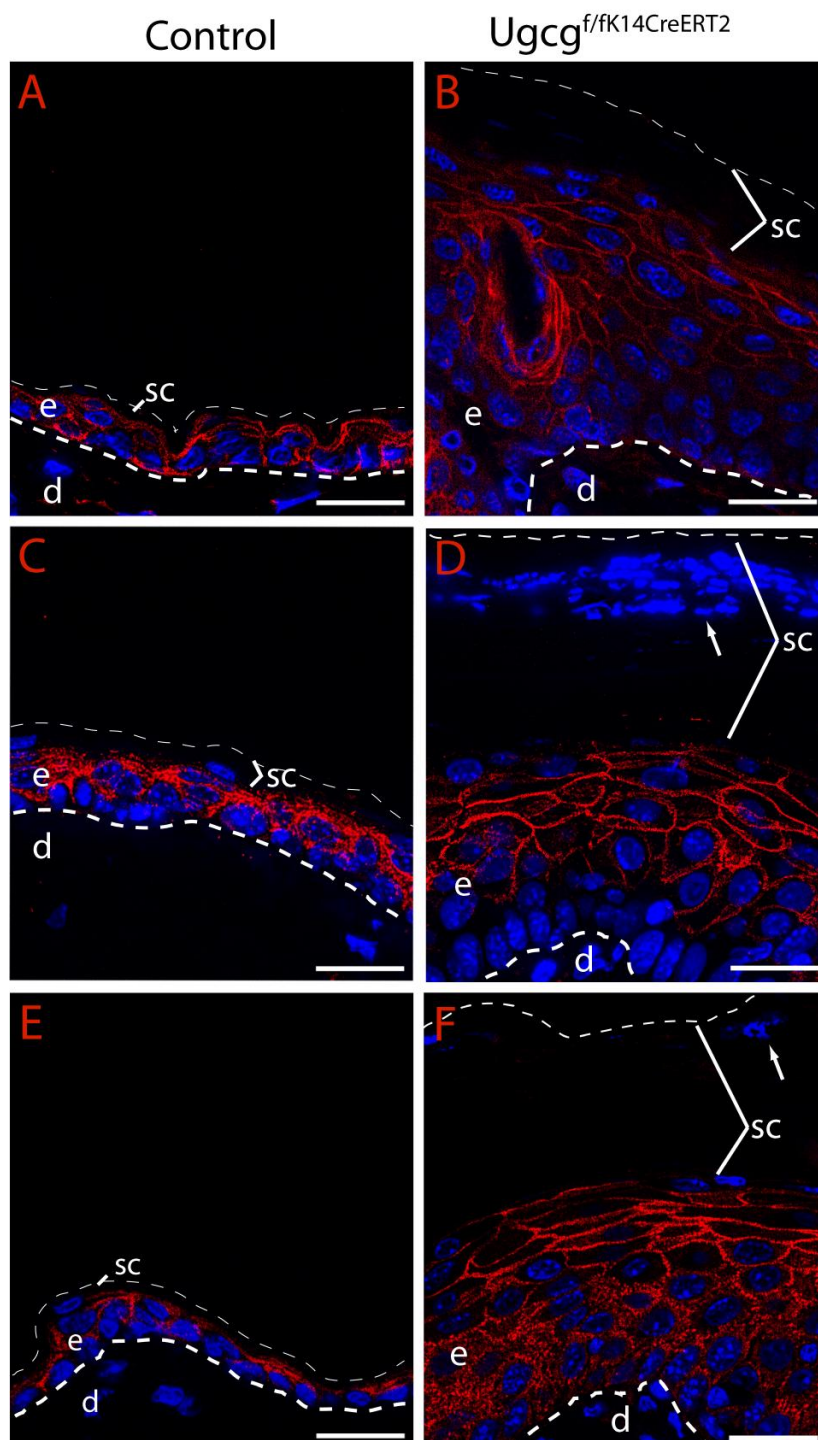
Figure 20.   Malformation of the junction protein barrier in *Ugcg*^*f/f K14CreERT2* mutants vs. controls.

IF microscopy of mouse skin sections from UGCG-deficient mutants and controls (red = a specific junction protein antibody; blue = nuclear staining with DAPI). Claudin 1 (**A**, **B**) and desmoglein 1 and desmoglein 2 (**C**, **D**) in SS/SG layers show weaker expression in *Ugcg* mutant epidermis. Desmoplakin (**E**, **F**) was detected as a diffuse cytosolic staining in the lower SS of mutant epidermis. Note the nuclear remnants present in SC layers of UGCG-deficient skin, reflecting the delay in terminal keratinocyte differentiation (**D**, **F**; arrows); e = epidermis; d = dermis; sc = stratum corneum; scale bars = 50 µm.

3.2.8   Corneocyte maturation and cornified envelope formation is impaired

The CE is formed early during corneocyte maturation. Its formation relies on intracellular synthesis of structural proteins which are stored in so-called keratohyalin granules (KGs) in granulocytes, which contain large F-granules (profilaggrin) and small L-granules (loricrin). During cornification, polymeric profilaggrin is processed into monomeric filaggrin (FLG) units, thus regulating the condensation of keratin intermediate filaments in the developing corneocyte. Monomeric FLG is then further processed into hydrophilic free amino acids (AA), which function as natural moisturizing factors (NMFs) and retain water in the SC (Brown and McLean, 2012).

In control skin, profilaggrin (proFLG) and FLG were normally located in the outer SG and SC whereas in mutant epidermis F-granules were present in almost all suprabasal layers, with highest accumulation in the SC (Figure 21 B,C). KGs were more numerous and larger in size throughout SS and SG layers of mutant epidermis vs. controls, suggesting a defect in proFLG synthesis and processing. Immunoblots (Figure 21 A) supported these results: mono-, di- and trimeric FLG (1 FLG, 2 FLG, 3 FLG) as well as polymeric FLG (FLG2) were detected in controls but were strongly reduced in mutants, where other proFLG peptides of abnormal chain lengths accumulated, giving a diffusive staining pattern (Figure 21 A).

During early CE assembly, involucrin (IVL) shifts from the cytosol to become aligned along the PM of granulocytes. At the SG/SC interface, this membrane is gradually replaced by a CE, indicated in control epidermis by the polarized staining pattern of IVL (Figure 21 D). In mutants IVL was strongly expressed in the cytosol of late SS and SG keratinocytes (Figure 21 E), indicating a delay in IVL processing in comparison with controls. Western blotting supported these results by revealing a reduced level of IVL in mutants (Figure 21 A).

Loricrin (LOR) is the major component of the CE (80-85% of total CE weight) and is initially expressed late during CE formation. In control skin, LOR expression appeared late at the SG/SC interface, whereas mutants displayed an earlier strong cytosolic staining for LOR as well as diffuse nuclear staining (Figure 21 F, G), indicating a delay in LOR processing. Western blot results demonstrated a large reduction of LOR expression in mutant epidermis (Figure 21 A). The delay in terminal keratinocyte differentiation (into anucleate corneocytes) was also apparent in the detection of nuclei (blue DAPI staining) in SC keratinocytes (Figure 21 C,G).
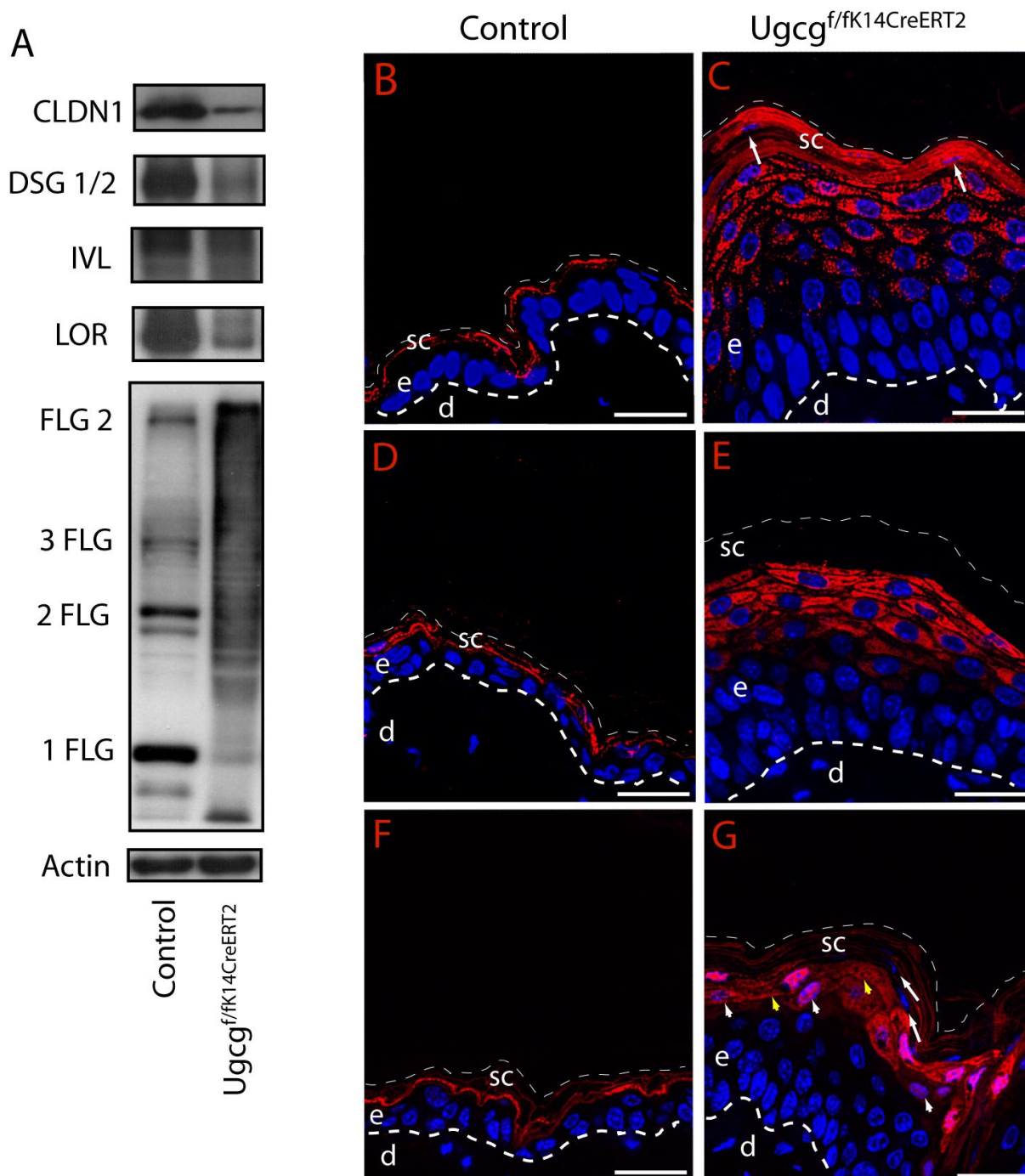
Figure 21. **Impaired cornification and CE formation in** $Ugcg^{f/f\,K14CreERT2}$ **mutants vs. controls.**

Western blot analysis (**A**) confirmed a deficit in protein expression or impaired processing in mutant epidermis. IF microscopy for the terminal differentiation marker (pro)filaggrin (**B**, **C**; red) revealed a strong dotted-like pattern in the upper epidermal layers of mutant skin. Involucrin (IVL) was expressed early in the late stratum spinosum cells in mutants and showed a more cytosolic staining pattern as compared to controls (**D**, **E**; red). Cornified envelope marker loricrin (LOR) (**F**, **G**; red) was strongly expressed in the stratum granulosum and stratum corneum (SC) of mutants. Its staining alternated throughout the granular layer, but clearly encircled the rim of F-granules in control and mutant skin (**G**, yellow arrows). Note the nuclear remnants (blue DAPI stain) in mutant SC (**C**, **G**; white arrows). Dashed lines indicate the dermal/epidermal junction zone and the apical margin of the SC, respectively; e = epidermis; d = dermis; scale bars = 50 µm.

3.2.9 Wound healing of full-thickness skin wounds is delayed in GlcCer-depleted skin and skin grafts

An *in vivo* wound healing model was chosen to investigate the function of GlcCers in epithelial differentiation. Wound healing experiments were performed in control and UGCG-deficient skin and skin grafts to investigate whether GlcCer-depletion affects reepithelialization. Transplantation experiments were conducted to exclude effects of a systemic factor on the outcome of wound healing. Control mice with grafted skin from either wild type or $Ugcg^{f/f\,K14CreERT2}$ litters were TAM-induced five weeks after transplantation, when grafts were fully adapted and hair growth was observed (Figure 22 A). Skin grafts were shaved previous to initiation of TAM induction (Figure 22B). After three weeks of induction, UGCG-deficient grafts were marked by dry scaly patches and pruritus (Figure 22), as observed in non-transplanted mutant mice (Figure 14 A). The same TAM induction and wound healing protocol was used for grafted and non-grafted mice (see Figure 9).

Full thickness skin wounds (5 mm in diameter) were applied on the lower back of control and mutant mice. Closure of wounds was significantly delayed at all investigated time points in *Ugcg* mutants vs. controls (Figure 23 A-J). Proliferation was investigated by Ki-67 staining and was significantly higher in mutant skin vs. controls in the early (6 h) and late (day 6) wound healing phase (Figure 23 K). Proliferation in controls at day two of wound healing increased as a normal response to injury.

To investigate the inflammatory response to wounding, HR3 and Giemsa stainings were performed (Figure 23 L,M). HR3-positive dendritic cells and macrophages were significantly increased in wound sites of mutant skin at all time points (Figure 23 L). In contrast, Giemsa-positive cells were not significantly different between the two groups, at least not during the early wound healing phase, but seemed to be slightly elevated in UGCG-deficient skin (Figure 23 M). At day 2, granulocyte numbers in control skin increased as a normal response to wounding, and also regressed in the late healing phase (at day 6). However, Giemsa-positive cells did not increase in mutant skin during the early wound healing phase (at day 2), indicating a delayed or impaired response to wounding. At day 6, mainly Giemsa-positive mast cells (not granulocytes) remained slightly elevated in mutant skin as a significant effect (Figure 23 M). In sum, dendritic cells and macrophages seemed to be the driving cells of an altered inflammatory response to wounding in *Ugcg* mutants, resulting in a delay in wound closure.

IF staining for the early differentiation markers keratin K14 and K10 revealed reepithelialization of the wounds to be completed in controls (Figure 24 A,C) and corresponding grafts (Figure 24 E,G) at day 9 post wounding. In contrast, wounds of GlcCer-deficient skin (Figure 24 B,D) and skin grafts (Figure 24 F,H) were not closed, as indicated by the lack of keratin K14- and K10-positive cells in the former wound center.
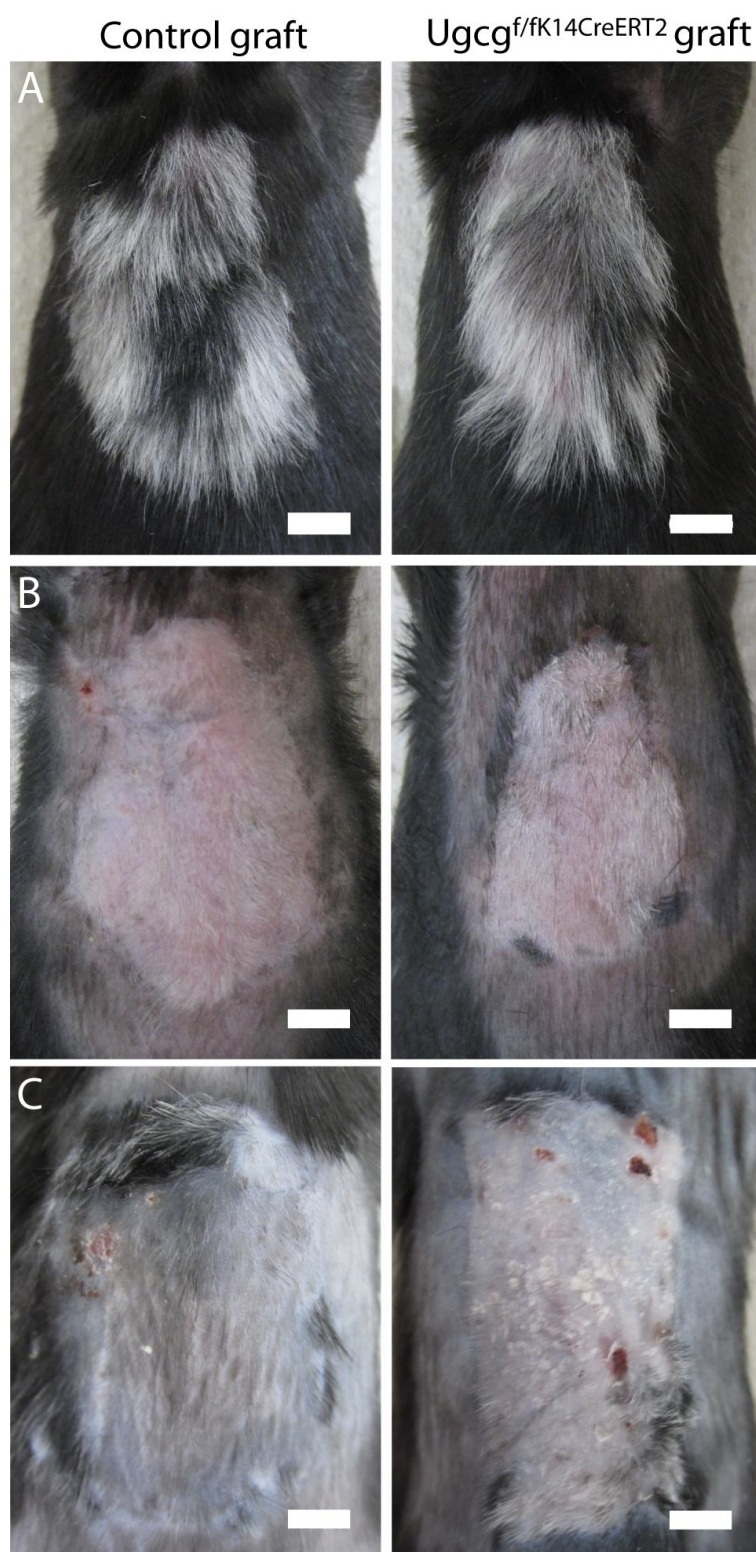
Figure 22. Skin grafts before and during TAM induction.

(**A**) Grafted skins were fully adapted five weeks post transplantation as indicated by hair growth in both control and mutant isografts. (**B**) Mice were shaved before TAM injection in week 6 after grafting. (**C**) Three weeks later, control grafts appeared normal, whereas UGCG-mutant grafts displayed dry, scaly patches and impaired hair growth. Due to pruritus, scratching led to sporadic crusts in lesional skin (**C**). Scale bars = 0.5 cm.
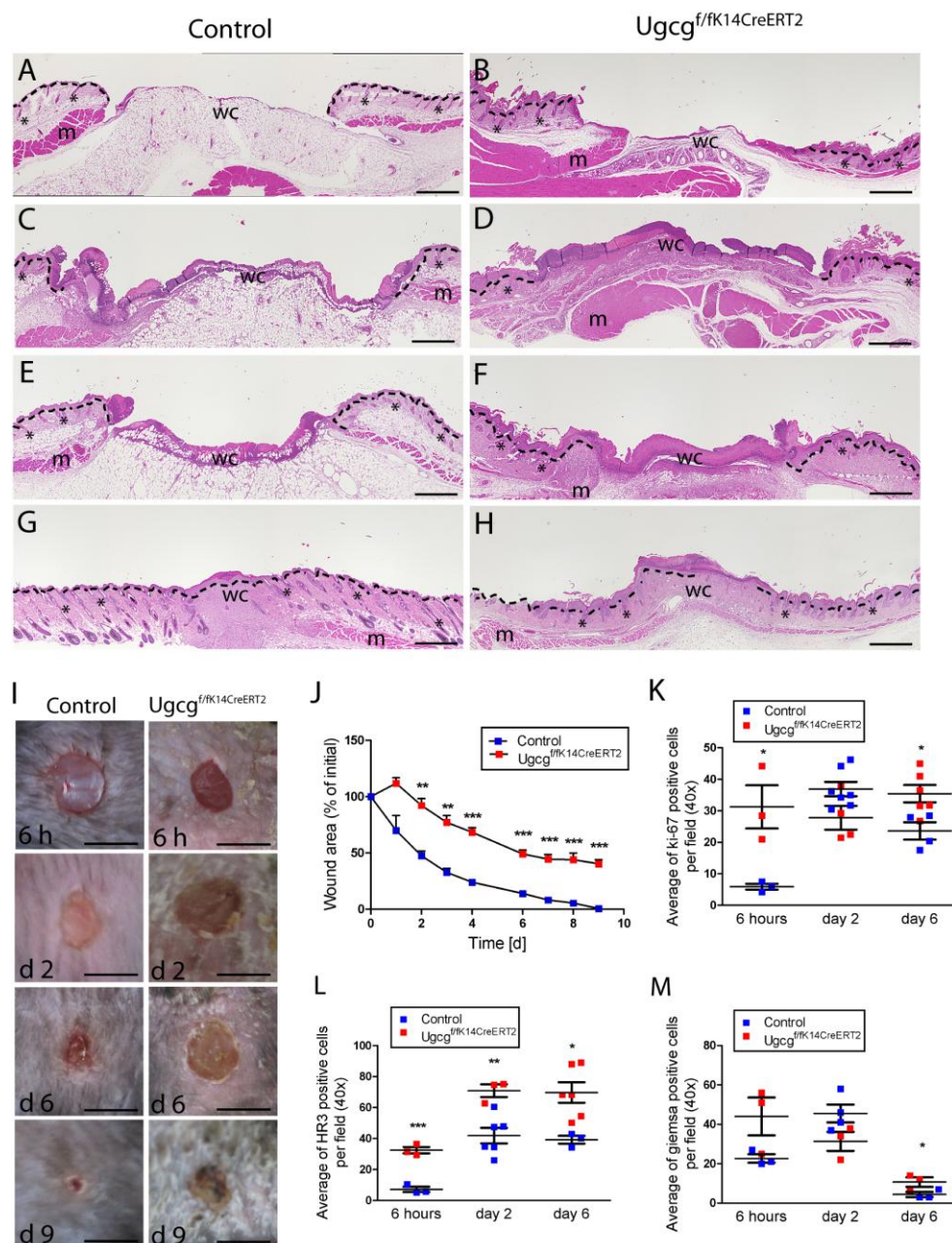
Figure 23. Wound healing is delayed in $Ugcg^{f/f\,K14CreERT2}$ mice.

H&E stainings were performed to investigate wound morphology at 6 h (**A**, **B**), day 2 (**C**, **D**), day 6 (**E**, **F**) and day 9 (**G**, **H**) after wounding. In contrast to controls, wounds of mutant mice were not fully reepithelialized by day 9. Wounds were monitored (**I**) and wound area (**J**) measured at different time points during wound healing, showing a significant delay in wound closure in mutants. Epidermal proliferation (**K**) was significantly enhanced in wound sites of mutants, except for day 2, when proliferation increased in controls in response to wounding. HR3-positive macrophages and dendritic cells (**L**) were the predominant immune cells in wound sites of mutant mice. (**M**) Granulocytes were slightly increased in mutant wound sites at 6 h and in controls at day 2 of healing. Cell numbers decreased until day 6, but mast cells remained significantly higher in mutant wound sites. d = dermis; e = epidermis; m = muscle; wc = wound center; dashed lines = dermal/epidermal junction zone; ∗ = hair follicles; scale bars = 600 μm (**A-H**) or 0.5 cm (**I**); mean values ± SD are shown for $n \geq 3$; significance levels for differences: $p < 0.05$ (*); $p < 0.01$ (**); $p < 0.001$ (***).
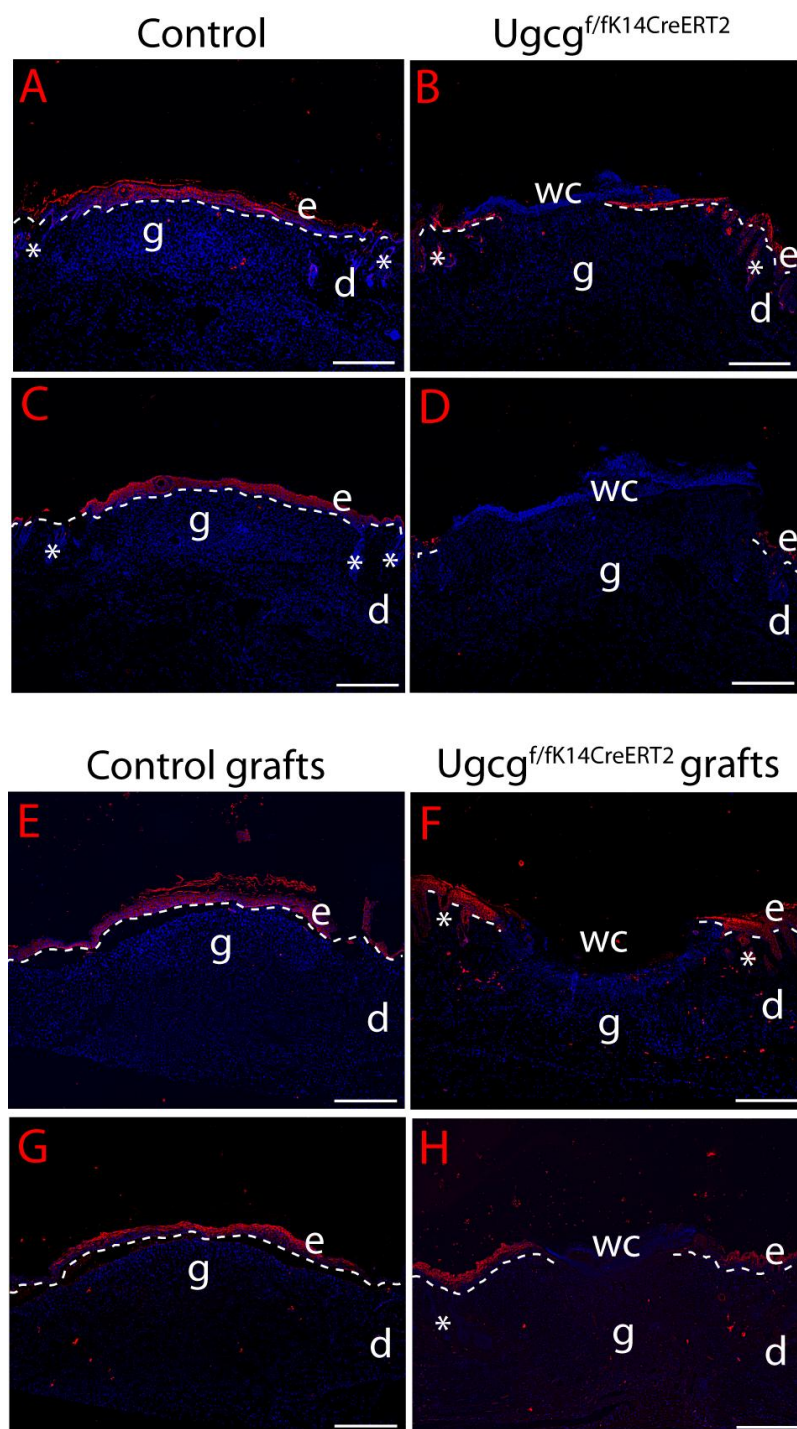
Figure 24. Reepithelialization is delayed in *Ugcg*^*f/f K14CreERT2*^ mutant skin and skin grafts vs. controls.

At day nine of wound healing, control wounds were fully reepithelialized as demonstrated by IF microscopy and staining (red) for keratin K14 (**A**) and keratin K10 (**C**) of controls. In contrast, reepithelialization was significantly delayed in wounds of mutants stained for K14 (**B**) and K10 (**D**). Wound healing in skin grafts (**E–H**) three weeks after TAM induction was also delayed for mutants vs. control grafts, as judged by expression of K14 (**E**,**F**) and K10 (**G**,**H**); d = dermis; e = epidermis; wc = wound center; dashed lines indicate dermal/epidermal junction zone; ∗ = infundibulum; scale bars = 200 µm.

3.2.10 Gene expression profiling reveals genes involved in lipid metabolism and epidermal development

In order to identify differentially expressed genes and enriched molecular networks resulting from epidermal *Ugcg* gene deletion, we conducted gene expression profiling and subsequent gene ontology (GO) enrichment analyses. Using the Genomatix single-probe approach, a total set of 362 differentially regulated transcripts was found from which 168 were induced and 194 were suppressed in the knockout epidermis (FDR = 0).

As described above, UGCG-deficient mice showed alterations in epidermal lipid composition and KC differentiation. GO enrichment analysis of the altered genes revealed the involvement of biological processes related to lipid metabolism (GO:0006629, GO:0008610, GO:0044255) and epidermal differentiation/proliferation (GO:0008544, GO:0031424, GO:0009611, GO:050678) (Appendix Table A2). The genes corresponding to these specific GO terms are shown in the differential expression plots in Figure 25. Selected genes in this collection were further validated by qRT-PCR (Appendix Figure A7) and western blot (Figure 25).

Regarding lipid metabolism, we found in particular upregulated genes which encode for enzymes of the Cer synthesis pathway such as (1) desaturase 2 (*Degs2,* FC 3.5), which catalyzes Cer formation from dihydroceramide, (2) neutral sphingomyelinase (*Smpd3,* FC 2.5), which catalyzes Cer formation from plasma-membrane derived SM, (3) sphingosine-1-phosphate phosphatase 2 (*Sgpp2,* FC 2.6), which generates Sph from Sph-1-P, and (4) CerS3 (encoded by the gene *Lass3,* FC 1.7), which converts dihydroceramide into Cer (Figure 25 and Figure 26).

Furthermore, two genes of the lipoxygenase (LOX) family were significantly altered: the epidermis-type *Alox12b* (encoding for 12R-LOX, FC 2.7) and *Alox12e* (encoding for eLOX-3, FC -4.1) (Figure 25). LOX enzymes are involved in the arachidonic acid (C20:4, ω–6) metabolism and thereby in eicosanoid biosynthesis. The enzymes 12R-LOX and eLOX-3 have been shown to act in concert, and lack of one or both of these has been related to SC hyperthickening and epidermal hyperplasia in patients with congenital ichthyosis (CI) (reviewed in (Furstenberger et al., 2007)).

Moreover, the gene encoding for bone morphogenic protein 6 (BMP6), a member of the TGF-β family, was downregulated (FC -1.4) in *Ugcg*-mutant skin (Figure 25). Among the 14 known BMP proteins, which are important for normal tissue function ((Schulz and Tseng, 2009)), BMP6 is normally expressed in the regenerating epidermis, repressing keratinocyte proliferation and inducing differentiation (Werner and Grose, 2003). The lack of *Bmp6* mRNA in *Ugcg*-mutant skin matches the phenotype of epidermal hyperplasia and impaired keratinocyte maturation.
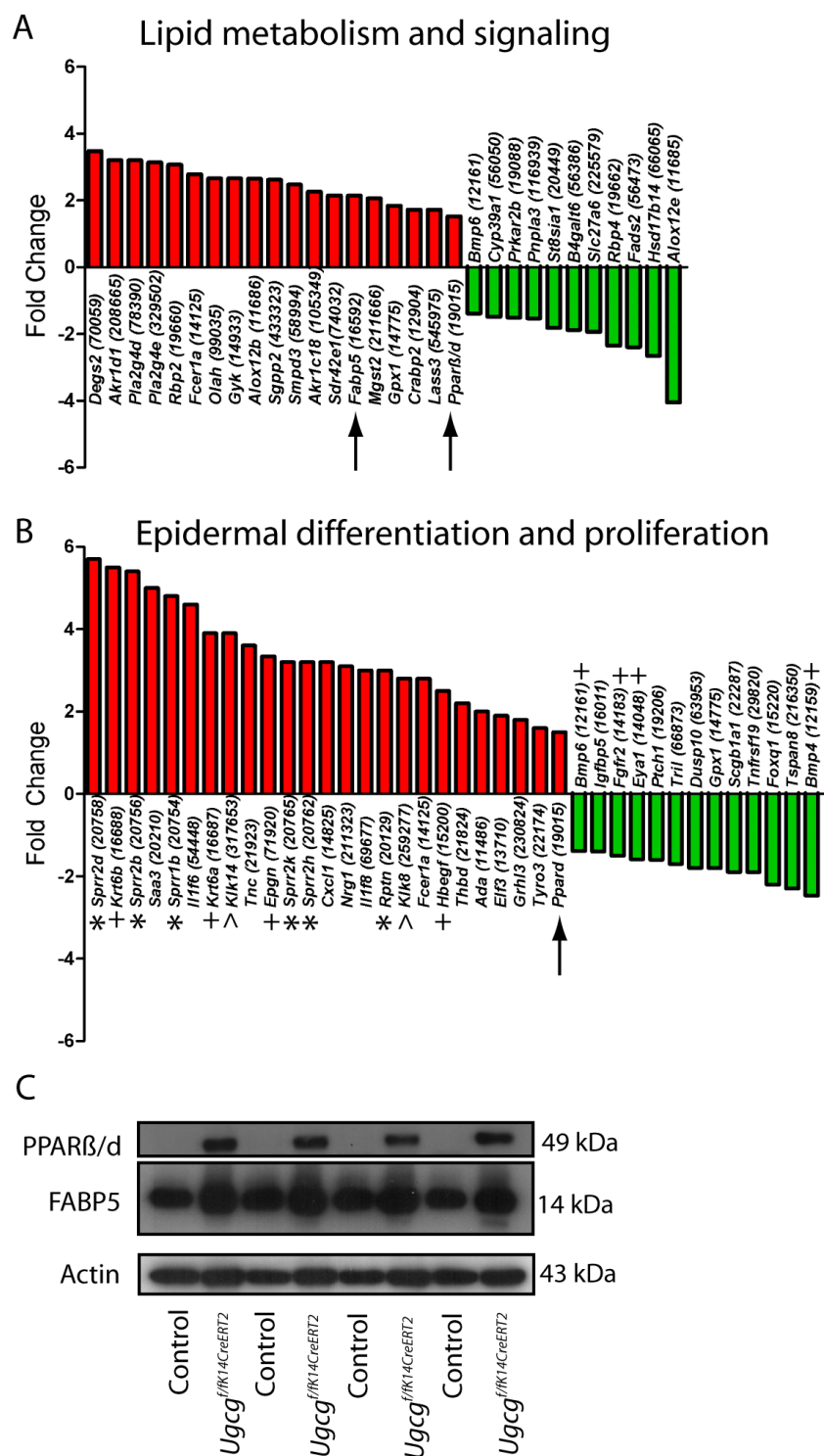
Figure 25.   Evaluation of differentially expressed genes.

Enrichment analysis of differentially expressed genes (mutant vs. controls) in GSL-depleted skin revealed a significant induction of proteins involved in lipid metabolism and signaling (**A**) as well as in epidermal differentiation (**B**). Numbers in parentheses indicate gene IDs. Arrows indicate the genes for the potential regulators PPARβ/δ and FABP5. Induction of these two proteins in mutant epidermis was demonstrated by Western blotting (**C**). (∗) indicates EDC genes; (+) indicates proliferation-related genes, i.e., *K6* keratins, epigen (*Epgn*) and heparin-binding EGF-like growth factor (*Hbegf*); (^) indicates kallikreins (*Klk14, Klk8*).
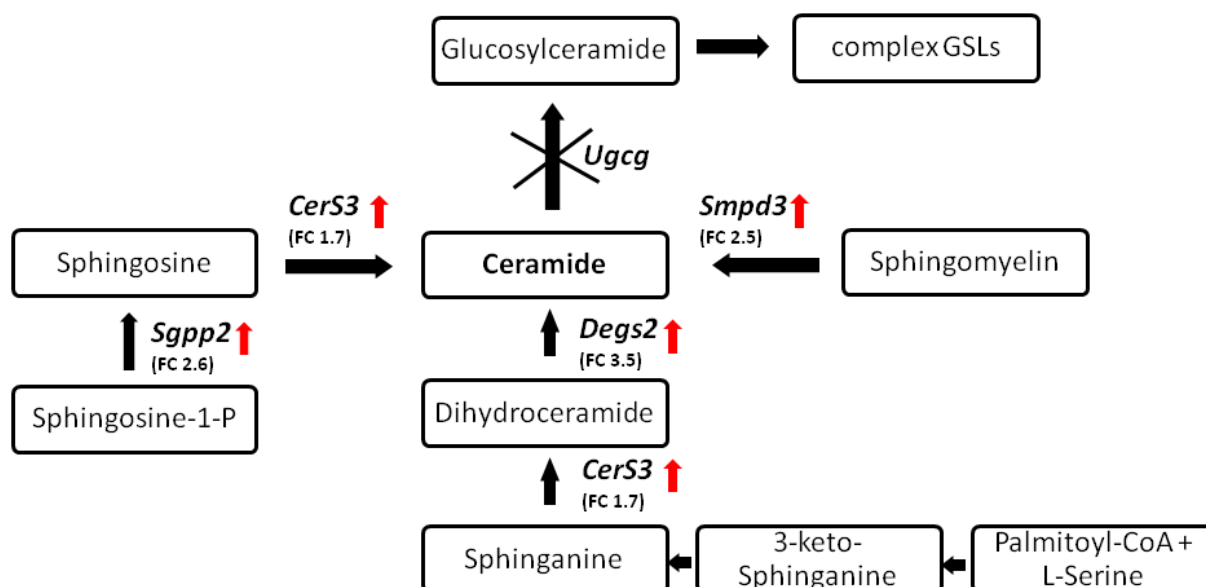
Figure 26. Induction of gene expression for proteins involved in Cer synthesis.

Gene expression profiling evidenced the upregulation (red arrows) of major Cer-synthesizing enzymes in *Ugcg* mutant skin. Gene names are: *CerS3*, ceramides synthase 3; *Degs2*, desaturase 2; *Smpd3*, neutral sphingomyelinase, *Sgpp2*, sphingosine phosphatase 2; *Ugcg*, glucosylceramide synthase. Numbers in parentheses indicate the fold change (FC) parameter used to quantify changes in expression.

The biggest group of differentially expressed genes was assigned to epidermal differentiation/proliferation. For example, we found that the transcriptional activators peroxisome proliferator-activated receptor β/δ (*Pparβ/δ*) and grainyhead-like 3 (*Grlh3*) were significantly upregulated (FC 1.8 and FC 1.5, respectively) (Figure 25). PPARβ/δ has been reported as a regulator of lipid transport, lipid signaling and differentiation in KCs (Jiang et al., 2009; Kannan-Thulasiraman et al., 2010; Tan et al., 2002). Furthermore, mRNA levels of potential PPARβ/δ target genes involved in proliferation and cell survival were significantly enhanced, e.g., members of the EGF family such as epigen (*Epgn*, FC 3.3) and heparin-binding EGF-like growth factor (*Hbegf*, FC 2.5) as well as lipid chaperones such as retinol binding protein 2 (*Rbp2*, FC 3.1), fatty acid binding protein 5 (*Fabp5*, FC 2.1) and cellular retinoic acid-binding protein 2 (*Crabp2*, FC 1.7).

Moreover, GRHL3 has been shown to play a pivotal role in differentiation of stratified epithelia, by regulating genes of the epidermal differentiation complex (EDC) (Kypriotou et al., 2012). This group of genes is altered in various human skin diseases such as lamellar ichthyosis, psoriasis or AD. EDC genes can be clustered into three distinct families encoding for (1) CE proteins such as involucrin (IVL), loricrin (LOR), small proline rich proteins (SPRR family) and late cornified envelope (LCE) proteins; (2) calcium-binding S100 proteins such as S100A8 (calgranulin A), S100A9 (calgranulin B); and (3) S100-fused proteins such as filaggrin (FLG), filaggrin-2 (FLG2) and repetin (RPTN), as reviewed in (Kypriotou et al., 2012).

Gene expression profiling uncovered major alterations in the expression of EDC gene members in *Ugcg* mutant skin. For example, *Sprr* genes (FC 3.2–5.7), *Rptn* (FC 3.0) (shown in Figure 25) and

71

Lce's (FC 4.0-5.8, not shown) were upregulated, while *Flg2* was downregulated (FC −2.8, not shown). Additionally, significant induction was found for the hyperproliferation markers keratin K6 (*Krt6b* (FC 3.9) and *Krt6a* (FC 5.5)) and the tissue kallikreins *Klk14* (FC 3.9) and *Klk8* (FC 2.8) (Figure 25). The KLKs belong to the group of secretory serine proteases, which are important for regular desquamation and/or protein shedding. Upregulation of the EDC genes, keratins K6 and KLKs, has been associated with hyperproliferative/inflammatory skin diseases such as psoriasis and AD (Bergboer et al., 2011; Iizuka et al., 2004; Komatsu et al., 2007).

To summarize, the identified gene subsets corroborate the observed phenotypes resulting from *Ugcg* gene deletion at the molecular level. Furthermore, the results obtained by gene expression profiling and western blotting suggest PPARβ/δ and FABP5 as potential transcriptional regulators of epidermal development. Thus, we propose that alterations in Cer homeostasis affect a PPARβ/δ-mediated signaling cascade as a likely mechanism for hyperproliferation in UGCG-deficient epidermis (see Discussion 4.4).

Additionally, analysis with the Genomatix software allowed for the correlation of differentially expressed genes to human diseases based on the Medical Subject Headings (MeSH) database (*http://www.nlm.nih.gov/mesh*). In line with the above results, the generated gene sets show the highest correlation to cancer and skin diseases such as psoriasis (Appendix Table A3).

4. Discussion

4.1 Glucosylceramides are Essential Barrier Lipids in Oral Stratified Epithelia

TAM induction of $Ugcg^{f/f\,K14CreERT2}$ mice led to $Ugcg$ gene deletion in the epidermis and in other K14-positive epithelia such as tongue, esophagus and forestomach, representing stratified squamous epithelia of the alimentary tract and an oral barrier against noxious luminal contents. The esophageal epithelium is rapidly renewed due to the high passage rate of food and mucus (Tobey, 1995).

In contrast to the epidermis, the esophagus is nonkeratinized and contains a (para)keratotic stratified squamous epithelium with typically more polar (GlcCers, cholesterol, phospholipids) than non-polar lipids (e.g., Cers) (Diaz-Del Consuelo et al., 2005). However, intercellular lipid lamellae and LB structures similar to those in the SC of the epidermis have been described (Elias et al., 1977). In our study, lipid analysis of control esophagus demonstrated the presence of GlcCers (NS, AS, OS) and most strikingly of linoleic acid-containing EOS-GlcCers, which so far have not been described in esophageal tissue. In contrast, the esophagus of $Ugcg$ mutants was almost devoid of GlcCers, in particular of EOS-GlcCers, explaining the observed alterations of the epithelial barrier which occurred by day 10 of TAM induction. Damage to the esophageal barrier resulted in epithelial hyperproliferation, most probably as a compensatory mechanism to rapidly repair the injured tissue. In addition to the role of GlcCers in the skin barrier, these results suggest a potential role of EOS-GlcCers in oral barrier homeostasis, which is to our knowledge a new finding. Investigations of the esophageal lipid barrier could be the subject of further studies, in particular with regard to improved treatment of human gastroesophageal reflux diseases (GERD).

4.2 Glucosylceramides are Unique Precursors for Epidermal Protein-linked Ceramides

Based on pathologies of human diseases such as Gaucher's disease and Harlequin ichthyosis, it has been concluded that Cers in the SC derive from glucosylated intermediates delivered by LBs from the underlying SG layer (Doering et al., 1999b; Zuo et al., 2008). Results from UGCG-deficient newborn mice ($Ugcg^{f/f\,K14Cre}$) only partially corroborated this "precursor concept", since epidermal POS-Cers were still present despite the loss of POS-GlcCers (Jennemann et al., 2007).

In the present study, induction of $Ugcg$ deletion in adult $Ugcg^{f/f\,K14CreERT2}$ mice resolved the apparent discrepancy by demonstrating that GlcCer-derived POS-Cers are significantly reduced in the mutant mice. These data support the hypothesis that the major portion of SC Cers derive from glucosylated intermediates (GlcCers) and suggest that Cer glucosylation, a prerequisite for lipid barrier formation, precedes the formation of POS-Cers by ω-esterification of Cers to proteins of the CE. Nevertheless, EOS-Cers were not lost in GlcCer-deficient skin, but instead accumulated, indicating no direct involvement of UGCG in the ω-esterification of FAs to Cers.

In GlcCer-deficient mice vs. controls the depletion of POS-Cers was accompanied by a significant increase in ωh-Cers and SMs. However, the increase in Cers (by ca. 4500 pmol/mg dry epidermis

weight) in UGCG-deficient epidermis cannot be accounted for alone by the concomitant loss of GlcCers (ca. 670 pmol/mg epidermal dry weight) in these mice. Instead, Cer accumulation might result from enhanced *de novo* Cer synthesis at the ER and/or to a lesser extend from Cer recycling in the salvage pathway, as compensation for barrier loss (Geilen et al., 1997; Grubauer et al., 1987). Recycling would explain the unchanged and even reduced levels of non-hydroxylated (NS) and α-hydroxylated (AS) SMs.

Moreover, long-chain (LC) and very-long-chain (VLC) Cers (C16–C24) are potential regulators of various cell fates, as evidenced from studies of human cancers and cancer cell lines. Increased levels of specific NS-Cers (C16, C24, C24:1), promote apoptosis and tumor progression (Eto et al., 2006; Hartmann et al., 2012; Koybasi et al., 2004; Schiffmann et al., 2009). In *Ugcg* mutants loss of NS-GlcCers and a significant increase of the corresponding NS-Cers did not lead to enhanced apoptosis in the epidermis (Figure A6), but may be responsible for the observed hyperproliferation and de-differentiation of GlcCer-deficient keratinocytes, as mediated by the nuclear transcription factor PPARβ/δ (see section 4.4).

4.3 Ceramide Glucosylation is Required for the Formation of a Competent Epidermal Permeability Barrier and for Barrier Restoration

GlcCer-deficient mice displayed severe ichthyosiform skin abnormalities within 3 to 4 weeks of induction. Hyperkeratosis with elevated TEWL and pH resulted in WPB loss. Morphologic alterations appeared to result from the early onset differentiation defect in K14-positive cells of the basal layer. UGCG-deficient keratinocytes lost their ability for normal maturation and expressed basal keratin K14 throughout all epidermal layers. This differentiation defect occurred together with a reduction of the junction barrier (involving the tight junction protein CLDN1 and the desmosomal junction proteins DSG1, DSG2 and DSP), potentiating the leakiness of the WPB. In patients suffering from congenital HI, dehydration becomes a lethal risk factor and results from accumulation of epidermal GlcCers, Cer loss and barrier loss. In comparison, GlcCer deficiency in $Ugcg^{f/f\,K14CreERT2}$ mice caused similar alterations, highlighting Cer glucosylation as a requirement for Cer processing and barrier formation. Nevertheless, *Ugcg* mutants sufficiently compensated the water loss by increasing their water uptake.

The SC of *Ugcg* mutants appeared as a thick rigid layer of partially undifferentiated corneocytes. The disorder in corneocyte maturation was further associated with altered processing of the terminal differentiation markers LOR, and (pro)FLG. Strong cytosolic and nuclear localization of LOR was observed in mutant skin and is a feature of loricrin keratoderma, e.g., Vohwinkel's syndrome (Ishida-Yamamoto et al., 2000). Furthermore, FLG depletion is characteristic for atopic skin of patients with *FLG* gene mutations (Palmer et al., 2006; Weidinger et al., 2006). Deficient proteolytic cleavage of proFLG in mutant skin was demonstrated by western blots which showed diffusive bands of FLG-like intermediates, and reduced levels of dimeric, trimeric and polymeric FLG (FLG2). FLG2 is a 250 kDa FLG polymer, which was found to be reduced in skin of atopic patients and in mice fed with an

essential FA-deficient diet (Hansmann et al., 2012) and displaying a skin phenotype similar to that of TAM-induced $Ugcg^{f/fK14CreERT2}$ mice. Loss of monomeric FLG might not only hinder keratin condensation in corneocytes (Sandilands et al., 2009), but also its degradation into water-retaining amino acids (e.g., histidine, glutamine, arginine) and their derivatives (e.g., *trans*-urocanic acid) within the SC, thus promoting further dehydration. Loss of the ability to retain water directly affects an increase in SC pH, which was indeed higher in mutants than in controls. Many enzymes secreted together with the lipids at the upper SG and SG/SC interface are typically found in the endosomal/lysosomal compartments and have an acidic activity optimum. Elevation of the SC pH in mutants implies reduced activity of such enzymes involved in lipid metabolism (e.g., glucosylceramidase, sphingomyelinases, phospholipases) (Fluhr et al., 2001; Holleran et al., 1992; Schmuth et al., 2000) and protein shedding (e.g., kallikreins) (Lin et al.; Ohman and Vahlquist, 1998), thereby contributing to hypercornification, impaired lamellar membrane formation and loss of barrier function.

Hyperproliferation and hyperkeratosis of UGCG-deficient skin was evidenced by K6-expression and increased numbers of Ki-67-positive keratinocytes, including the lower suprabasal layers. In addition, enhanced signs of inflammation, i.e., infiltration of HR3-positive macrophages and dendritic cells into dermis and epidermis, were observed for mutants vs. controls. Dendritic cells are normally recruited by chemotactic stimuli synthesized by keratinocytes (e.g., IL-1, TGFα) (Wang et al., 2004; Werner and Grose, 2003). Accordingly, GlcCer-depleted keratinocytes themselves may have activated epidermal dendritic cells (e.g., Langerhans cells), dermal-resident cells (e.g., macrophages) or peripheral immune-competent cells (e.g., neutrophils) as a stress response to barrier loss.

During wound healing, a tight regulation of the inflammatory phases is important for efficient cutaneous tissue repair, whereas excessive or chronic inflammation can lead to impaired wound healing (e.g., diabetic wounds) (Eming et al., 2007). Although, at the onset of wounding, mutant skin contained significantly more HR3-positive cells than control skin, the immune response upon wounding was similar in mutants and controls and did not alter granulation tissue formation. The lack of K14- and K10-positive cells in wound tissue suggested rather a defect in reepithelialization as the cause for delayed wound closure. To exclude the possibility of a systemic effect of factors such as water and electrolyte loss as well as low body temperature (Figure A5) on delayed wound closure, wound healing experiments were performed on skin isografts of control and $Ugcg^{f/fK14CreERT2}$ mice upon TAM induction. These experiments corroborated the delay in keratinization in *Ugcg* mutants and excluded a relevant role for systemic effects. In summary, the pronounced defect in differentiation of GlcCer-depleted keratinocytes can explain the delay in wound closure (reepithelialization) and provide evidence for a pivotal role of GlcCers in keratinocyte differentiation and barrier restoration.

4.4 Ceramide Potentially Regulates Keratinocyte Differentiation Mediated by Epidermis-type PPARβ/δ

The molecular events induced upon *Ugcg* gene deletion in the epidermis were addressed by performing gene expression profiling and GO enrichment analysis. The clustering of differentially

expressed genes disclosed pathways specifically related to lipid metabolism and epidermal development. Genes of the lipid metabolic pathway are involved in (1) Cer synthesis (*CerS3, Degs2, Smpd3, Sgpp2*) (Figure 26), (2) Cer signaling (*Pparβ/δ*) and (3) lipid transport (*Rbp2, Fabp5, Crabp2*).

The upregulation of genes promoting Cer synthesis (Figure 26) clearly supports the lipid results obtained from TLC and quantitative MS analysis, demonstrating a significant increase in epidermal Cers in *Ugcg* mutants. The major increase in ωh-ULC-Cers can be accounted for by the blockage of Cer processing (Cer glucosylation) in the suprabasal living epidermal layers upon *Ugcg* gene deletion. Additionally, accumulation of LC- and VLC-Cers may result from the upregulation of *CerS3* and *Degs2* genes, thus promoting Cer *de novo* synthesis as a compensatory mechanism for barrier loss. Moreover, induction of *Smpd3* and *Sgpp2* implies the activation of the salvage pathway (SM recycling) in favor of Cer synthesis. Cers (with LC- and VLC-FA moieties) are known for their crucial function in cell signaling with the activation of a variety of key enzymes involved in protein phosphorylation (e.g., CAPP, PKC, JNK) and phospholipid hydrolysis (e.g., PLA, PLD) (Geilen et al., 1997; Perry and Hannun, 1998). However, gene expression profiling did not reveal significant alterations in expression of the described Cer targets.

Instead, induction of the Cer-responsive gene *Pparβ/δ* was conclusive. PPARβ/δ is not expressed in normal adult skin but is activated by proliferative stimuli such as injury or inflammation, exerting a protective effect on keratinocytes and promoting efficient wound healing (Di-Poi et al., 2003). A conformational change in PPARβ/δ, as induced by cognate ligands, e.g., C2-ceramide (*N*-acetyl-D-sphingosine) and C6-ceramide (*N*-hexanoyl-D-sphingosine), linoleic acid derivatives, saturated and polyunsaturated fatty acids (PUFAs) (Coll et al., 2010; Jiang et al., 2009; Naruhn et al., 2010), leads to its activation via heterodimerization with nuclear retinoic X receptors (RXR; in particular RXRα) and binding to peroxisome proliferator responsive elements (PPRE) in the promoter region of target genes (e.g., *Fabp5, Vegf*) (Schachtrup et al., 2004; Wang et al., 2006). Both, FABP5 and PPARβ/δ, have been suggested as (cooperative) lipid-responsive regulators of transcription in skin. In this context, FABP5 may act as either a coactivator of PPARβ/δ, delivering lipophilic ligands to *Pparβ/δ* in the nucleus (Tan et al., 2002), or its gene may act as a target, mediating PPARβ/δ function (Schachtrup et al., 2004). As coactivator, FABP5 may be induced by epidermal growth factors (e.g., EPGN, HBEGF) in an NF-κB-mediated manner (Kannan-Thulasiraman et al., 2010), as observed in hyperproliferative settings such as psoriasis, wound healing or cancer (Di-Poi et al., 2003; Kannan-Thulasiraman et al., 2010; Ogawa et al., 2011). However, in *Ugcg* mutants mRNA transcription levels of *Nf-κb* were not significantly altered.

Furthermore, we analyzed PPARβ/δ and FABP5 protein expression in control and mutant epidermis. Our results showed a strong induction in GlcCer-deficient skin as compared to controls. The expression of both proteins may explain the hyperproliferative state of keratinocytes in *Ugcg* mutants, directed by the alterations in Cer composition. This conclusion was corroborated by the observation of enhanced mRNA levels from potential PPARβ/δ target genes such as the lipid transporters (*Fabp5, Crapb2, Rbp2*) and EGF family members (*Epgn, Hbegf*) (Figure 25) (Han et al., 2009; Morgan et al., 2010).

A proposed mechanism of Cer function inducing keratinocyte proliferation and de-differentiation is summarized in Figure 27. However, further evidence is needed to confirm this hypothesis which could be the subject of future investigations, e.g., *in vitro* using a 3D culture system ("skin equivalents") of primary keratinocytes. The cells have been successfully isolated from control and *Ugcg*-mutant skin, and could provide substantial information for elucidating the underlying mechanism of GlcCer-dependent epithelial cell differentiation.
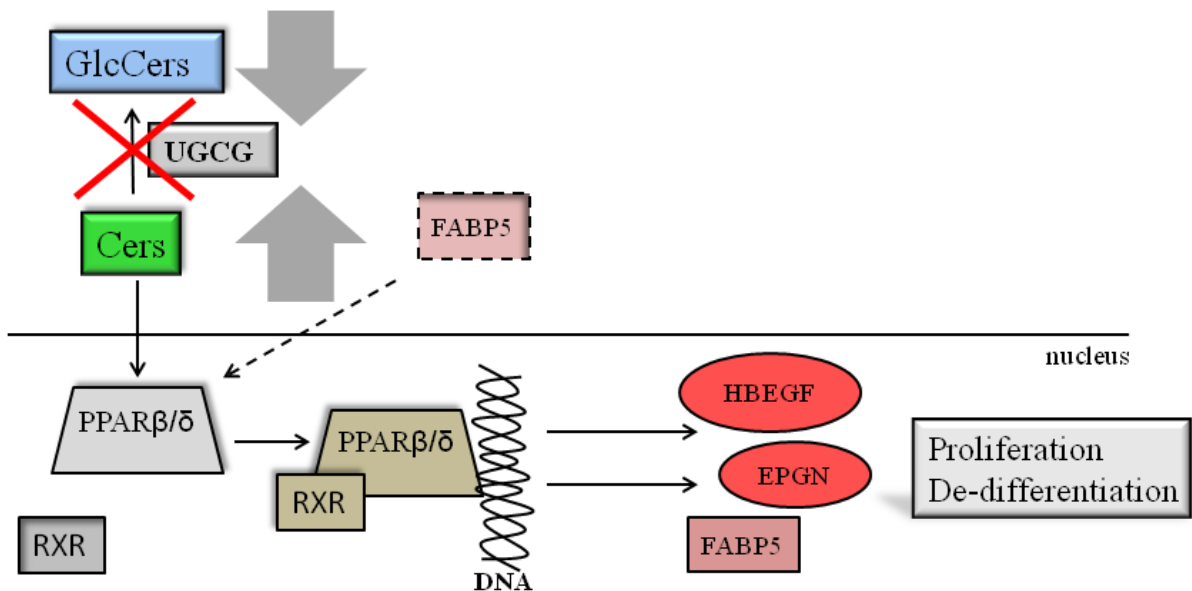
Figure 27. Schematic representation of processes induced upon *Ugcg* deletion and subsequent Cer accumulation in mouse epidermis.

Elimination of GlcCer synthesis in mutant epidermis leads to Cer accumulation and induction of proliferation and de-differentiation processes mediated by the peroxisome proliferator-activated receptor β/δ (PPARβ/δ), fatty acid binding protein 5 (FABP5) and potential target genes encoding for proteins such as heparin-binding EGF-like growth factor (HBEGF), epigen (EPGN) and fatty acid binding protein 5 (FABP5).

5. Conclusions

Intensive investigations over the last two decades led to major advances in SL research and confirmed the roles of distinct SLs and GSLs in human skin diseases such as ichthyosis, psoriasis, AD and xerosis (Coderch et al., 2003). GlcCer has long been identified as the major GSL in the epidermis, comprising ca. 4% of the total epidermal lipid mass (Madison et al., 1986). Its synthesis is known to depend on the enzyme UGCG, which catalyzes Cer glucosylation as the initial step in GSL biosynthesis. GlcCer itself is thought to function as an intracellular precursor and carrier for extracellular Cers. The aim of this thesis project was to prove this hypothesis and, furthermore, to investigate the potential role of GlcCer in epithelial cell differentiation using a TAM-inducible tissue-specific *Ugcg* knockout mouse model.

Although no human skin disorder has been directly related to mutations of the *Ugcg* gene, the UGCG enzyme catalyzes the key metabolic step in Cer processing (i.e., glucosylation), and resolution of these key steps are important for fully understanding the metabolic functions of Cers, in particular in relation to human pathologies such as skin diseases and cancer.

Previously, UGCG has been shown to be of vital importance during embryogenesis and for the epidermal WPB in newborn mice. TAM-inducible *Ugcg* deletion in adult mice allowed for a longer and more detailed investigation of lipid barrier formation. UGCG depletion resulted in a significant decrease (by 80%) of epidermal GlcCers and an increase in free extractable Cers and ωh SMs. More importantly, protein-linked POS-Cers were significantly reduced, indicating that sequential Cer processing was blocked. Hence, we conclude that Cer glucosylation is pivotal for transport and ω-esterification of Cers into the CE – a prerequisite for barrier formation in the skin and esophagus.

GlcCer depletion in basal cells directly affected keratinocyte maturation and hampered cornification as well as wound reepithelialization.

Gene expression data were conclusive and pointed to alterations in Cer composition and induction of a PPARβ/δ-mediated signaling cascade as a likely mechanism for de-differentiation and hyperproliferation in UGCG-deficient epidermis (Figure 27).

In conclusion, the results of the present thesis work provide important evidence concerning the function of GlcCers in epithelial differentiation and barrier homeostasis in the epidermal and esophageal epithelium. The underlying mechanism of the observed ichthyosiform defects may be regulated by Cers via activation of the nuclear receptor PPARβ/δ and target genes involved in epidermal differentiation. In addition, modulation of the inflammatory signaling cascade and epidermal healing does occur with a deficiency in UGCG (and in GlcCers) and with an increase in epidermal Cers.

6. References

Aerts, J.M., R. Ottenhoff, A.S. Powlson, A. Grefhorst, M. van Eijk, P.F. Dubbelhuis, J. Aten, F. Kuipers, M.J. Serlie, T. Wennekes, J.K. Sethi, S. O'Rahilly, and H.S. Overkleeft. 2007. Pharmacological inhibition of glucosylceramide synthase enhances insulin sensitivity. *Diabetes*. 56:1341-1349.

Akiyama, M., K. Sakai, C. Takayama, T. Yanagi, Y. Yamanaka, J.R. McMillan, and H. Shimizu. 2008. CGI-58 is an alpha/beta-hydrolase within lipid transporting lamellar granules of differentiated keratinocytes. *Am J Pathol*. 173:1349-1360.

Akiyama, M., D. Sawamura, Y. Nomura, M. Sugawara, and H. Shimizu. 2003. Truncation of CGI-58 protein causes malformation of lamellar granules resulting in ichthyosis in Dorfman-Chanarin syndrome. *J Invest Dermatol*. 121:1029-1034.

Akiyama, M., Y. Sugiyama-Nakagiri, K. Sakai, J.R. McMillan, M. Goto, K. Arita, Y. Tsuji-Abe, N. Tabata, K. Matsuoka, R. Sasaki, D. Sawamura, and H. Shimizu. 2005. Mutations in lipid transporter ABCA12 in harlequin ichthyosis and functional recovery by corrective gene transfer. *J Clin Invest*. 115:1777-1784.

Angstrom, J., S. Teneberg, and K.A. Karlsson. 1994. Delineation and comparison of ganglioside-binding epitopes for the toxins of Vibrio cholerae, Escherichia coli, and Clostridium tetani: evidence for overlapping epitopes. *Proc Natl Acad Sci U S A*. 91:11859-11863.

Ashton, G.H., P. Sorelli, J.E. Mellerio, F.M. Keane, R.A. Eady, and J.A. McGrath. 2001. Alpha 6 beta 4 integrin abnormalities in junctional epidermolysis bullosa with pyloric atresia. *Br J Dermatol*. 144:408-414.

Bartke, N., and Y.A. Hannun. 2009. Bioactive sphingolipids: metabolism and function. *J Lipid Res*. 50 Suppl:S91-96.

Bergboer, J.G., G.S. Tjabringa, M. Kamsteeg, I.M. van Vlijmen-Willems, D. Rodijk-Olthuis, P.A. Jansen, J.Y. Thuret, M. Narita, A. Ishida-Yamamoto, P.L. Zeeuwen, and J. Schalkwijk. 2011. Psoriasis risk genes of the late cornified envelope-3 group are distinctly expressed compared with genes of other LCE groups. *Am J Pathol*. 178:1470-1477.

Bibel, D.J., R. Aly, and H.R. Shinefield. 1992. Antimicrobial activity of sphingosines. *J Invest Dermatol*. 98:269-273.

Bollinger, C.R., V. Teichgraber, and E. Gulbins. 2005. Ceramide-enriched membrane domains. *Biochim Biophys Acta*. 1746:284-294.

Bourbon, N.A., J. Yun, and M. Kester. 2000. Ceramide directly activates protein kinase C zeta to regulate a stress-activated protein kinase signaling complex. *J Biol Chem*. 275:35617-35623.

Bouwstra, J.A., P.L. Honeywell-Nguyen, G.S. Gooris, and M. Ponec. 2003. Structure of the skin barrier and its modulation by vesicular formulations. *Prog Lipid Res*. 42:1-36.

Brandner, J.M., M. Haftek, and C.M. Niessen. 2010. Adherens junctions, desmosomes and tight junctions in epidermal barrier function. *The Open Dermatology Journal*. 4:14-20.

Brown, S.J., and W.H. McLean. 2012. One remarkable molecule: filaggrin. *J Invest Dermatol*. 132:751-762.

Cameron, D.J., Z. Tong, Z. Yang, J. Kaminoh, S. Kamiyah, H. Chen, J. Zeng, Y. Chen, L. Luo, and K. Zhang. 2007. Essential role of Elovl4 in very long chain fatty acid synthesis, skin permeability barrier function, and neonatal survival. *Int J Biol Sci*. 3:111-119.

Candi, E., R. Schmidt, and G. Melino. 2005. The cornified envelope: a model of cell death in the skin. *Nat. Rev. Mol. Cell Biol*. 6:328-340.

Chalfant, C.E., and S. Spiegel. 2005. Sphingosine 1-phosphate and ceramide 1-phosphate: expanding roles in cell signaling. *J Cell Sci*. 118:4605-4612.

Chomczynski, P., and N. Sacchi. 2006. The single-step method of RNA isolation by acid guanidinium thiocyanate-phenol-chloroform extraction: twenty-something years on. *Nat Protoc*. 1:581-585.

Coderch, L., O. Lopez, A. de la Maza, and J.L. Parra. 2003. Ceramides and skin function. *Am J Clin Dermatol*. 4:107-129.

Coll, T., E. Barroso, D. Alvarez-Guardia, L. Serrano, L. Salvado, M. Merlos, X. Palomer, and M. Vazquez-Carrera. 2010. The Role of Peroxisome Proliferator-Activated Receptor beta/delta on the Inflammatory Basis of Metabolic Disease. *PPAR Res*. 2010.

De Libero, G., A. Donda, H.J. Gober, V. Manolova, Z. Mazorra, A. Shamshiev, and L. Mori. 2002. A new aspect in glycolipid biology: glycosphingolipids as antigens recognized by T lymphocytes. *Neurochem Res*. 27:675-685.

Demerjian, M., D.A. Crumrine, L.M. Milstone, M.L. Williams, and P.M. Elias. 2006. Barrier dysfunction and pathogenesis of neutral lipid storage disease with ichthyosis (Chanarin-Dorfman syndrome). *J Invest Dermatol*. 126:2032-2038.

Di-Poi, N., L. Michalik, N.S. Tan, B. Desvergne, and W. Wahli. 2003. The anti-apoptotic role of PPARbeta contributes to efficient skin wound healing. *The Journal of steroid biochemistry and molecular biology*. 85:257-265.

Diaz-Del Consuelo, I., Y. Jacques, G.P. Pizzolato, R.H. Guy, and F. Falson. 2005. Comparison of the lipid composition of porcine buccal and esophageal permeability barriers. *Arch Oral Biol*. 50:981-987.

Diaz, L.A., M.R. Heaphy, N.J. Calvanico, T.B. Tomasi, and R.E. Jordon. 1977. Separation of epidermis from dermis with sodium thiocyanate. *J Invest Dermatol*. 68:36-38.

Doering, T., W.M. Holleran, A. Potratz, G. Vielhaber, P.M. Elias, K. Suzuki, and K. Sandhoff. 1999a. Sphingolipid activator proteins are required for epidermal permeability barrier formation. *J Biol Chem*. 274:11038-11045.

Doering, T., R.L. Proia, and K. Sandhoff. 1999b. Accumulation of protein-bound epidermal glucosylceramides in beta-glucocerebrosidase deficient type 2 Gaucher mice. *FEBS Lett*. 447:167-170.

Drake, D.R., K.A. Brogden, D.V. Dawson, and P.W. Wertz. 2008. Thematic review series: skin lipids. Antimicrobial lipids at the skin surface. *J Lipid Res*. 49:4-11.

Edgar, R., M. Domrachev, and A.E. Lash. 2002. Gene Expression Omnibus: NCBI gene expression and hybridization array data repository. *Nucleic Acids Res*. 30:207-210.

el Marjou, F., K.P. Janssen, B.H. Chang, M. Li, V. Hindie, L. Chan, D. Louvard, P. Chambon, D. Metzger, and S. Robine. 2004. Tissue-specific and inducible Cre-mediated recombination in the gut epithelium. *Genesis*. 39:186-193.

Elias, P., K.R. Feingold, and M. Fartasch. 2006. The epidermal lamellar body as a multifunctional secretory organelle. *Skin Barrier*:261-272.

Elias, P.M. 2005. Stratum corneum defensive functions: an integrated view. *J Invest Dermatol*. 125:183-200.

Elias, P.M., N.S. McNutt, and D.S. Friend. 1977. Membrane alterations during cornification of mammalian squamous epithelia: a freeze-fracture, tracer, and thin-section study. *The Anatomical record*. 189:577-594.

Elias, P.M., M. Schmuth, Y. Uchida, R.H. Rice, M. Behne, D. Crumrine, K.R. Feingold, W.M. Holleran, and D. Pharm. 2002. Basis for the permeability barrier abnormality in lamellar ichthyosis. *Exp Dermatol*. 11:248-256.

Elias, P.M., M.L. Williams, M.E. Maloney, J.A. Bonifas, B.E. Brown, S. Grayson, and E.H. Epstein, Jr. 1984. Stratum corneum lipids in disorders of cornification. Steroid sulfatase and cholesterol sulfate in normal desquamation and the pathogenesis of recessive X-linked ichthyosis. *J Clin Invest*. 74:1414-1421.

Eming, S.A., T. Krieg, and J.M. Davidson. 2007. Inflammation in wound repair: molecular and cellular mechanisms. *J Invest Dermatol*. 127:514-525.

Eto, M., J. Bennouna, O.C. Hunter, M.T. Lotze, and A.A. Amoscato. 2006. Importance of C16 ceramide accumulation during apoptosis in prostate cancer cells. *Int J Urol*. 13:148-156.

Feingold, K.R. 2007. Thematic review series: skin lipids. The role of epidermal lipids in cutaneous permeability barrier homeostasis. *J Lipid Res*. 48:2531-2546.

Fluhr, J.W., and P. Elias. 2002. Stratum corneum pH: Formation and function of the Acid Mantle. *Exog. Dermatol.* 1:163–175.

Fluhr, J.W., J. Kao, M. Jain, S.K. Ahn, K.R. Feingold, and P.M. Elias. 2001. Generation of free fatty acids from phospholipids regulates stratum corneum acidification and integrity. *J Invest Dermatol*. 117:44-51.

Furstenberger, G., N. Epp, K.M. Eckl, H.C. Hennies, C. Jorgensen, P. Hallenborg, K. Kristiansen, and P. Krieg. 2007. Role of epidermis-type lipoxygenases for skin barrier function and adipocyte differentiation. *Prostaglandins & other lipid mediators*. 82:128-134.

Furuse, M., M. Hata, K. Furuse, Y. Yoshida, A. Haratake, Y. Sugitani, T. Noda, A. Kubo, and S. Tsukita. 2002. Claudin-based tight junctions are crucial for the mammalian epidermal barrier: a lesson from claudin-1-deficient mice. *J Cell Biol*. 156:1099-1111.

Geilen, C.C., T. Wieder, and C.E. Orfanos. 1997. Ceramide signalling: regulatory role in cell proliferation, differentiation and apoptosis in human epidermis. *Arch Dermatol Res*. 289:559-566.

Ghazizadeh, S., and L.B. Taichman. 2001. Multiple classes of stem cells in cutaneous epithelium: a lineage analysis of adult mouse skin. *EMBO J*. 20:1215-1222.

Greenspan, P., E.P. Mayer, and S.D. Fowler. 1985. Nile red: a selective fluorescent stain for intracellular lipid droplets. *J Cell Biol*. 100:965-973.

Grubauer, G., K.R. Feingold, and P.M. Elias. 1987. Relationship of epidermal lipogenesis to cutaneous barrier function. *J Lipid Res*. 28:746-752.

Halprin, K.M. 1972. Epidermal "turnover time"--a re-examination. *Br J Dermatol*. 86:14-19.

Hamanaka, S., M. Hara, H. Nishio, F. Otsuka, A. Suzuki, and Y. Uchida. 2002. Human epidermal glucosylceramides are major precursors of stratum corneum ceramides. *J Invest Dermatol*. 119:416-423.

Han, J., M. Kioi, W.S. Chu, J.L. Kasperbauer, S.E. Strome, and R.K. Puri. 2009. Identification of potential therapeutic targets in human head & neck squamous cell carcinoma. *Head Neck Oncol*. 1:27.

Hanada, K. 2003. Serine palmitoyltransferase, a key enzyme of sphingolipid metabolism. *Biochim Biophys Acta*. 1632:16-30.

Hanada, K. 2006. Discovery of the molecular machinery CERT for endoplasmic reticulum-to-Golgi trafficking of ceramide. *Mol Cell Biochem*. 286:23-31.

Hansmann, B., K. Ahrens, Z. Wu, E. Proksch, U. Meyer-Hoffert, and J.M. Schroder. 2012. Murine filaggrin-2 is involved in epithelial barrier function and down-regulated in metabolically induced skin barrier dysfunction. *Exp Dermatol*. 21:271-276.

Hartmann, D., J. Lucks, S. Fuchs, S. Schiffmann, Y. Schreiber, N. Ferreiros, J. Merkens, R. Marschalek, G. Geisslinger, and S. Grosch. 2012. Long chain ceramides and very long chain ceramides have opposite effects on human breast and colon cancer cell growth. *Int J Biochem Cell Biol*. 44:620-628.

Holleran, W.M., K.R. Feingold, M.Q. Man, W.N. Gao, J.M. Lee, and P.M. Elias. 1991. Regulation of epidermal sphingolipid synthesis by permeability barrier function. *J Lipid Res*. 32:1151-1158.

Holleran, W.M., Y. Takagi, G. Imokawa, S. Jackson, J.M. Lee, and P.M. Elias. 1992. beta-Glucocerebrosidase activity in murine epidermis: characterization and localization in relation to differentiation. *J Lipid Res*. 33:1201-1209.

Hong, K.K., H.R. Cho, W.C. Ju, Y. Cho, and N.I. Kim. 2007. A study on altered expression of serine palmitoyltransferase and ceramidase in psoriatic skin lesion. *J Korean Med Sci*. 22:862-867.

Hou, S.Y., A.K. Mitra, S.H. White, G.K. Menon, R. Ghadially, and P.M. Elias. 1991. Membrane structures in normal and essential fatty acid-deficient stratum corneum: characterization by ruthenium tetroxide staining and x-ray diffraction. *J Invest Dermatol*. 96:215-223.

Huelsken, J., R. Vogel, B. Erdmann, G. Cotsarelis, and W. Birchmeier. 2001. beta-Catenin controls hair follicle morphogenesis and stem cell differentiation in the skin. *Cell*. 105:533-545.

Huwiler, A., B. Johansen, A. Skarstad, and J. Pfeilschifter. 2001. Ceramide binds to the CaLB domain of cytosolic phospholipase A2 and facilitates its membrane docking and arachidonic acid release. *FASEB J*. 15:7-9.

Ichikawa, S., K. Ozawa, and Y. Hirabayashi. 1998. Molecular cloning and characterization of the mouse ceramide glucosyltransferase gene. *Biochem Biophys Res Commun*. 253:707-711.

Iizuka, H., H. Takahashi, M. Honma, and A. Ishida-Yamamoto. 2004. Unique keratinization process in psoriasis: late differentiation markers are abolished because of the premature cell death. *J Dermatol*. 31:271-276.

Irizarry, R.A., B. Hobbs, F. Collin, Y.D. Beazer-Barclay, K.J. Antonellis, U. Scherf, and T.P. Speed. 2003. Exploration, normalization, and summaries of high density oligonucleotide array probe level data. *Biostatistics*. 4:249-264.

Ishida-Yamamoto, A., H. Kato, H. Kiyama, D.K. Armstrong, C.S. Munro, R.A. Eady, S. Nakamura, M. Kinouchi, H. Takahashi, and H. Iizuka. 2000. Mutant loricrin is not crosslinked into the cornified cell envelope but is translocated into the nucleus in loricrin keratoderma. *J Invest Dermatol*. 115:1088-1094.

Ishida-Yamamoto, A., and M. Kishibe. 2011. Involvement of corneodesmosome degradation and lamellar granule transportation in the desquamation process. *Med Mol Morphol*. 44:1-6.

Ito, M., Y. Liu, Z. Yang, J. Nguyen, F. Liang, R.J. Morris, and G. Cotsarelis. 2005. Stem cells in the hair follicle bulge contribute to wound repair but not to homeostasis of the epidermis. *Nat Med*. 11:1351-1354.

Jameson, J., K. Ugarte, N. Chen, P. Yachi, E. Fuchs, R. Boismenu, and W.L. Havran. 2002. A role for skin gammadelta T cells in wound repair. *Science*. 296:747-749.

Jeckel, D., A. Karrenbauer, K.N. Burger, G. van Meer, and F. Wieland. 1992. Glucosylceramide is synthesized at the cytosolic surface of various Golgi subfractions. *J Cell Biol*. 117:259-267.

Jennemann, R., S. Kaden, R. Sandhoff, V. Nordstrom, S. Wang, M. Volz, S. Robine, N. Amen, U. Rothermel, H. Wiegandt, and H.J. Grone. 2012a. Glycosphingolipids are essential for intestinal endocytic function. *J Biol Chem*. 287:32598-32616.

Jennemann, R., M. Rabionet, K. Gorgas, S. Epstein, A. Dalpke, U. Rothermel, A. Bayerle, F. van der Hoeven, S. Imgrund, J. Kirsch, W. Nickel, K. Willecke, H. Riezman, H.J. Grone, and R. Sandhoff. 2012b. Loss of ceramide synthase 3 causes lethal skin barrier disruption. *Human molecular genetics*. 21:586-608.

Jennemann, R., A. Rodden, B.L. Bauer, H.D. Mennel, and H. Wiegandt. 1990. Glycosphingolipids of human gliomas. *Cancer Res*. 50:7444-7449.

Jennemann, R., R. Sandhoff, L. Langbein, S. Kaden, U. Rothermel, H. Gallala, K. Sandhoff, H. Wiegandt, and H.J. Grone. 2007. Integrity and barrier function of the epidermis critically depend on glucosylceramide synthesis. *J Biol Chem*. 282:3083-3094.

Jennemann, R., R. Sandhoff, S. Wang, E. Kiss, N. Gretz, C. Zuliani, A. Martin-Villalba, R. Jager, H. Schorle, M. Kenzelmann, M. Bonrouhi, H. Wiegandt, and H.J. Grone. 2005. Cell-specific deletion of glucosylceramide synthase in brain leads to severe neural defects after birth. *Proc Natl Acad Sci U S A*. 102:12459-12464.

Jiang, Y.J., Y. Uchida, B. Lu, P. Kim, C. Mao, M. Akiyama, P.M. Elias, W.M. Holleran, C. Grunfeld, and K.R. Feingold. 2009. Ceramide stimulates ABCA12 expression via peroxisome proliferator-activated receptor {delta} in human keratinocytes. *J Biol Chem*. 284:18942-18952.

Jobard, F., C. Lefevre, A. Karaduman, C. Blanchet-Bardon, S. Emre, J. Weissenbach, M. Ozguc, M. Lathrop, J.F. Prud'homme, and J. Fischer. 2002. Lipoxygenase-3 (ALOXE3) and 12(R)-lipoxygenase (ALOX12B) are mutated in non-bullous congenital ichthyosiform erythroderma (NCIE) linked to chromosome 17p13.1. *Human molecular genetics*. 11:107-113.

Kannagi, R., M. Izawa, T. Koike, K. Miyazaki, and N. Kimura. 2004. Carbohydrate-mediated cell adhesion in cancer metastasis and angiogenesis. *Cancer Sci*. 95:377-384.

Kannan-Thulasiraman, P., D.D. Seachrist, G.H. Mahabeleshwar, M.K. Jain, and N. Noy. 2010. Fatty acid-binding protein 5 and PPARbeta/delta are critical mediators of epidermal growth factor receptor-induced carcinoma cell growth. *J Biol Chem*. 285:19106-19115.

Karlsson, K.A. 1989. Animal glycosphingolipids as membrane attachment sites for bacteria. *Annu Rev Biochem*. 58:309-350.

Katz, P.O., L.B. Gerson, and M.F. Vela. 2013. Guidelines for the Diagnosis and Management of Gastroesophageal Reflux Disease. *Am J Gastroenterol*.

Kendall, A.C., and A. Nicolaou. 2012. Bioactive lipid mediators in skin inflammation and immunity. *Prog Lipid Res*. 52:141-164.

Keusch, G.T., M. Jacewicz, M. Mobassaleh, and A. Donohue-Rolfe. 1991. Shiga toxin: intestinal cell receptors and pathophysiology of enterotoxic effects. *Rev Infect Dis*. 13 Suppl 4:S304-310.

Kirschner, N., P. Houdek, M. Fromm, I. Moll, and J.M. Brandner. 2010. Tight junctions form a barrier in human epidermis. *Eur J Cell Biol*. 89:839-842.

Kolter, T., R.L. Proia, and K. Sandhoff. 2002. Combinatorial ganglioside biosynthesis. *J Biol Chem*. 277:25859-25862.

Komatsu, N., K. Saijoh, C. Kuk, A.C. Liu, S. Khan, F. Shirasaki, K. Takehara, and E.P. Diamandis. 2007. Human tissue kallikrein expression in the stratum corneum and serum of atopic dermatitis patients. *Exp Dermatol*. 16:513-519.

Koybasi, S., C.E. Senkal, K. Sundararaj, S. Spassieva, J. Bielawski, W. Osta, T.A. Day, J.C. Jiang, S.M. Jazwinski, Y.A. Hannun, L.M. Obeid, and B. Ogretmen. 2004. Defects in cell growth regulation by C18:0-ceramide and longevity assurance gene 1 in human head and neck squamous cell carcinomas. *J Biol Chem*. 279:44311-44319.

Kypriotou, M., M. Huber, and D. Hohl. 2012. The human epidermal differentiation complex: cornified envelope precursors, S100 proteins and the 'fused genes' family. *Exp Dermatol*. 21:643-649.

Lahiri, S., and A.H. Futerman. 2007. The metabolism and function of sphingolipids and glycosphingolipids. *Cell Mol Life Sci*. 64:2270-2284.

Lavie, Y., H. Cao, S.L. Bursten, A.E. Giuliano, and M.C. Cabot. 1996. Accumulation of glucosylceramides in multidrug-resistant cancer cells. *J Biol Chem*. 271:19530-19536.

Levade, T., N. Andrieu-Abadie, B. Segui, N. Auge, M. Chatelut, J.P. Jaffrezou, and R. Salvayre. 1999. Sphingomyelin-degrading pathways in human cells role in cell signalling. *Chem Phys Lipids*. 102:167-178.

Li, W., R. Sandhoff, M. Kono, P. Zerfas, V. Hoffmann, B.C. Ding, R.L. Proia, and C.X. Deng. 2007. Depletion of ceramides with very long chain fatty acids causes defective skin permeability barrier function, and neonatal lethality in ELOVL4 deficient mice. *Int J Biol Sci*. 3:120-128.

Lin, T.K., D. Crumrine, L.D. Ackerman, J.L. Santiago, T. Roelandt, Y. Uchida, M. Hupe, G. Fabrias, J.L. Abad, R.H. Rice, and P.M. Elias. Cellular changes that accompany shedding of human corneocytes. *J Invest Dermatol*. 132:2430-2439.

Liu, Y., Y. Su, M. Wiznitzer, O. Epifano, and S. Ladisch. 2008. Ganglioside depletion and EGF responses of human GM3 synthase-deficient fibroblasts. *Glycobiology*. 18:593-601.

Macheleidt, O., H.W. Kaiser, and K. Sandhoff. 2002. Deficiency of epidermal protein-bound omega-hydroxyceramides in atopic dermatitis. *J Invest Dermatol*. 119:166-173.

Madison, K.C. 2003. Barrier function of the skin: "la raison d'etre" of the epidermis. *J Invest Dermatol*. 121:231-241.

Madison, K.C., P.W. Wertz, J.S. Strauss, and D.T. Downing. 1986. Lipid composition of cultured murine keratinocytes. *J Invest Dermatol*. 87:253-259.

Marekov, L.N., and P.M. Steinert. 1998. Ceramides are bound to structural proteins of the human foreskin epidermal cornified cell envelope. *J Biol Chem*. 273:17763-17770.

Markwell, M.A., L. Svennerholm, and J.C. Paulson. 1981. Specific gangliosides function as host cell receptors for Sendai virus. *Proc Natl Acad Sci U S A*. 78:5406-5410.

Masukawa, Y., H. Narita, E. Shimizu, N. Kondo, Y. Sugai, T. Oba, R. Homma, J. Ishikawa, Y. Takagi, T. Kitahara, Y. Takema, and K. Kita. 2008. Characterization of overall ceramide species in human stratum corneum. *J Lipid Res*. 49:1466-1476.

McGovern, M.M., and E.H. Schuchman. 1993. Acid Sphingomyelinase Deficiency.

Melton, J.L., P.W. Wertz, D.C. Swartzendruber, and D.T. Downing. 1987. Effects of essential fatty acid deficiency on epidermal O-acylsphingolipids and transepidermal water loss in young pigs. *Biochim Biophys Acta*. 921:191-197.

Mertens, A.E., T.P. Rygiel, C. Olivo, R. van der Kammen, and J.G. Collard. 2005. The Rac activator Tiam1 controls tight junction biogenesis in keratinocytes through binding to and activation of the Par polarity complex. *J Cell Biol*. 170:1029-1037.

Mizukoshi, K., K. Matsumoto, R. Hirose, T. Fujita, A. Ishida-Yamamoto, and H. Iizuka. 2011. Effects of serine palmitoyltransferase inhibitor ISP-I on the stratum corneum of intact mouse skin. *Biol Pharm Bull*. 34:1383-1389.

Morgan, E., P. Kannan-Thulasiraman, and N. Noy. 2010. Involvement of Fatty Acid Binding Protein 5 and PPARbeta/delta in Prostate Cancer Cell Growth. *PPAR Res*. 2010.

Naruhn, S., W. Meissner, T. Adhikary, K. Kaddatz, T. Klein, B. Watzer, S. Muller-Brusselbach, and R. Muller. 2010. 15-hydroxyeicosatetraenoic acid is a preferential peroxisome proliferator-activated receptor beta/delta agonist. *Molecular pharmacology*. 77:171-184.

Natoli, T.A., L.A. Smith, K.A. Rogers, B. Wang, S. Komarnitsky, Y. Budman, A. Belenky, N.O. Bukanov, W.R. Dackowski, H. Husson, R.J. Russo, J.A. Shayman, S.R. Ledbetter, J.P. Leonard, and O. Ibraghimov-

Beskrovnaya. 2010. Inhibition of glucosylceramide accumulation results in effective blockade of polycystic kidney disease in mouse models. *Nat Med*. 16:788-792.

Nemes, Z., L.N. Marekov, L. Fesus, and P.M. Steinert. 1999. A novel function for transglutaminase 1: attachment of long-chain omega-hydroxyceramides to involucrin by ester bond formation. *Proc Natl Acad Sci U S A*. 96:8402-8407.

Nordström, V., M. Willershäuser, S. Herzer, J. Rozman, O. von Bohlen und Halbach, S. Meldner, U. Rothermel, S. Kaden, F.C. Roth, C. Waldeck, N. Gretz, M. Hrabě de Angelis, A. Draguhn, M. Klingenspor, H.-J. Gröne, and R. Jennemann. 2013. Neuronal Expression of Glucosylceramide Synthase in Central Nervous System Regulates Body Weight and Energy Homeostasis. *Plos Biology*. 11.

Ogawa, E., Y. Owada, S. Ikawa, Y. Adachi, T. Egawa, K. Nemoto, K. Suzuki, T. Hishinuma, H. Kawashima, H. Kondo, M. Muto, S. Aiba, and R. Okuyama. 2011. Epidermal FABP (FABP5) regulates keratinocyte differentiation by 13(S)-HODE-mediated activation of the NF-kappaB signaling pathway. *J Invest Dermatol*. 131:604-612.

Ohman, H., and A. Vahlquist. 1998. The pH gradient over the stratum corneum differs in X-linked recessive and autosomal dominant ichthyosis: a clue to the molecular origin of the "acid skin mantle"? *J Invest Dermatol*. 111:674-677.

Owens, D.M., M.R. Romero, C. Gardner, and F.M. Watt. 2003. Suprabasal alpha6beta4 integrin expression in epidermis results in enhanced tumourigenesis and disruption of TGFbeta signalling. *J Cell Sci*. 116:3783-3791.

Palmer, C.N., A.D. Irvine, A. Terron-Kwiatkowski, Y. Zhao, H. Liao, S.P. Lee, D.R. Goudie, A. Sandilands, L.E. Campbell, F.J. Smith, G.M. O'Regan, R.M. Watson, J.E. Cecil, S.J. Bale, J.G. Compton, J.J. DiGiovanna, P. Fleckman, S. Lewis-Jones, G. Arseculeratne, A. Sergeant, C.S. Munro, B. El Houate, K. McElreavey, L.B. Halkjaer, H. Bisgaard, S. Mukhopadhyay, and W.H. McLean. 2006. Common loss-of-function variants of the epidermal barrier protein filaggrin are a major predisposing factor for atopic dermatitis. *Nat Genet*. 38:441-446.

Perry, D.K., and Y.A. Hannun. 1998. The role of ceramide in cell signaling. *Biochim Biophys Acta*. 1436:233-243.

Pewzner-Jung, Y., S. Ben-Dor, and A.H. Futerman. 2006. When do Lasses (longevity assurance genes) become CerS (ceramide synthases)?: Insights into the regulation of ceramide synthesis. *J Biol Chem*. 281:25001-25005.

Potten, C.S., R. Saffhill, and H.I. Maibach. 1987. Measurement of the transit time for cells through the epidermis and stratum corneum of the mouse and guinea-pig. *Cell and tissue kinetics*. 20:461-472.

Pruett, S.T., A. Bushnev, K. Hagedorn, M. Adiga, C.A. Haynes, M.C. Sullards, D.C. Liotta, and A.H. Merrill, Jr. 2008. Biodiversity of sphingoid bases ("sphingosines") and related amino alcohols. *J Lipid Res*. 49:1621-1639.

Rabionet , M. 2011. Ceramide synthase 3 and its essential role in skin barrier function and male fertility. *Dissertation*.

Raffaghello, L., D. Marimpietri, G. Pagnan, F. Pastorino, E. Cosimo, C. Brignole, M. Ponzoni, and P.G. Montaldo. 2003. Anti-GD2 monoclonal antibody immunotherapy: a promising strategy in the prevention of neuroblastoma relapse. *Cancer Lett*. 197:205-209.

Raja, K. Sivamani, M.S. Garcia, and R.R. Isseroff. 2007. Wound re-epithelialization: modulating keratinocyte migration in wound healing. *Front Biosci*. 12:2849-2868.

Rodriguez, C.I., F. Buchholz, J. Galloway, R. Sequerra, J. Kasper, R. Ayala, A.F. Stewart, and S.M. Dymecki. 2000. High-efficiency deleter mice show that FLPe is an alternative to Cre-loxP. *Nat Genet*. 25:139-140.

Rosenwald, A.G., and R.E. Pagano. 1993. Intracellular transport of ceramide and its metabolites at the Golgi complex: insights from short-chain analogs. *Adv Lipid Res*. 26:101-118.

Salic, A., and T.J. Mitchison. 2008. A chemical method for fast and sensitive detection of DNA synthesis in vivo. *Proc Natl Acad Sci U S A*. 105:2415-2420.

Sandhoff, K. 1969. Variation of beta-N-acetylhexosaminidase-pattern in Tay-Sachs disease. *FEBS Lett*. 4:351-354.

Sandhoff, R. 2009. Very long chain sphingolipids: tissue expression, function and synthesis. *FEBS Lett*. 584:1907-1913.

Sandilands, A., C. Sutherland, A.D. Irvine, and W.H. McLean. 2009. Filaggrin in the frontline: role in skin barrier function and disease. *J Cell Sci*. 122:1285-1294.

Sato, J., M. Denda, J. Nakanishi, J. Nomura, and J. Koyama. 1998. Cholesterol sulfate inhibits proteases that are involved in desquamation of stratum corneum. *J Invest Dermatol*. 111:189-193.

Schachtrup, C., T. Emmler, B. Bleck, A. Sandqvist, and F. Spener. 2004. Functional analysis of peroxisome-proliferator-responsive element motifs in genes of fatty acid-binding proteins. *The Biochemical journal*. 382:239-245.

Schiffmann, S., J. Sandner, K. Birod, I. Wobst, C. Angioni, E. Ruckhaberle, M. Kaufmann, H. Ackermann, J. Lotsch, H. Schmidt, G. Geisslinger, and S. Grosch. 2009. Ceramide synthases and ceramide levels are increased in breast cancer tissue. *Carcinogenesis*. 30:745-752.

Schmuth, M., C.M. Haqq, W.J. Cairns, J.C. Holder, S. Dorsam, S. Chang, P. Lau, A.J. Fowler, G. Chuang, A.H. Moser, B.E. Brown, M. Mao-Qiang, Y. Uchida, K. Schoonjans, J. Auwerx, P. Chambon, T.M. Willson, P.M. Elias, and K.R. Feingold. 2004. Peroxisome proliferator-activated receptor (PPAR)-beta/delta stimulates differentiation and lipid accumulation in keratinocytes. *J Invest Dermatol*. 122:971-983.

Schmuth, M., M.Q. Man, F. Weber, W. Gao, K.R. Feingold, P. Fritsch, P.M. Elias, and W.M. Holleran. 2000. Permeability barrier disorder in Niemann-Pick disease: sphingomyelin-ceramide processing required for normal barrier homeostasis. *J Invest Dermatol*. 115:459-466.

Schulz, T.J., and Y.H. Tseng. 2009. Emerging role of bone morphogenetic proteins in adipogenesis and energy metabolism. *Cytokine & growth factor reviews*. 20:523-531.

Simpson, C.L., D.M. Patel, and K.J. Green. 2011. Deconstructing the skin: cytoarchitectural determinants of epidermal morphogenesis. *Nat Rev Mol Cell Biol*. 12:565-580.

Soriano, P. 1999. Generalized lacZ expression with the ROSA26 Cre reporter strain. *Nat Genet*. 21:70-71.

Sprong, H., B. Kruithof, R. Leijendekker, J.W. Slot, G. van Meer, and P. van der Sluijs. 1998. UDP-galactose:ceramide galactosyltransferase is a class I integral membrane protein of the endoplasmic reticulum. *J Biol Chem*. 273:25880-25888.

Tan, N.S., G. Icre, A. Montagner, B. Bordier-ten-Heggeler, W. Wahli, and L. Michalik. 2007. The nuclear hormone receptor peroxisome proliferator-activated receptor beta/delta potentiates cell chemotactism, polarization, and migration. *Mol Cell Biol*. 27:7161-7175.

Tan, N.S., N.S. Shaw, N. Vinckenbosch, P. Liu, R. Yasmin, B. Desvergne, W. Wahli, and N. Noy. 2002. Selective cooperation between fatty acid binding proteins and peroxisome proliferator-activated receptors in regulating transcription. *Mol Cell Biol*. 22:5114-5127.

Thudichum, J.L.W. 1884. A treatise on the chemical constitution of the brain.

Tobey, N.A. 1995. How does the esophageal epithelium maintain its integrity? *Digestion*. 56 Suppl 1:45-50.

Uchida, Y., and S. Hamanaka. 2006. Stratum Corneum Ceramides: Function, Origins, and Therapeutic Applications. *Skin Barrier*:43-64.

Uchida, Y., M. Hara, H. Nishio, E. Sidransky, S. Inoue, F. Otsuka, A. Suzuki, P.M. Elias, W.M. Holleran, and S. Hamanaka. 2000. Epidermal sphingomyelins are precursors for selected stratum corneum ceramides. *J Lipid Res*. 41:2071-2082.

van Echten-Deckert, G., A. Klein, T. Linke, T. Heinemann, J. Weisgerber, and K. Sandhoff. 1997. Turnover of endogenous ceramide in cultured normal and Farber fibroblasts. *J Lipid Res*. 38:2569-2579.

Van Kaer, L. 2005. alpha-Galactosylceramide therapy for autoimmune diseases: prospects and obstacles. *Nat Rev Immunol*. 5:31-42.

Vielhaber, G., S. Pfeiffer, L. Brade, B. Lindner, T. Goldmann, E. Vollmer, U. Hintze, K.P. Wittern, and R. Wepf. 2001. Localization of ceramide and glucosylceramide in human epidermis by immunogold electron microscopy. *J Invest Dermatol*. 117:1126-1136.

Wang, D., H. Wang, Y. Guo, W. Ning, S. Katkuri, W. Wahli, B. Desvergne, S.K. Dey, and R.N. DuBois. 2006. Crosstalk between peroxisome proliferator-activated receptor delta and VEGF stimulates cancer progression. *Proc Natl Acad Sci U S A*. 103:19069-19074.

Wang, X.P., M. Schunck, K.J. Kallen, C. Neumann, C. Trautwein, S. Rose-John, and E. Proksch. 2004. The interleukin-6 cytokine system regulates epidermal permeability barrier homeostasis. *J Invest Dermatol*. 123:124-131.

Watt, F.M. 2002a. Role of integrins in regulating epidermal adhesion, growth and differentiation. *EMBO J*. 21:3919-3926.

Watt, F.M. 2002b. The stem cell compartment in human interfollicular epidermis. *J Dermatol Sci*. 28:173-180.

Weerheim, A., and M. Ponec. 2001. Determination of stratum corneum lipid profile by tape stripping in combination with high-performance thin-layer chromatography. *Arch Dermatol Res*. 293:191-199.

Weidinger, S., T. Illig, H. Baurecht, A.D. Irvine, E. Rodriguez, A. Diaz-Lacava, N. Klopp, S. Wagenpfeil, Y. Zhao, H. Liao, S.P. Lee, C.N. Palmer, C. Jenneck, L. Maintz, T. Hagemann, H. Behrendt, J. Ring, M.M. Nothen, W.H. McLean, and N. Novak. 2006. Loss-of-function variations within the filaggrin gene predispose for atopic dermatitis with allergic sensitizations. *J Allergy Clin Immunol*. 118:214-219.

Werner, S., and R. Grose. 2003. Regulation of wound healing by growth factors and cytokines. *Physiological reviews*. 83:835-870.

Wertz, P.W. 2006. Biochemistry of human stratum corneum lipids. *Skin Barrier*.

Wertz, P.W., P.S. Cox, C.A. Squier, and D.T. Downing. 1986. Lipids of epidermis and keratinized and non-keratinized oral epithelia. *Comp Biochem Physiol B*. 83:529-531.

Westwick, J.K., A.E. Bielawska, G. Dbaibo, Y.A. Hannun, and D.A. Brenner. 1995. Ceramide activates the stress-activated protein kinases. *J Biol Chem*. 270:22689-22692.

Wood, L.C., S.M. Jackson, P.M. Elias, C. Grunfeld, and K.R. Feingold. 1992. Cutaneous barrier perturbation stimulates cytokine production in the epidermis of mice. *J Clin Invest*. 90:482-487.

Yamashita, T., A. Hashiramoto, M. Haluzik, H. Mizukami, S. Beck, A. Norton, M. Kono, S. Tsuji, J.L. Daniotti, N. Werth, R. Sandhoff, K. Sandhoff, and R.L. Proia. 2003. Enhanced insulin sensitivity in mice lacking ganglioside GM3. *Proc Natl Acad Sci U S A*. 100:3445-3449.

Yang, L., F. Francois, and Z. Pei. 2012. Molecular pathways: pathogenesis and clinical implications of microbiome alteration in esophagitis and Barrett esophagus. *Clin Cancer Res*. 18:2138-2144.

Yates, A.J. 1986. Gangliosides in the nervous system during development and regeneration. *Neurochem Pathol*. 5:309-329.

Zuo, Y., D.Z. Zhuang, R. Han, G. Isaac, J.J. Tobin, M. McKee, R. Welti, J.L. Brissette, M.L. Fitzgerald, and M.W. Freeman. 2008. ABCA12 maintains the epidermal lipid permeability barrier by facilitating formation of ceramide linoleic esters. *J Biol Chem*. 283:36624-36635.

7. Appendix

7.1   Supplementary Figures
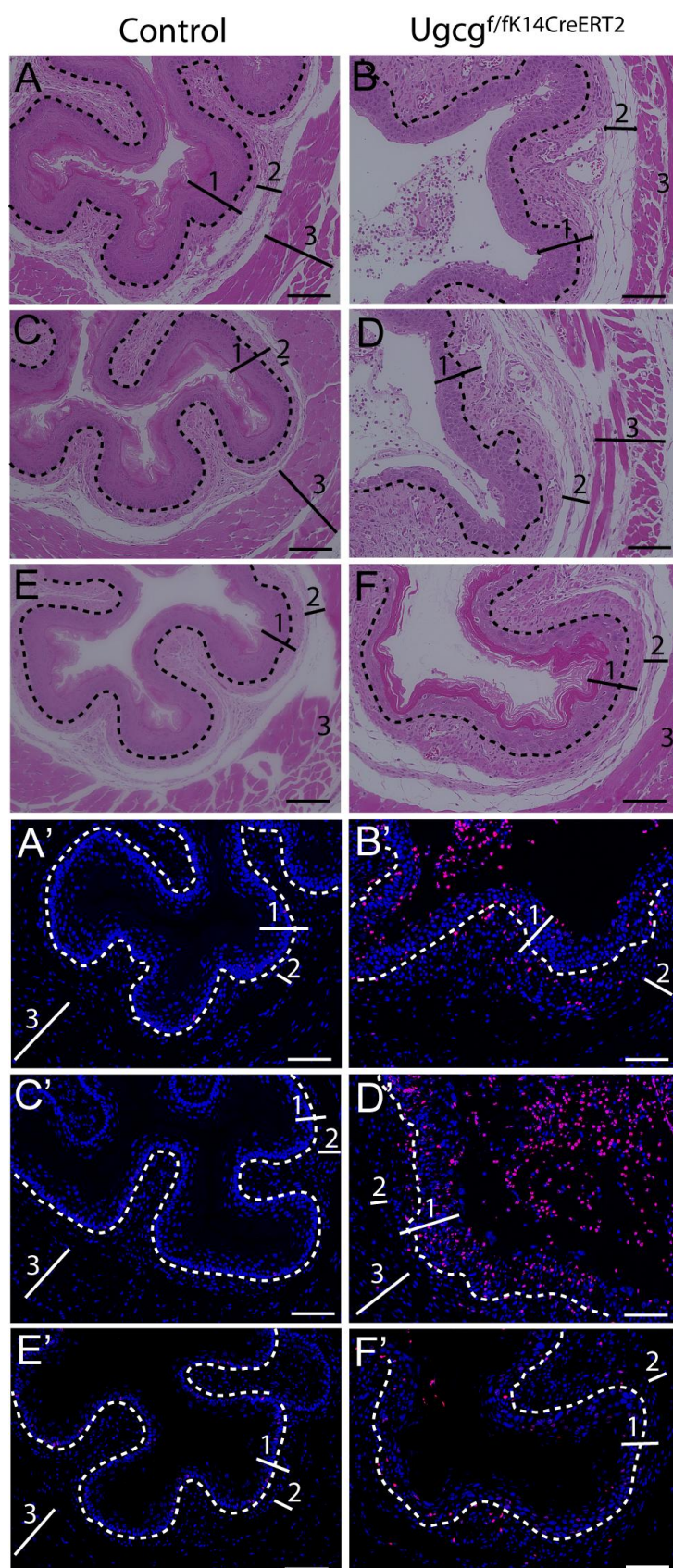
Figure A1. Epithelial alterations and hyperproliferation in esophageal tissue are observed already on day 10 after initiation of TAM induction.

LM of H&E-stained cervical (**A**, **B**), thoracic (**C**, **D**) and abdominal (**E**, **F**) esophagus showed a less coherent morphology of the stratified epithelium in *Ugcg* mutants compared to controls in week 2 of TAM induction. (**A'-F'**) EdU staining of corresponding esophageal sections (cervical (**A'**, **B'**), thoracic (**C'**, **D'**), abdominal (**E'**, **F'**)) 24 h after EdU injection (200 µg) revealed significantly more EdU-positive cells in *Ugcg* mutant samples. Due to dissociation of parts of the apical epithelium (**B**, **B'**, **D**, **D'**, **F'**), EdU-positivity is observed in the esophageal lumen (**B'**, **D'**). Dashed line indicates epithelial basement membrane. Tissue types are (para)keratotic squamous epithelia (lamina propria, muscularis mucosae, (**1**); submucosa (**2**); muscularis externa (smooth and striated muscle, (**3**); scale bars = 100 µm.
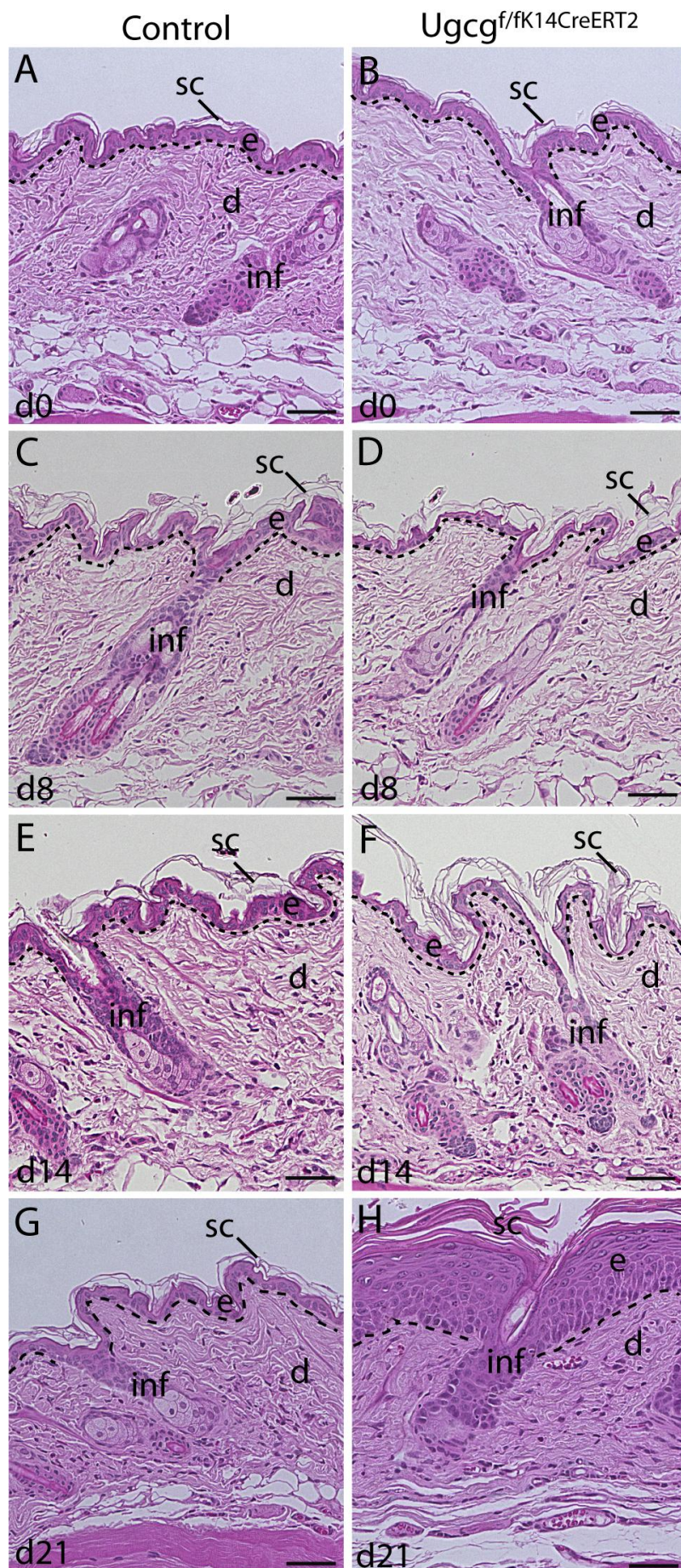
Figure A2. Hyperstratification of *Ugcg* mutant epidermis occurs first 3 weeks after TAM induction.

LM of H&E-stained control (**A**, **C**, **E**, **G**) and mutant mouse skin sections (**B**, **D**, **F**, **H**) revealed the first significant alterations of epidermal morphology at day 21 of TAM induction. UGCG-deficient skin displayed a hyperstratified epidermis with a fivefold increase in epidermal layers (**H**) as compared to controls (**G**). Representative sections from four independent experiments with $n = 4$ each are shown (e = epidermis; d = dermis; inf = infundibulum; sc = stratum corneum; scale bars = 50 µm).
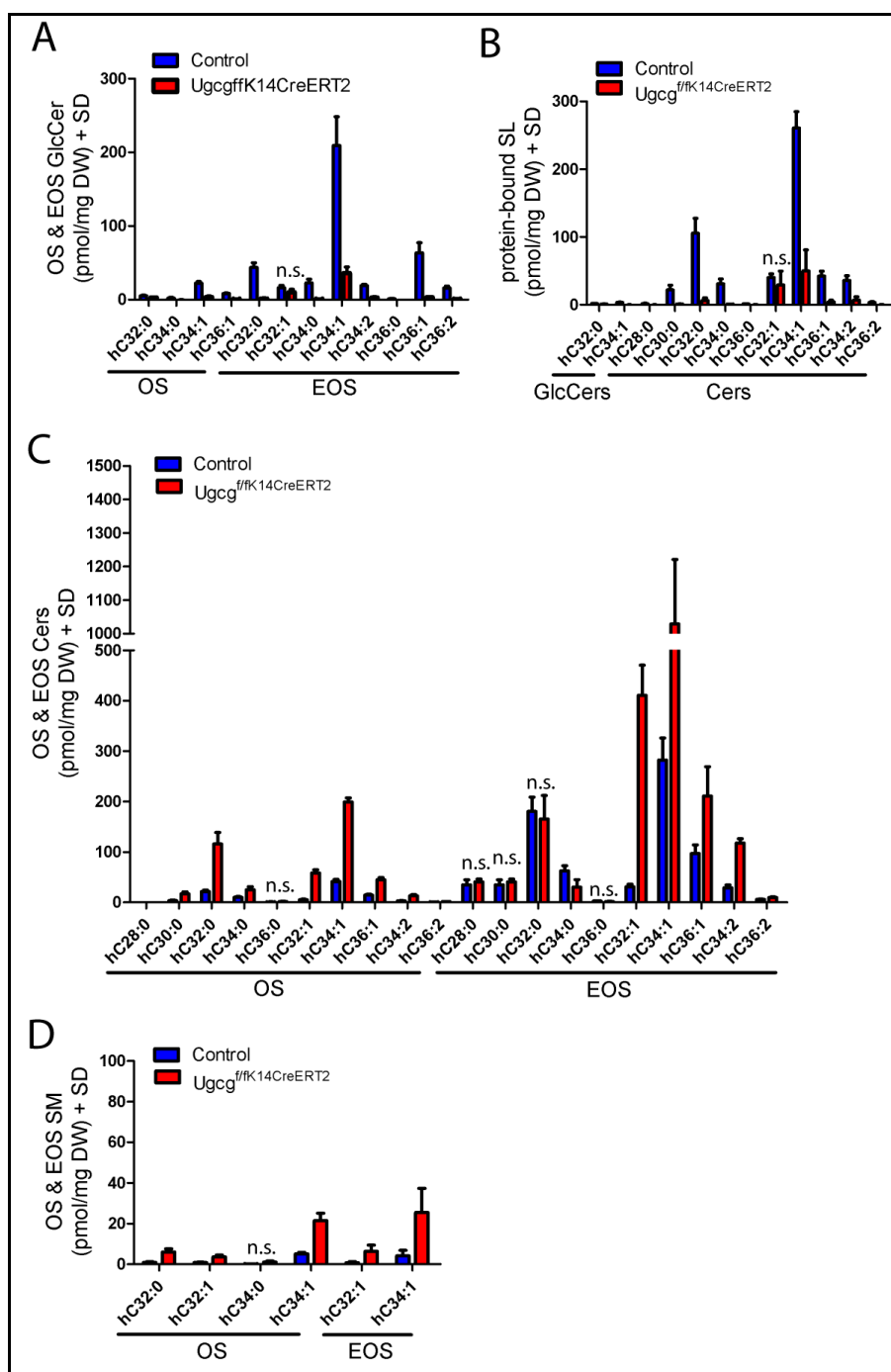
Figure A3. MS analysis of OS-, EOS- and POS-SLs in epidermis of $Ugcg^{f/f\,K14CreERT2}$ mice.

The epidermal composition of ωh-ULC-SLs was investigated by quantitative MS and revealed for all SL species (except for those denoted with n.s. (not significant)) significant differences between control and mutant epidermal extracts. (**A**) OS- and EOS-GlcCers were significantly reduced in mutant epidermis, the hydroxylated FA components hC32:0, hC34:1 and hC36:1 showed the largest decrease by weight for mutants vs. controls. (**B**) The largest decrease was observed for POS-SLs such as POS-Cers containing hC32:0, hC34:1, hC34:2 and hC36:1 FAs. (**C**) Furthermore, Cers were significantly increased in mutant epidermis, and most species contained FAs similar to those found in the corresponding depleted GlcCer fraction (e.g., hC32:0, hC34:1, hC34:2, hC36:1). (**D**) ULC-SMs only occur to a minor extent in murine epidermis; those with a C32:0, C32:1 or C34:1 FA were significantly elevated. Mean values ± SD are shown for $n = 4$.
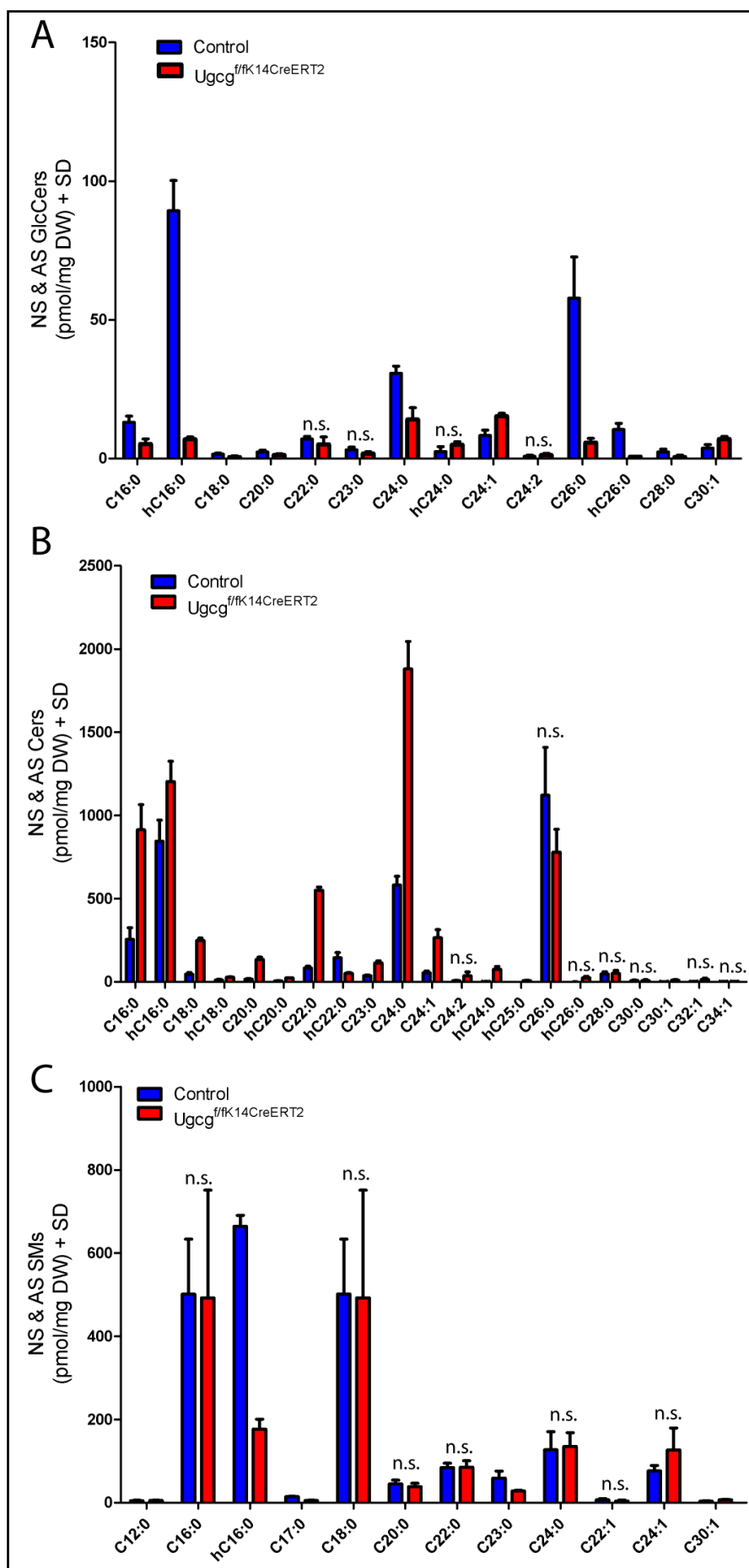
Figure A4. MS analysis of epidermal NS- and AS-SLs in $Ugcg^{f/f\,K14CreERT2}$ mice.

Significant differences in the SL pattern regarding nonhydroxylated (NS) and α-hydroxylated (AS) species were observed for mutant vs. control epidermis. (**A**) For NS- and AS-GlcCers, those containing a C16, C24 or C26 FA chain showed the most prominent decrease. (**B**) In general, the corresponding NS- and AS-Cers were significantly increased in mutants. In particular, FA-containing Cers with C18:0, C20:0, C22:0 and C24:0 were elevated. (**C**) The NS- and AS-SMs showed little differences between mutants and controls, except for C17:0 and hC16:0 species. Mean values ± SD are shown for $n = 4$; all differences were statistically significant except those denoted with n.s.

Control   *Ugcg^{f/f K14CreERT2}*
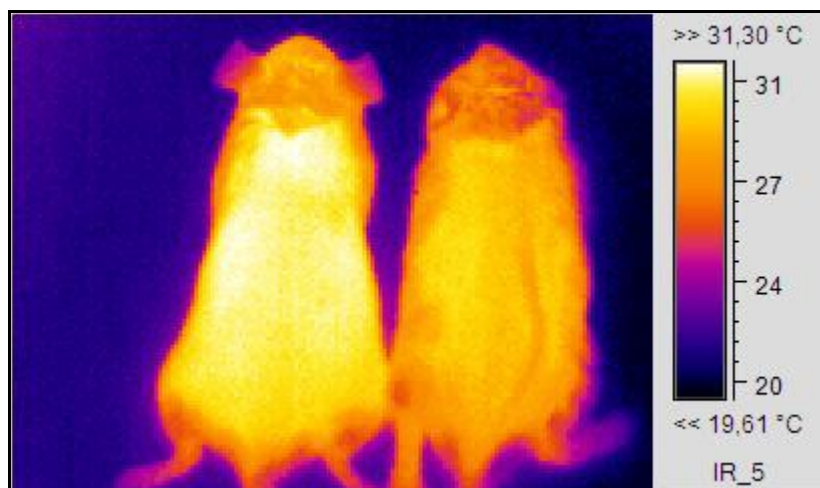
Figure A5. Infrared thermography of control and UGCG-deficient mice.

The body surface temperature of mice was analyzed using an infrared camera. The thermal image shows that skin temperature decreased by a few °C for mutant vs. control.
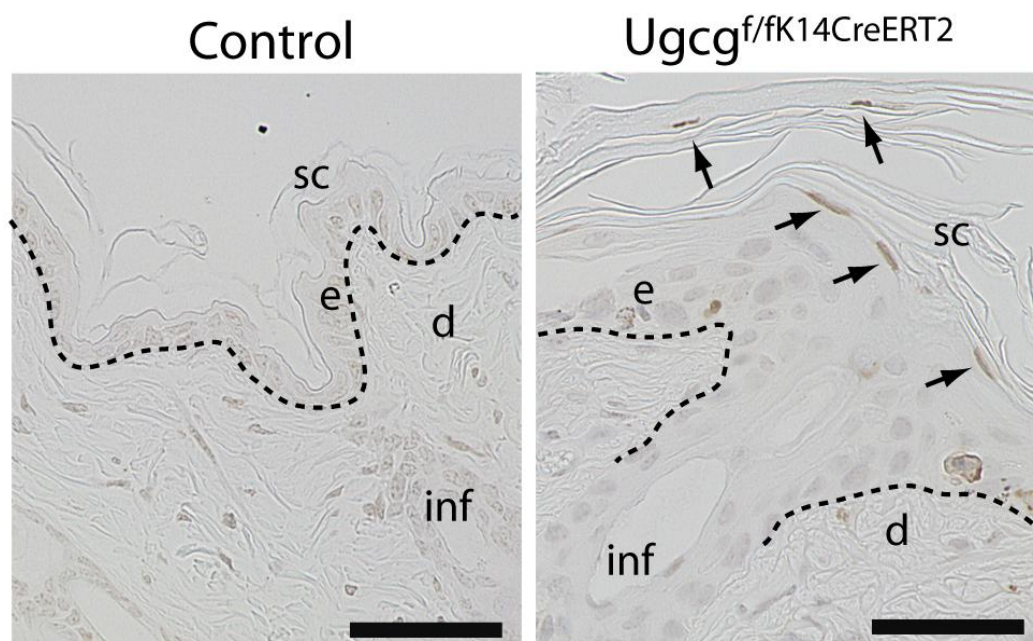
Figure A6. Investigation of apoptosis by TUNEL staining.

Right Panel: TUNEL staining performed on paraffin sections of skins from 12 week-old mice showed apoptotic nuclei in the lower und upper stratum corneum layers of epidermis from *Ugcg* mutants (arrows), indicating a defect in corneocyte maturation rather than enhanced apoptosis. **Left Panel:** control epidermis was TUNEL-negative. Representative sections from three independent experiments with *n* = 3 each are shown (e = epidermis; d = dermis; inf = infundibulum; sc = stratum corneum; scale bars = 25 μm).
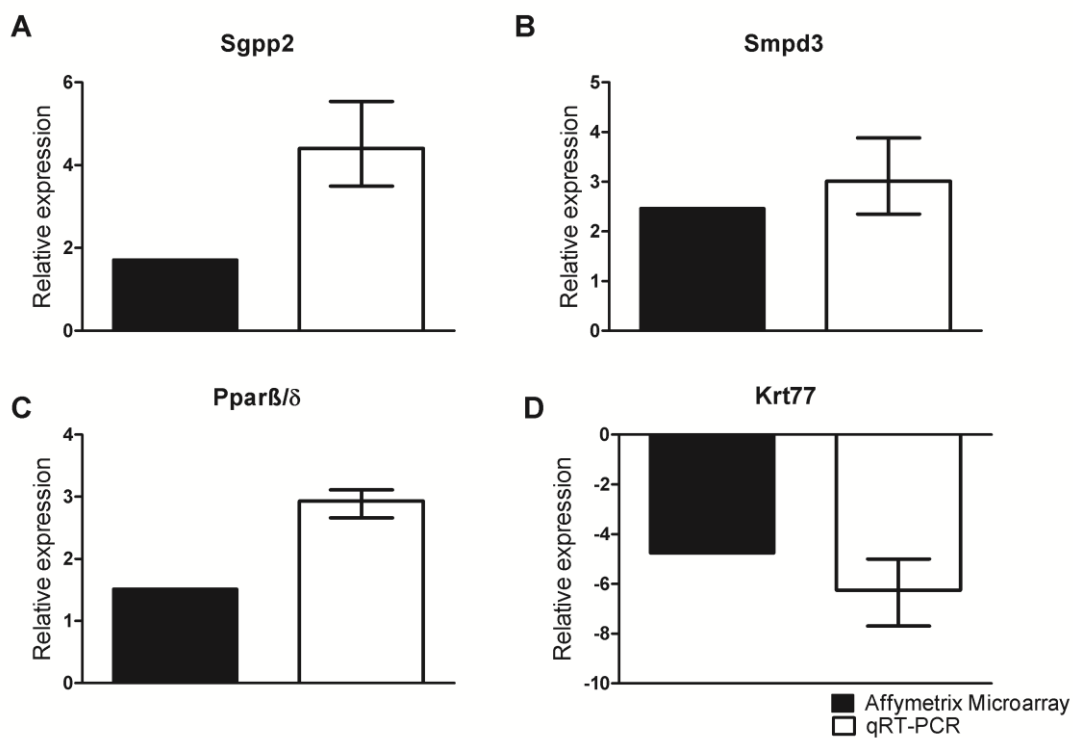
Figure A7. Relative expression of selected genes in microarray and qRT-PCR experiments.

Differentially expressed genes involved in lipid metabolic pathways (**A-C**) and/or in epidermal differentiation (**C, D**) were additionally analyzed via qRT-PCR in order to corroborate the array data. White Bars show the relative fold changes of the corresponding genes normalized to GAPDH. Black bars show fold changes. For abbreviations see 7.3.

7.2   Supplementary Tables

Table A1.   Epidermal sphingolipids in control and mutant mice, as quantified by tandem mass spectrometry. [a]

FA component[b]	Glucosylceramides [pmol/mg dw] ± SD		Ceramides [pmol/mg dw] ± SD		Sphingomyelins [pmol/mg dw] ± SD	
	Control	Mutant	Control	Mutant	Control	Mutant
NS (C16-C36)	130.8 ± 17.6	58.0 ± 10.3	2263.1 ± 253.8	5010.8 ± 265.3	1425.9 ± 346.6	1421.4 ± 618.0
AS (C16-C26)	102.3 ± 11.6	12.5 ± 2	1009.0 ± 125.7	1415.5 ± 120.9	664.5 ± 26.1	177.0 ± 24.1
OS (C28-C36)	38.4 ± 3.8	7.0 ± 1.4	10.2 ± 1.1	47.7 ± 3	7.0 ± 1.1	32.0 ± 4.3
EOS (C28-C36)	391.6 ± 64.2	55.3 ± 11.8	761.0 ± 107.8	2057.6 ± 345.4	5.4 ± 3.9	34.0 ±15.9
POS (C28-C36)	6.9 ± 1.2	1.0 ± 0.3	544.6 ± 73.4	99.1 ± 63.7	0	0

[a] mutant = TAM-induced $Ugcg^{f/f\ K14CreERT2}$; dw = dry wt.

[b] NS, nonhydroxylated; AS, α-hydroxylated; OS, ω-hydroxylated; EOS, ω-hydroxylated, esterified to an FA; POS, ω-hydroxylated, linked to protein.

Table A2.   Gene ontology (GO) enrichment analysis.

GO term	description (biological process)	*p*-value
GO:0008152	metabolic process	3.09 E-16
GO:0032502	developmental process	7.57 E-16
GO:0048856	anatomical structure development	5.78 E-15
GO:0007275	multicellular organismal development	7.91 E-15
GO:0048731	system development	1.71 E-15
GO:0010951	negative regulation of endopeptidase activity	1.96 E-13
GO:0010466	negative regulation of peptidase activity	1.78 E-12
GO:0009987	cellular process	3.09 E-12
GO:0030154	cell differentiation	4.13 E-12
GO:0009653	anatomical structure morphogenesis	6.65 E-12
GO:0048869	cellular developmental process	1.31 E-11
GO:0065007	biological regulation	1.36 E-11
GO:0051346	negative regulation of hydrolase activity	4.36 E-11
GO:0052547	regulation of peptidase activity	1.69 E-10
GO:0052548	regulation of endopeptidase activity	3.40 E-10
GO:0048513	organ development	1.11 E-9
GO:0032501	multicellular organismal process	1.54 E-9
GO:0044238	primary metabolic process	1.76 E-9
GO:0051239	regulation of multicellular organismal process	1.98 E-9
GO:0050790	regulation of catalytic activity	3.03 E-9
GO:0009888	tissue development	3.09 E-9
GO:0008544	**epidermis development**	**5.55 E-9**
GO:0050789	regulation of biological process	5.90 E-9
GO:0006629	**lipid metabolic process**	**1.02 E-8**
GO:0008610	**lipid biosynthetic process**	**1.24 E-8**
GO:0031424	**keratinization**	**1.89 E-8**
GO:0044255	**cellular lipid metabolic process**	**2.20 E-8**
GO:0065009	regulation of molecular function	2.98 E-8
GO:0019222	regulation of metabolic process	4.43 E-8
GO:0043086	negative regulation of catalytic activity	5.89 E-8
GO:0048583	regulation of response to stimulus	5.94 E-8
GO:0050896	response to stimulus	8.81 E-8
GO:0009611	**response to wounding**	**1.31 E–6**
GO:0050678	**regulation of epithelial cell proliferation**	**4.4 E-4**

Table A3.   List of human diseases from the Medical Subject Headings database (MeSH) correlating to differentially expressed genes.

MeSH Diseases	*p*-value
Head and Neck Neoplasms	1.46 E-13
Psoriasis	1.64 E-13
Skin Diseases, Papulosquamous	7.95 E-13
Esophageal Neoplasms	2.10 E-11
Esophageal Diseases	5.26 E-11
Skin Diseases	8.08 E-11
Inflammation	2.45 E-10
Neoplastic Processes	2.68 E-10
Skin and Connective Tissue Diseases	2.85 E-10
Carcinomas, Squamous Cell	2.40 E-9
Neoplasms, Squamous Cell	4.76 E-9
Dermatitis	8.24 E-9
Metaplasia	1.16 E-8
Gastrointestinal Neoplasms	1.65 E-8
Neoplasm Invasiveness	1.67 E-8
Skin Neoplasms	1.69 E-8
Skin Diseases, Genetic	1.86 E-8

As expected from the observed phenotype of *Ugcg* mutants, the gene sets derived from expression analysis show the highest correlation to cancer, skin and esophageal diseases (lowest *p* values).

7.3 Catalog of Abbreviations, Terminology and Proteins

For the following list of abbreviations IUPAC and IUBMB standards and the recommendations of the HGNC (genes, proteins) and BRENDA (enzymes) data bases have been used wherever possible. Where relevant, common synonyms for proteins or genes are given. The following conventions have been applied for symbolic names: human and mouse proteins are upper-case, roman type; human genes are upper-case, italics; mouse genes are italics, first character upper-case; greek letters (e.g., α, β) are replaced by there roman equivalents as suffixes. For enzymes alternative names and EC numbers are given where available. In some cases only protein root symbols are given to designate a protein family or the symbol *n* is attached; for specific members the appropriate arabic numeral is attached. In general, when an abbreviation is used in a plural sense (families, classes), a lower-case s is attached.

12R-LOX	arachidonate 12-lipoxygenase (EC 1.13.11.31)
AA	amino acids
ABCA12	ATP-binding cassette, sub-family A (ABC1), member 12
AD	atopic dermatitis
aGSL	acidic glycosphingolipid (carbohydrate headgroup with carboxyl, sulfate, or phosphate substituents)
Alox12b	gene encoding for 12R-LOX
Alox12e	gene encoding for eLOX-3
AP	alkaline phosphatase (EC 3.1.3.1)
ARCI	autosomal recessive congenital ichthyosis
AS	α-hydroxylated FA
acid SMase, aSMase	sphingomyelin phosphodiesterase (EC 3.1.4.12); acid sphingomyelinase
AJ	adherens junction
AJAP1	adherens junctions associated protein 1
B4GALT6	UDP-Gal:betaGlcNAc β-1,4-galactosyltransferase, polypeptide 6
bFGF	basic fibroblast growth factor
BglII	restriction endonuclease (*Bacillus globigii*), site II
BM	basement membrane
BMP6	bone morphogenic protein 6
bp	base pair
BSA	bovine serum albumin
CAPP	ceramide-activated protein phosphatase (EC 3.1.3-)
caspase-8	apototic cysteine protease 8 (EC 3.4.22.61)

CD	corneodesmosome
CDH1	cadherin 1, type 1, E-cadherin (epithelial)
CDH3	cadherin 3, type 1, P-cadherin (placental)
cDNA	complementary DNA
CDSN	corneodesmosin
CE	cornified envelope
Cer	ceramide
Cer-1-*P*	ceramide 1-phosphate
ceramidase	*N*-acylsphingosine amidohydrolase (EC 3.5.1.23)
CerS	ceramide synthase family; sphingosine *N*-acyltransferase (EC 2.3.1.24)
CERT	ceramide transfer protein
CGI-58	1-acylglycerol-3-phosphate O-acyltransferase (EC 2.3.1.51); also known as AGPAT
Cho-*P*	phosphocholine
CI	congenital ichthyosis
ClaI	restriction endonuclease (*Caryophanon latum* L), site I
CLDN1	claudin 1 (tight junction protein)
CLE	cornified lipid envelope
CoA	Coenzyme A
CRABP	cellular retinoic acid binding protein
Cre	Cre-recombinase enzyme (Cre = cyclization recombination), a tyrosine recombinase
CreERT2	a genetic modification introducing tamoxifen-inducible Cre-recombinase activity
CSPD	Disodium 3-(4-methoxyspiro {1,2-dioxetane-3,2'-(5'-chloro)tricyclo [3.3.1.13,7]decan}-4-yl)phenyl phosphate, a chemiluminescent substrate for alkaline phosphatase
CTNNB1	catenin (cadherin-associated protein), beta 1, 88kDa
DAG	diacylglycerol
DAPI	4',6-diamidino-2-phenylindole, a fluorescent stain for A-T rich DNA regions
DDC	dermal dendritic cell
dd H_2O	doubly distilled, autoclaved water
DEAE	diethylaminoethyl (Sephadex)
DEGS2	sphingolipid delta(4)-desaturase/C4-hydroxylase
delta-neo	deleted neomycin cassette
DETC	dendritic epidermal T-cell
DES1	dihydroceramide desaturase 1

DIG	digoxigenin, a steroid hapten from *Digitalis* plants, used as immunohistochemical marker for in situ hybridization
DNA	deoxyribonucleic acid
dNTP	2′-deoxyribonucleoside-5′-triphosphate
DSC*n*	desmocollin *n* (*n* = 1, 2, 3)
DSG*n*	desmoglein *n* (*n* = 1, 2); desmosomal cadherin proteins
DSP	desmoplakin (desmosomal catenin protein)
dw	dry weight
ECL	enhanced chemiluminescence
ECM	extracellular matrix
EcoRV	restriction endonuclease V (*E. coli*) type II, site-specific deoxyribonuclease (site V) (EC 3.1.21.4)
EDC	epidermal differentiation complex
EDTA	ethylenediaminetetraacetic acid
EdU	5-ethynyl-2′-deoxyuridine
EFAD	essential fatty acid deficiency
EGF	epidermal growth factor
ELOVL	elongation of very-long-chain fatty acyl-CoA; fatty acid elongase; icosanoyl-CoA synthase (EC 2.3.1.119)
eLOX3	hydroperoxide dehydratase (EC 4.2.1.92)
EOS	ω-hydroxylated FA esterified primarily to linoleic acid
EPGN	epigen growth factor
ER	endoplasmic reticulum
ER-HR3	anti-hematopoiesis-related macrophage antibody
ERT2	estrogen receptor T2
ES	embryonic stem cells
EVPL	envoplakin
FA	fatty acid
FABP5	fatty acid binding protein 5 (epidermal)
FAS	Fas (TNF receptor superfamily, member 6); APO-1, CD95
FATP4	solute carrier family 27 (fatty acid transporter), member 4; SLC27A4
FCS	fetal calf serum
FDR	false discovery rate (chip statistics)
F-granules	filaggrin/profilaggrin-containing granules
FGF	fibroblast growth factor

FLG	filaggrin (protein monomer)
FLG2	filaggrin family member 2 (polymeric)
floxed	"flanked by LoxP"; a DNA sequence is sandwiched between to two *loxP* sites which are targeted by Cre recombinase
FLP	site-specific tyrosine recombinase (*Saccharomyces cerevisiae*), targets FRT site
FLP-deleter	a mouse strain used to remove Frt-flanked selection cassettes in vivo
Frt	FLP recombinase target site
GalCer	galactosylceramide; galactocerebroside e.g., galactosylceramide (d18:1/18:0) = *N*-(octadecanoyl)-1-β-D-galactosyl-sphingosine
GAPDH	glyceraldehyde 3-phosphate dehydrogenase (EC 1.2.1.12/13/59)
GERD	gastroesophageal reflux disease
Giemsa	a stain prepared from a mixture of methylene blue, eosin, and Azure B
GlcCer	glucosylceramide; glucocerebroside e.g., glucosylceramide (d18:1/18:0) = *N*-(octadecanoyl)-1-β-D-glucosyl-sphingosine;
GlcCerase	glucosylceramidase (EC 3.2.1.45), β-glucocerebrosidase; D-glucosyl-*N*-acylsphingosine glucohydrolase
GM3	NeuAc-Gal-Glc-Cer (a ganglioside containing *N*-acetylneuraminic acid)
GO	gene ontology
GRHL3	grainy head-like protein 3
GSL	glycosphingolipid
HBEGF	heparin-binding EGF-like growth factor
H&E	hematoxylin & eosin stain for DNA (pink) and protein (blue)
HMG-CoA	3-hydroxy-3-methyl-glutaryl-CoA
HI	harlequin ichthyosis
HPTLC	high-performance thin-layer chromatography
HRP	horse radish peroxidase (EC 1.11.1.7)
iCre	codon-improved Cre recombinase gene
IF	immunofluorescence
IL	interleukin
ITGA6B4	integrin-α6β4, laminin receptor (adhesive protein in basal keratinocytes)
IVL	involucrin
JNK	janus kinase
JUP	junction plakoglobin; previously PKGB or CTNNG
KAc	potassium acetate

kb	kilobases (in DNA)
KDSR	3-ketodihydrosphingosine reductase (EC 1.1.1.102); 3-dehydrosphinganine reductase (DSR)
KG	keratohyalin granule
Ki-67 (MKI67)	a nuclear protein associated with proliferation
KLK*n*	kallikrein protein family
KpnI	restriction endonuclease (Klebsiella pneumoniae) type II site-specific deoxyribonuclease (EC 3.1.21.4)
KRT*n*	keratin protein family
LacZ	β-galactosidase reporter gene
LAMA5	laminin, alpha 5; laminin-α5 (basement membrane protein)
Lass	the longevity assurance gene family; six LASS proteins function as ceramide synthases
LB	lamellar body
LC	long-chain, referring to FA chain length
LC-ESI	liquid chromatography electrospray ionization (for mass spectrometry)
L-granules	loricrin-containing granules
LI1, LI2	lamellar ichthyosis type 1 and type 2
LIN	linoleic acid (C18:2, ω–6; cis,cis-Δ^9,Δ^{12})
LM	light microscopy
LOR	loricrin
LoxP, *loxP*	"locus of X-over P1"; a DNA sequence derived from bacteriophage P1; a pair of LoxP sites flanking a gene are used as targets for Cre recombinase, e.g. for gene deletion.
MS	mass spectrometry
MS/MS	tandem mass spectrometry (fragmentation of selected parent ions)
neo	neomycin, an aminoglycoside antibiotic
nGSL	neutral glycosphingolipid (uncharged carbohydrate headgroup)
NFκB	nuclear factor 'kappa light chain enhancer' (transcription factor)
NheI	restriction endonuclease (*Neisseria mucosa* heidelbergensis), site I
NMF	natural moisturizing factor
NP-40	nonyl phenoxypolyethoxylethanol, a detergent
NS	nonhydroxylated FA
nSMase	neutral sphingomyelinase
ωh	ω-hydroxylated
Ole	oleic acid (C18:1, ω–9; cis-Δ^9)
OS	ω-hydroxylated FA

O/N	overnight
PacI	restriction endonuclease (*Pseudomonas alcaligenes*), site I
PAS	periodic acid Schiff stain
PBS	phosphate-buffered saline
PCR	polymerase chain reaction
PFA	paraformaldehyde
PFU	proof-reading polymerase
PGK-DTA	phosphoglycerate kinase I promoter from the diphtheria toxin gene
PKC	protein kinase C
PLA2	phospholipase A2
PLD	phospholipase D
PM	plasma membrane
PMNL	polymorphonuclear leukocytes
POS	ω-hydroxylated FA esterified to a protein
PPARβ/δ	peroxisome proliferator-activated receptor β/δ
PPL	periplakin
PPRE	peroxisome proliferator responsive elements
PSAP	prosaposin; sphingolipid activator protein-1
PtdCho	phosphatidyl choline
proFLG	profilaggrin (polymeric FLG)
proteinase K	peptidase K (EC 3.4.21.64) from *Engyodontium album*
PUFA	Polyunsaturated fatty acid
qRT-PCR	quantitative (real-time) reverse transcription polymerase chain reaction
RBP2	retinol binding protein 2
RNA	ribonucleic acid
RNAse A	bovine pancreatic ribonuclease A (EC 3.1.27.5)
RNaseOUT™	recombinant RNase inhibitor (Invitrogen)
Rosa26	Rosaβgeo26 (gene locus in the mouse)
RPTN	repetin
RT	room temperature
RXR	retinoic X receptor
S100A8	calgranulin A
S100A9	calgranulin B
SB	stratum basale

SC	stratum corneum
SCD2	acyl-CoA desaturase 2 (EC 1.14.19.1); stearoyl-CoA desaturase 2
SDS-PAGE	sodium dodecyl sulfate polyacrylamide gel electrophoresis
SG	stratum granulosum
SGPP2	sphingosine-1-phosphate phosphatase 2
SL	sphingolipid
SLC9A1	solute carrier family 9, subfamily A (NHE1, cation proton antiporter 1), member 1
SM	sphingomyelin
SMase	sphingomyelinase, sphingomyelin phosphodiesterase (EC 3.1.4.12)
SMPD1	gene for sphingomyelin phosphodiesterase 1, acid lysosomal SMase
SMPD2	gene for sphingomyelin phosphodiesterase 2, neutral SMase
SM synthase	sphingomyelin synthase (EC 2.7.8.27)
SpeI	restriction endonuclease (*Sphaerotilus natans*), site I
Sph	sphingosine = (4*E*)-sphingenine = (*E*,2*S*,3*R*)-2-aminooctadec-4-ene-1,3-diol
Sph-1-*P*	sphingosine-1-*P*
sPLA2	secretory phospholipase A2 (EC 3.1.1.4)
SPRRs	small proline-rich proteins (family)
SPT	serine C-palmitoyltransferase (EC 2.3.1.50)
SS	stratum spinosum
Sst II (SstII)	restriction endonuclease (*Streptomyces stanford*), site II
TAE	TRIS-acetate-EDTA
TAM	tamoxifen, a selective estrogen receptor modulator with tissue-specific activity
TE	transesterification
TEWL	transepidermal water loss
TJ	tight junction
TJ1	tight junction protein 1; zona occludens 1
TLC	thin-layer chromatography
TG	transglutaminase (EC 2.3.2.13)
TG1	protein-glutamine gamma-glutamyltransferase 1 (EC 2.3.2.13)
TGF	transforming growth factor
TJP1	tight junction protein 1
TNFα	tumor necrosis factor α
TRIS	tris(hydroxymethyl)-aminomethane
Triton X-100	4-octylphenol polyethoxylate, a detergent

Tween® 20	nonionic detergent, polyethylene glycol sorbitan monolaurate
tUCA	*trans*-urocanic acid
UDP-Glc	Uridine(5′)diphospho(1)-α-D-glucose
UGCG	UDP-glucose:ceramide glucosyltransferase; glucosylceramide synthase (EC 2.4.1.80)
ULC	ultra-long-chain
VEGF	vascular endothelial growth factor
VLC	very-long-chain
WPB	water permeability barrier
wt	wild-type: natural or most common phenotype of a species; normal gene or allele
ww	wet weight
XRI	X-linked recessive ichthyosis

Acknowledgements

Publications and Presentations

Parts of the present work have been published or presented elsewhere:

Amen, N., Mathow, M., Rabionet, M., Sandhoff, R., Langbein, L., Gretz, N., Jäckel, C., Gröne, H.-J., Jennemann, R. 2013. Differentiation of epidermal keratinocytes is dependent on glucosylceramide:ceramide processing. *Hum Mol Genet*, submitted, in review.

Poster presentation at the German Cancer Research Center, Nov. 2012.

Poster presentation on the "Stratum Corneum VII" Conference in Cardiff, England, Sept. 10-12, 2012.

Scientific talk at the PhD Retreat of the German Cancer Research Center in Weil der Stadt, Stuttgart, Germany, September 2011.

Further publications:

Jennemann, R., Kaden, S., Sandhoff, R., Nordstrom, V., Wang, S., Volz, M., Robine, S., **Amen, N.,** Rothermel, U., Wiegandt, H., and Grone, H.-J. 2012. Glycosphingolipids are essential for intestinal endocytic function. *J Biol Chem* 287:32598-32616.